ULTRA-WIDEBAND RANGING IN DENSE MULTIPATH ENVIRONMENTS

by

Joon-Yong Lee

A Dissertation Presented to the
FACULTY OF THE GRADUATE SCHOOL
UNIVERSITY OF SOUTHERN CALIFORNIA
In Partial Fulfillment of the
Requirements for the Degree
DOCTOR OF PHILOSOPHY
(ELECTRICAL ENGINEERING)

May 2002

Dedication

To my loving God and my dear parents...

Acknowledgements

I give my most sincere thanks to my advisor, Prof. Robert Scholtz, for his support and encouragement over the past 4 years, his guidance on this thesis, and especially for helping me know the kind of researcher I aspire to become. It has truly been a great privilege to work with him. I am greatly indebted to Profs. Charles Weber, Keith Chugg, Urbashi Mitra and Won Namgoong at Electrical Engineering Department for their valuable suggestions and contributions on my research. I am also very thankful to Prof. Peter Baxendale at Mathematics Department for the help he has offered in the probabilistic analysis.

My gratitude goes to the staffs at Communication Science Institute, especially Milly Montenegro, Mayumi Thrasher and Gerrielyn Ramos, for their exceptional administrative help. And I should thank my colleagues at Ultra-Wideband Radio Laboratory for their thoughtful comments and suggestions. The work proposed was supported by the U.S. Office of Naval Research under Contract No. N00014-00-0221, and by the Integrated Media System Center, a National Science Foundation Engineering Research Center. I deeply appreciate their support. I'd like to acknowledge Time Domain, Inc. for the assistance they have provided in taking propagation

data. Finally I am very much grateful to my parents in Korea, Dal-Keun Lee and Soon-Ok Cho. Their unconditional love and undoubted belief in me have sustained me throughout. Without them this work would not have been possible.

Contents

Dedication ii

Acknowledgements iii

List Of Figures vii

Abstract xi

1 Introduction 1
- 1.1 Motivation . . . 1
- 1.2 Existing Location Systems . . . 3
- 1.3 Problems . . . 5
- 1.4 Overview . . . 7

2 UWB Indoor Propagation Measurement 8
- 2.1 Review of the Measurement . . . 8
- 2.2 Measurement of Antenna System Function . . . 12
- 2.3 Sources of Interference to UWB System . . . 16

3 ToA Measurement Algorithm for Detection of the Direct Path Signal 23
- 3.1 Introduction . . . 23
- 3.2 Signal Representation . . . 24
- 3.3 ToA Algorithm Using GML Estimation . . . 28

4 Error Analysis for ToA Algorithm 33
- 4.1 Statistical Modeling of Ranging Parameters . . . 33
  - 4.1.1 Modeling of Marginal Densities . . . 33
  - 4.1.2 Modeling of the Joint Density of (δ, ρ) . . . 37
- 4.2 Error Analysis . . . 42
  - 4.2.1 Probability of an Early False Alarm . . . 43
  - 4.2.2 Probability of a Missed Direct Path Error . . . 46

5 Threshold Setting and Test for the ToA Algorithm **49**
5.1 Threshold Setting Criteria 49
5.2 Test on Measured Data 56

6 Design of an UWB Ranging System **66**
6.1 Introduction 66
6.2 System Description 68
6.3 Evaluation of Noise Power 70
6.4 Two-Way Ranging Scheme 73

7 Application of ToA algorithm for UWB Scanning Receiver **76**
7.1 Modification of the Algorithm 77
7.2 Sampling Issues 78

8 Conclusion **88**

Appendix A
Evaluation of High Level Crossing Probability of a Continuous Random Process 94

Appendix B
UWB Ambiguity Function 98
B.1 Derivation UWB Ambiguity Function 98
B.2 Computer Plots of UWB Ambiguity functions 103

Appendix C
Maximum A Posteriori Estimation for ToA Measurement: Two-Path Model 110
C.1 Introduction 110
C.2 ToA Estimation Using a Two-Path Model 113

List Of Figures

1.1 (a) Front-end of the received signal which was transmitted with a clear line of sight and (b) its magnitude spectrum 2

2.1 Experimental setup for propagation test. 8
2.2 Output of Avtech pulser. 9
2.3 Basement floor plan of the building where the experiments were conducted. Interior walls are metal stud and dry wall construction. Circular marks stand for the locations of the receiving antenna and the rectangular mark indicates the transmitting antenna's location. . . . 10
2.4 Measured signals at location 1, 5, 7, 10, 13, and 16. The vertical axis indicates signal strength in millivolts. The vertical scales of each plot are different, indicating differences in channel attenuation. The signal shown in the first plot was measured with a clear LoS and the others were measured in the presence of LoS blockages. 13
2.5 Initial portions of signals measured at location 1, 5, 7, 10, 13, and 16. Notice the existence of stronger multipath components. 14
2.6 An average of 32 traces of $|H_{\mathrm{a}}(f)|^2$. Distance between the two antennas were 1m and the relative orientation between them were kept the same. 15
2.7 Measurement of interference signals using spectrum analyzer. The resolution bandwidth of the spectrum analyzer was 300 kHz and noise floor of the equipment was -94.5 dBm. 19
2.8 Interfering signals in the frequency band from 1.08 Hz to 2.16 GHz. The resolution bandwidth of the spectrum analyzer was 300 kHz and noise floor of the equipment was -94.5 dBm. 20
2.9 Interfering signals in the frequency band from 2.16 Hz to 3.24 GHz. No significant signal but noise floor of the equipment was observed. . 21
2.10 Outputs of two ideal bandpass filters whose passbands are 780 MHz - 2.05 GHz and 960 MHz - 1.93 GHz, respectively. The waveform in solid line is the initial portion of a signal measured with a clear LoS. . 22

3.1 Model for the template signal $s(t)$. 25

3.2 Estimated ToA's of signals measured at location 8 and 15. The threshold θ_δ was fixed at 100 ns and θ_ρ was varied. Dashed lines represent of ToA's of each signal evaluated with measured range assuming the presence of a clear LoS. Threshold setting techniques using different criteria are discussed in chapter 5. 32

4.1 Floor plan of the building where the propagation data was taken. . . 34
4.2 Normalized histograms of (a) $\boldsymbol{\delta}$ and (b) $\boldsymbol{\rho}$ and approximation of marginal densities using curve-fitting. 35
4.3 Histogram of $\boldsymbol{\rho}$ and $\boldsymbol{\delta}$. Total volume was normalized to 1. 38
4.4 Joint probability density function of δ and ρ. 41
4.5 Simulation result of $E(\boldsymbol{\lambda})$. $\boldsymbol{u}(\beta)$ was simulated and $\boldsymbol{\lambda}$ for a given γ was observed over 100 occurrences and averaged. 45
4.6 Plot of (a) P_{FA} and (b) P_{M} with a peak SNR of 18 dB. 48

5.1 Threshold setting using criterion A.1 with $\alpha_{\mathrm{FA}} = 0.005$. Each curve is the collection of θ_δ and θ_ρ which satisfy $P_{\mathrm{FA}} = \alpha_{\mathrm{FA}}$. The circular mark on each curve represents the thresholds that minimize P_{M}. . . . 52
5.2 Threshold setting using criterion A.2. The value of θ_δ corresponding to $\alpha_{\mathrm{M}} = 0.001$ is 102.8 ns and each curve represents θ_ρ's which satisfy the given early false alarm setting (α_{F}). Notice that with this criterion, θ_ρ is set independently of the PDF of $\boldsymbol{\rho}$. 53
5.3 Threshold setting using criterion B.1. Each circular mark represents the optimum θ_δ and θ_ρ that minimize $P_{\mathrm{FA}} + P_{\mathrm{M}}$ with a given peak SNR. 54
5.4 Threshold setting with criterion B.2. The value of θ_δ corresponding to $\alpha_{\mathrm{M}} = 0.001$ is 102.8 ns and each curve is a plot of P_{M} vs. P_{FA} with a given peak SNR. Circular mark on each curve represents the optimum θ_δ and θ_ρ that minimize $P_{\mathrm{FA}} + P_{\mathrm{M}}$. 55
5.5 ToA algorithm tested on measured signal at location 2 and 3 with thresholds set by criterion B.2. The vertical scale is in millivolts. Vertical line in each plot show the ToA of the direct path signal based on true measured range, assuming the presence of a clear LoS. The threshold θ_δ was set at 102.8 ns with $\alpha_{\mathrm{M}} = 0.001$ and the values of θ_ρ were (a) 0.060 and (b) 0.056. Notice that the ToA of the signal was defined as the center of the pulse. (See figure 3.1) 57
5.6 ToA algorithm tested on measured signal at location 4 and 5 with thresholds set by criterion B.2. Vertical line in each plot show the ToA of the direct path signal based on true measured range, assuming the presence of a clear LoS. The threshold θ_δ was set at 102.8 ns with $\alpha_{\mathrm{M}} = 0.001$ and the values of θ_ρ were (a) 0.038 and (b) 0.060. Notice that the ToA of the signal was defined as the center of the pulse. (See figure 3.1) 58

5.7 ToA algorithm tested on measured signal at location 6 and 7 with thresholds set by criterion B.2. Vertical line in each plot show the ToA of the direct path signal based on true measured range, assuming the presence of a clear LoS. The threshold θ_δ was set at 102.8 ns with $\alpha_{\mathrm{M}} = 0.001$ and the values of θ_ρ were (a) 0.034 and (b) 0.020. Notice that the ToA of the signal was defined as the center of the pulse. (See figure 3.1) 59
5.8 ToA algorithm tested on measured signal at location 8 and 9 with thresholds set by criterion B.2. Vertical line in each plot show the ToA of the direct path signal based on true measured range, assuming the presence of a clear LoS. The threshold θ_δ was set at 102.8 ns with $\alpha_{\mathrm{M}} = 0.001$ and the values of θ_ρ were (a) 0.030 and (b) 0.050. Notice that the ToA of the signal was defined as the center of the pulse. (See figure 3.1) 60
5.9 ToA algorithm tested on measured signal at location 10 and 11 with thresholds set by criterion B.2. Vertical line in each plot show the ToA of the direct path signal based on true measured range, assuming the presence of a clear LoS. The threshold θ_δ was set at 102.8 ns with $\alpha_{\mathrm{M}} = 0.001$ and the values of θ_ρ were (a) 0.082 and (b) 0.102. Notice that the ToA of the signal was defined as the center of the pulse. (See figure 3.1) 61
5.10 ToA algorithm tested on measured signal at location 12 and 13 with thresholds set by criterion B.2. Vertical line in each plot show the ToA of the direct path signal based on true measured range, assuming the presence of a clear LoS. The threshold θ_δ was set at 102.8 ns with $\alpha_{\mathrm{M}} = 0.001$ and the values of θ_ρ were (a) 0.112 and (b) 0.154. Notice that the ToA of the signal was defined as the center of the pulse. (See figure 3.1) 62
5.11 ToA algorithm tested on measured signal at location 14 and 15 with thresholds set by criterion B.2. Vertical line in each plot show the ToA of the direct path signal based on true measured range, assuming the presence of a clear LoS. The threshold θ_δ was set at 102.8 ns with $\alpha_{\mathrm{M}} = 0.001$ and the values of θ_ρ were (a) 0.152 and (b) 0.184. Notice that the ToA of the signal was defined as the center of the pulse. (See figure 3.1) 63
5.12 ToA algorithm tested on measured signal at location 16 and 17 with thresholds set by criterion B.2. Vertical line in each plot show the ToA of the direct path signal based on true measured range, assuming the presence of a clear LoS. The threshold θ_δ was set at 102.8 ns with $\alpha_{\mathrm{M}} = 0.001$ and the values of θ_ρ were (a) 0.288 and (b) 0.458. Notice that the ToA of the signal was defined as the center of the pulse. (See figure 3.1) 64

5.13 Range estimation errors (estimated range - measured range) incurred in the test using threshold setting criterion B.2. The numbers are the index of measurement positions. 65

6.1 Receiver schematic of UWB ranging system. 67
6.2 Evaluation of the signal round-trip time using 2-way ranging technique. 74

7.1 Search for the earliest arrival of the signal using uniform sampling. Search is performed in a positive direction along the time axis. 78
7.2 Reconstruction of signal using MMSE estimation based on two samples. Solid curve indicates the reconstructed signal and the dotted line shows the error deviation. 80
7.3 Transmission and reception of signal in UWB scanning receiver system link. The channel function $h_{\mathrm{b}}(t)$ can be approximated using the measured antenna system function. 81
7.4 Spectral density of $p(t)$ and $u(t)$. The template signal $u(t)$ was modeled using $s(t)$ shown in figure 3.1 84
7.5 Plots of (a) $S'_{\mathrm{w}}(f)$ and (b) $R'_{\mathrm{w}}(\tau)$. $S'_{\mathrm{w}}(f)$ is evaluated by (7.7). 85
7.6 Evaluation of error variance in MMSE estimation based on 2 samples. Error variance decreases with sampling rate. 86
7.7 Evaluation of error variance in MMSE estimation based on different number of samples. Sampling rate was fixed at 2GHz and it was assumed that estimation was done with given number of closest samples. 87

A.1 Evaluation of level crossing probability. λ denotes the time between successive down-crossing and up-crossing and ζ is the first occurrence time. 95

B.1 UWB ambiguity function of a single pulse. 106
B.2 UWB ambiguity function of a periodic train of 64 pulses. The pulse repetition rate is 10 Mpps. 107
B.3 UWB ambiguity function of 64 time hopped pulses with $N_{\mathrm{h}} = 16$, $T_{\mathrm{f}} = 100$ ns, and $T_{\mathrm{c}} = 2$ ns. 108
B.4 UWB ambiguity function of 64 time hopped pulses with $N_{\mathrm{h}} = 32$, $T_{\mathrm{f}} = 100$ ns, and $T_{\mathrm{c}} = 2$ ns. 109

Abstract

Ultra-wideband (UWB) radio, a new carrierless communication scheme using impulses, is a candidate technology for future communication and ranging applications. Recent progress on both in the technical and regulatory side of this technology has made this possible. The fine time resolution and material penetration capability of UWB signals has created a vision of novel ranging and positioning applications to augment existing narrowband systems operating in dense multipath environments.

In this thesis, a time-of-arrival (ToA) based ranging scheme using an UWB radio link is proposed. This ranging scheme, based on maximum likelihood estimation, implements a search algorithm for the detection of the direct path signal in the presence of dense multipath. Models for critical parameters in the algorithm are based on statistical analysis of propagation data, and the algorithm is tested on another independent set of propagation measurements. The proposed UWB ranging system uses a correlator and a parallel sampler with a high speed measurement capability in each transceiver to accomplish two-way ranging between them in the absence of a common clock. The UWB ambiguity function illustrates the effects of time offset and scaling factor (or clock offset) on the receiver's correlator output.

Chapter 1

Introduction

1.1 Motivation

According to the Defense Advanced Research Projects Agency's definition, ultra-wideband (UWB) radio is a communication system which utilizes a signal whose 3 dB bandwidth is greater than 25% of its center frequency. Typical UWB radios communicate with sub-nanosecond wide pulses without a carrier. The radar community has been using similar pulse signals for ground-penetration radars for many years. The reason why a communication scheme using narrow pulse signals has been proposed is because of their novel properties which possess advantages over conventional narrow-band or wide-band signals. First, range resolution is extremely fine, which provides a good potential for the applications in ranging and positioning. The radar range resolution Δr is defined as

$$\Delta r = \frac{c}{2B}, \tag{1.1}$$

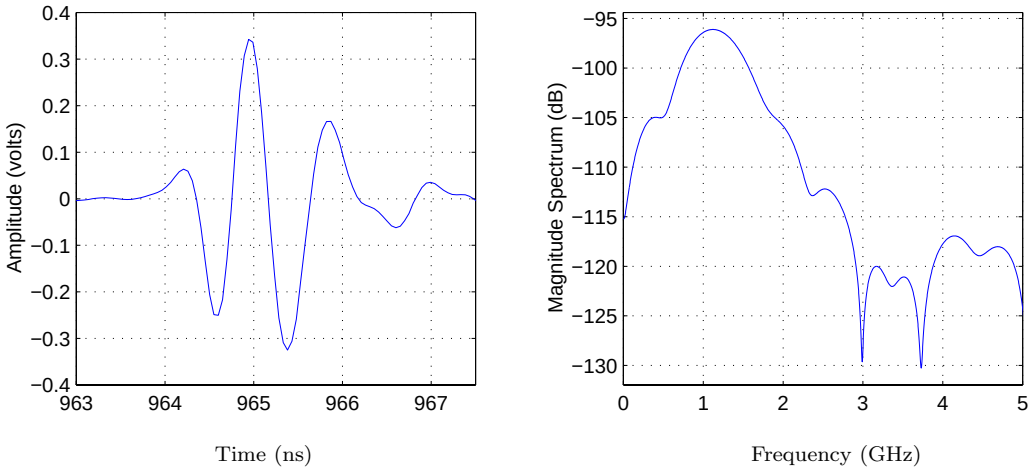

(a) (b)

Figure 1.1: (a) Front-end of the received signal which was transmitted with a clear line of sight and (b) its magnitude spectrum

where B is the bandwidth of the signal and c is the speed of light. The inverse proportionality to the bandwidth makes the inherent range resolution of UWB signals 100 to 1000 times finer than that of narrow-band signals [16]. Secondly, UWB signal supplies that bandwidth at a lower center frequency, which is advantageous for penetration of materials and for operation in shadowed environments. Resolvable multipath and the penetration capability enable a vision of potential UWB radio applications in complex multipath environments, including indoor wireless local area network (LAN). Furthermore, the absence of a sinusoidal carrier may allow a simpler radio architecture because no intermediate frequency (IF) stage is necessary.

Figure 1.1 shows (a) the front-end of a typical received signal which was transmitted with a clear line of sight (LoS) and (b) its magnitude spectrum. The 3 dB

bandwidth of the signal is approximately 753 MHz. Due to the fact that UWB radios operate in a portion of the radio spectrum which is already occupied by existing radio systems, the risk of interfering with other systems has been an important issue ever since UWB communication systems were proposed. Especially important is the protection of systems which use low-power signals related to public safety, e.g., Global Positioning System (GPS) L-band signals. The Federal Communications Commission (FCC) issued a proposed rule making (NPRM) on May, 2000, and approved a UWB radio regulation in February, 2002, limiting UWB power spectral densities, and forcing applications to frequencies above 3.1 GHz. The ranging techniques developed in this thesis, with data taken at frequencies just below 3.1 GHz, are applicable to systems in this somewhat higher frequency range.

1.2 Existing Location Systems

There has been a growing need for wireless systems that provide accurate position location. For example, a robust positioning using mobile stations (MS) which satisfy FCC's requirements for Enhanced 911 [35, 34, 1, 9, 23, 4], is one of the hottest topics in radio location. Indoor positioning to track personnel or assets in laboratories, warehouses, and hospitals is becoming more popular [25]. Applications of wireless positioning for search-and-rescue operations by military commanders and fire-fighters have become important because of increasing interest in security services.

One of the most successful classic ground-based navigation systems is Loran (Long Range Area Navigation); Loran-C was developed for civilian use and Loran-D for military purposes. A Loran-C system uses a series of pulsed 100 kHz signals [36, 27]. Use of the signal reflected from the ionosphere, namely sky wave, as well as ground wave propagation, extends the range of coverage up to 2,500 miles. A Line of sight (LoS) propagation path is not required by Loran-C, however its accuracy is strongly affected by the poor geometry of the environment. Accuracy of ground wave navigation is approximately 1,500 feet [20].

GPS (Global Positioning System) is currently the most widely used positioning system. It was originally developed for military purposes but now has useful commercial uses, even with reduced accuracy. Selective availability (SA), which is an intentional degradation of GPS positioning accuracy introduced for non-military users by US Department of Defense (DOD), has recently been removed. According to a 24 hour test result performed by the Federal Geodetic Data Committee (FGDC), the 95% probable horizontal accuracy without SA is better than 6.3 meter (www.ngs.noaa.gov). However, GPS requires LoS for location estimation to its full capability, which limits its utility in shadowed environments.

Since the FCC's E-911 mandate, considerable effort has been made to improve the accuracy of geo-positioning using mobile stations (MS). The FCC adopted standards for Phase II location accuracy of 50 meters for handset-based solutions and 100 meters for network-based solutions for 67% of calls. Several mobile station location

techniques have been proposed and typical systems incorporate time of arrival (ToA) and/or angle or arrival (AoA) information. Recently, a network-aided GPS approach also has been considered.

1.3 Problems

There exist many different elements which may cause errors in range estimation. Corruption of ToA measurement by noise and interference is one of them. However, one of the most significant obstacles in accurate ranging and positioning is the non-line of sight (NLoS) problem, which occurs in shadowed environments where a signal that propagated with a clear LoS may not be available. This is a major limiting factor in location using GPS in urban areas or indoors. For mobile location, this problem has been recognized as a "killer issue" [32, 3]. Several different NLoS error mitigation techniques recently have been proposed for MS location [42, 13, 41]. These utilize statistical information on the scale of NLoS errors to estimate location. However, the accuracy of these techniques is not good enough due to the large variance of the errors.

A novel aspect of UWB ranging is the capability to detect the direct path signal accurately using the fine time resolution of an UWB signal. However, it is still a complicated problem because of a number of unknown spatial variables which make the characterization of UWB signal propagation difficult. The algorithm for ToA estimation of the direct path signal proposed herein is related to multipath resolution

techniques. Time delay estimation problems have been studied and several different techniques proposed, including Maximum likelihood (ML), MUSIC, and ESPRIT [21, 43, 10, 29]. Li et al. [18] formulated the time delay estimation problem as a nonlinear least squares fitting problem in the frequency domain. For UWB systems, Win and Scholtz [38] developed ML detector and Cramer at al. [7, 6, 5] used the CLEAN algorithm to develop a UWB channel model involving angle of arrival (AoA) as well as ToA. In this dissertation a simple ranging algorithm based on generalized maximum likelihood (GML) estimation is introduced and modifications to the algorithm made to determine the ToA of the direct path signal [16, 15] . It is known that GML estimation provides a sub-optimal solution for time delay estimation. Utilizing GML estimation, we can avoid a computationally complex process to remove all nuisance parameters, which is necessary if they are modeled as random variables. By doing this, the estimation errors caused by potentially large variances of nuisance parameters can also be avoided.

Part of the work proposed herein is related to Time Domain, Inc., who has a senior level partnership with Integrated Media Systmes Center at University of Southern California. The UWB scanning receiver system which was introduced by Withington et al. [40] at Time Domain serves as a baseline for the design of the UWB ranging system posed in chapter 6, while the ToA measurement algorithm described in chapter 3 was developed independently by the author.

1.4 Overview

Following this chapter, a set of indoor propagation tests is introduced in chapter 2. The propagation measurement data with range calibration to an accuracy of a few inches will give insight into the problems inherent in the detection of the direct-path signal. Antenna system function measurement using a network analyzer and measurements to identify interference from other radiators are also introduced. In chapter 3, a ToA measurement algorithm using GML estimation for detection of the direct path signal is developed. Chapter 4 models statistically the critical parameters incorporated in the ranging algorithm introduced in chapter 3. Probabilistic analysis of different kinds of ToA errors provides a way of determining the thresholds used in the ranging algorithm, as well as estimating the algorithm's performance. In chapter 5, different kinds of threshold setting techniques are presented and the ToA algorithm is tested on the set of propagation data introduced in chapter 2. A schematic design of UWB ranging system with a high speed measurement capability is presented in chapter 6. The two-way ranging scheme used in this system is based on a remote synchronization technique [19] employed in satellite systems. Modification of ToA algorithms for application for existing UWB scanning receiver technology and related sampling issues are also discussed in chapter 7. Appendix C discusses a maximum a posteriori (MAP) estimation approach for the direct path signal detection. Due to unavailability of a proven UWB channel model, a simple two-path model is used to develop the estimator.

Chapter 2

UWB Indoor Propagation Measurement

2.1 Review of the Measurement

One of the scenarios in which an UWB ranging system has advantages over conventional narrowband systems is a dense multipath environment, e.g. indoor propagation. A set of propagation measurements was conducted in an indoor environment to verify the applicability of UWB signals for ranging. This propagation data was used to test ToA measurement algorithm introduced in chapter 3.

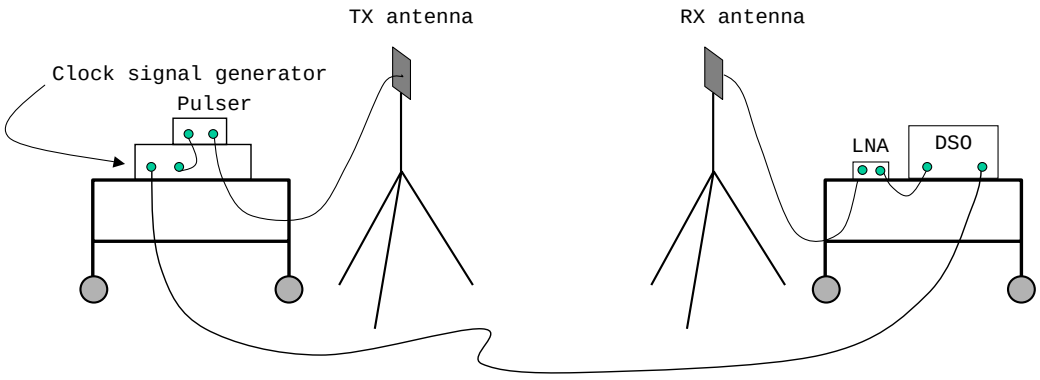

Figure 2.1: Experimental setup for propagation test.

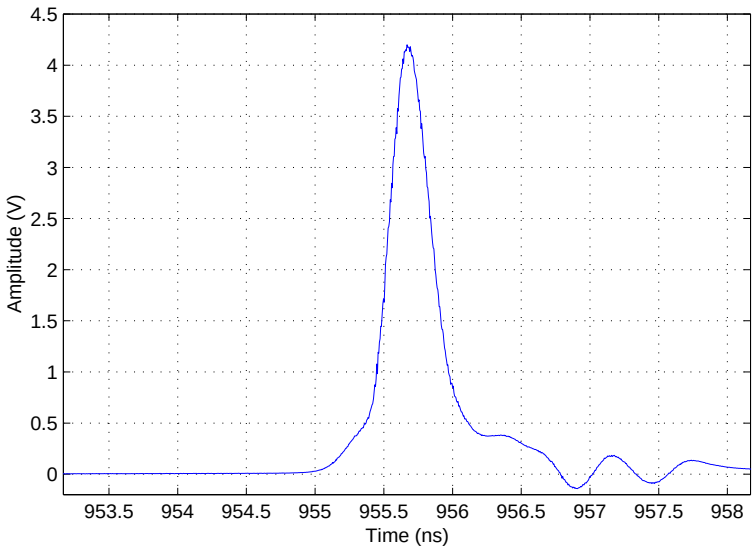

Figure 2.2: Output of Avtech pulser.

Figrue 2.1 shows the experimental setup of the measurement. The transmitter employs a pulser and a clock signal generator to generate a periodic train of UWB pulses. The pulser, made by Avtech Electrosystems Ltd. (AVP-1-P-DSRCA1), and generates pulses with a sub-nanosecond width when triggered by an input from the regular frame clock. Figure 2.2 is the plot of the pulser output. The 3 dB width of the pulse is less than a half nanosecond. Pulses were transmitted with one microsecond spacing which is large enough relative to the temporal profile of the received signal that successive received signals do not overlap. The transmitter and receiver antennas were vertically polarized diamond dipoles [30], approximately 5 feet above the floor. The received signal was measured with a digital sampling scope (HP54750A). At the receiver front-end, a low-noise amplifier (JCA04-239) with 28 dB gain was employed to amplify the received signal. Sampled waveforms were averaged 512 times to acquire a higher signal-to-noise ratio (SNR). The clock

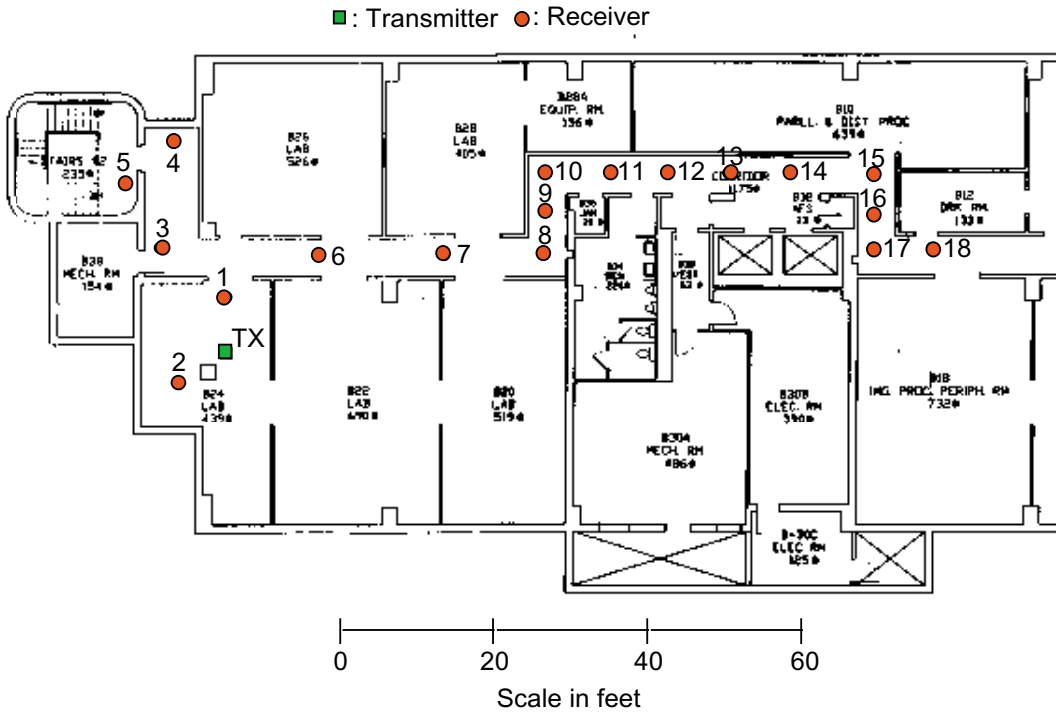

Figure 2.3: Basement floor plan of the building where the experiments were conducted. Interior walls are metal stud and dry wall construction. Circular marks stand for the locations of the receiving antenna and the rectangular mark indicates the transmitting antenna's location.

signal which triggerd the pulser was also used to trigger the sampling scope. In each measurement, two consecutive sampled waveforms with a time span of 200 ns were concatenated to provide a 400 ns measurement time span, assuming that the channel is stationary.

The experiments were conducted in the basement of Electrical Engineering Department building at University of Southern California, where different laboratories are located. Compared to higher floors of the building, the basement is more quiet since the interference from the outside of the building is relatively well blocked. The walls in the building are made of cinder blocks or wood. In the Ultra-Wideband Radio Laboratory (UltraLab) where the transmitter is located, there were computers and various test equipments. Figure 2.3 is the floor plan of the building where the measurements were taken. Signals were measured at 18 different locations while the transmitter was fixed in the UltraLab. The measurements were taken with ranges up to 93 feet and the distance at each location was surveyed using 2 feet $\times$ 2 feet grid structure, assuming the perpendicularity. The errors in the range measurements are supposed to be in the order of a few inches. At location 1, the signal was measured with a visually clear line-of-sight (LoS) and used to calibrate the arrival time of the direct path signal. The other 17 signals were measured with a blocked LoS. In these measurements, signals propagated through one or multiple walls. At location 16, 17, and 18, the LoS path was completely blocked by an elevator (a metallic structure), so the direct path signal could not be measured while multipath could be observed.

Figure 2.4 shows the samples of signals taken at location 1, 5, 7, 10, 13, and 16, respectively. Vertical scales are millivolts. We can observe that the quality and the temporal profile of the signal is varied with range and the geometry of the environment. Figure 2.5 shows the same set of signals shown in figure 2.4 with a finer time scale. Notice that all signals shown in this figure except the first one, which was measured with a clear LoS, have stronger multipath components than the direct path signal. In these cases, if a ranging system synchronizes with the strongest signal component for the purpose of range estimation, a large-scale error will occur. The presence of reflected signals that are stronger than the direct path signal makes ranging to the full capabilities of ultra-wideband signals challenging.

2.2 Measurement of Antenna System Function

UWB signal propagations are critically affected by the characteristic of the antenna system. The pulse used in the propagation measurement is reshaped by an filtering actions of antennas. Let's define the antenna system $H_{\mathrm{a}}(f)$ as the transfer function from the input of the transmitter antenna to the output of the receiver antenna. Then $H_a(f)$ can be expressed by

$$H_{\mathrm{a}}(f) = H_{\mathrm{t}}(f)H_{\mathrm{ch}}(f)H_{\mathrm{r}}(f), \tag{2.1}$$

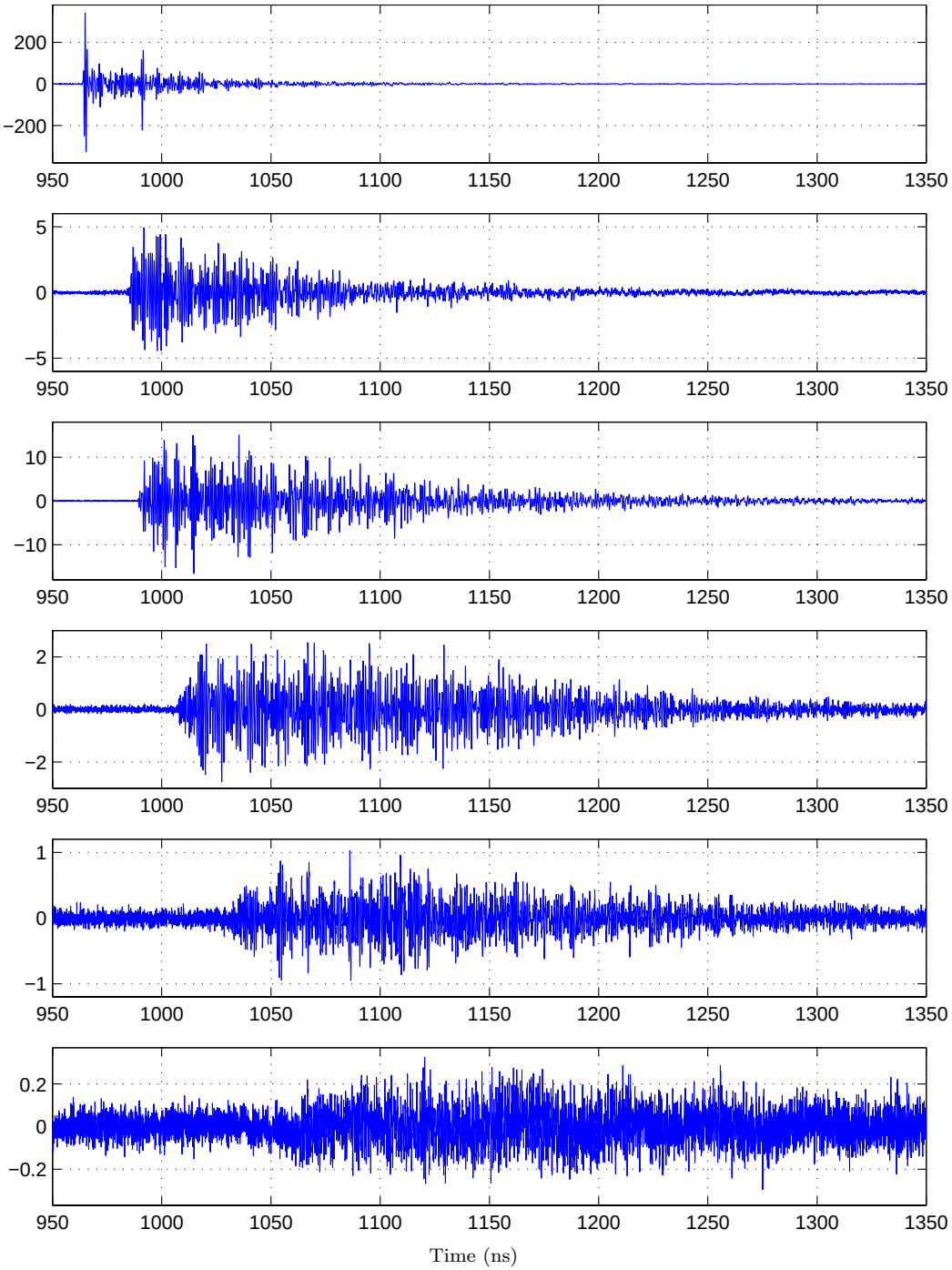

Figure 2.4: Measured signals at location 1, 5, 7, 10, 13, and 16. The vertical axis indicates signal strength in millivolts. The vertical scales of each plot are different, indicating differences in channel attenuation. The signal shown in the first plot was measured with a clear LoS and the others were measured in the presence of LoS blockages.

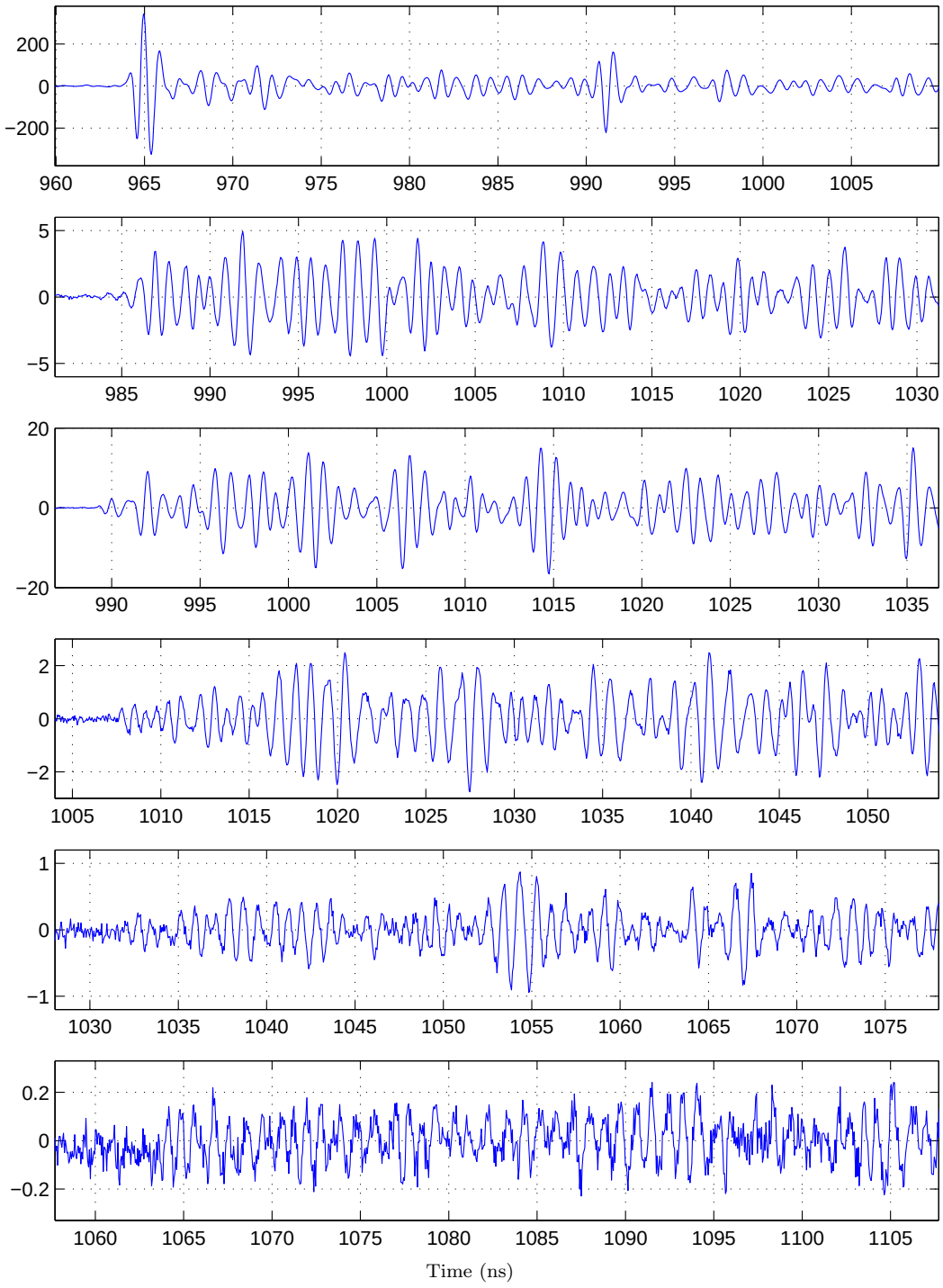

Figure 2.5: Initial portions of signals measured at location 1, 5, 7, 10, 13, and 16. Notice the existence of stronger multipath components.

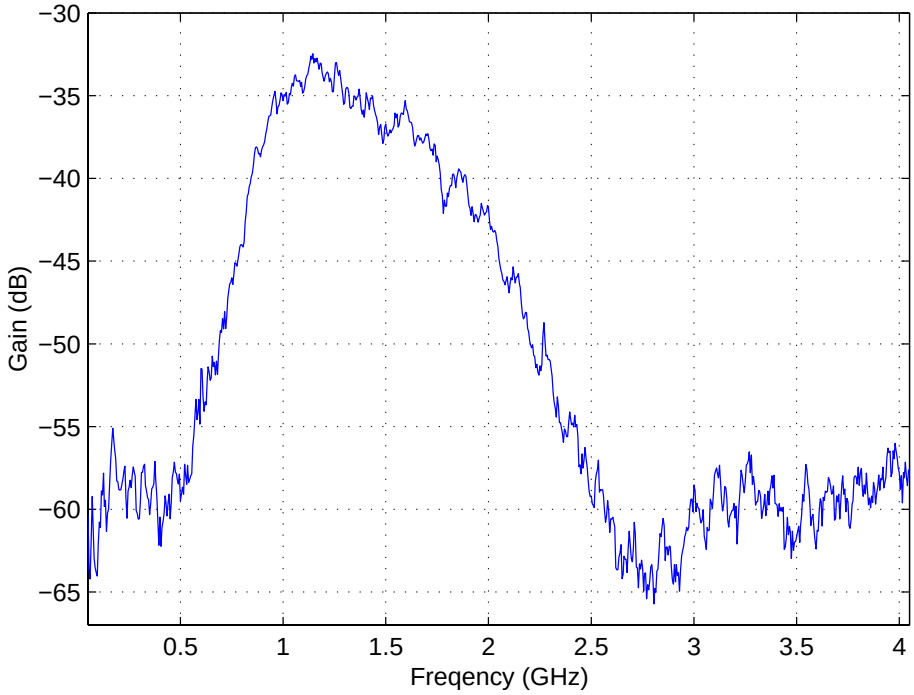

Figure 2.6: An average of 32 traces of $|H_{\mathrm{a}}(f)|^2$. Distance between the two antennas were 1m and the relative orientation between them were kept the same.

where $H_{\mathrm{t}}(f)$ is the transmitting transfer function from the antenna terminal to the electric field reference point near the transmitting antenna. The channel transfer function $H_{\mathrm{ch}}(f)$ is the transfer function from the reference point near the transmitting antenna to the other reference point near the receiving antenna, and $H_{\mathrm{r}}(f)$ denotes the receiving transfer function. Figure 2.6 shows an averaged trace of $|H_{\mathrm{a}}(f)|^2$ which was measured using a network analyzer. The transmitter and receiver antennas were hooked up to port 1 and port 2 of network analyzer, respectively and S_{21} parameter of this antenna system was measured. To compensate the effect of multipath, traces were taken at 32 different locations in the laboratory and hallway and then averaged. The relative orientation between two antennas were kept the same by fixing them on two ends of a piece of PVC pipe with 1m length. Based on this trace, 95%-bandwidth of the antenna system is approximated to be 1.18GHz (from 820MHz to 2GHz). The antenna system function will change depending on the channel, however this measurement gives an intuition on the approximate pass-band of the system.

2.3 Sources of Interference to UWB System

Since the UWB receivers operate over a very wide bandwidth, various external radiators in this bandwidth can affect the UWB receiver [31]. As an effort to identify these potential interferers, a frequency domain measurement using a spectrum analyzer was conducted in a common office environment. An UWB antenna used in

the propagation test described in this chapter was installed in an office on the fifth floor of Electrical Engineering building. The antenna was located approximately 10 feet away from the window of the office which is facing north. The resolution bandwidth of the spectrum analyzer was 300 kHz and the measured noise floor of the equipment was -94.5dBm. Figure 2.9 shows the measurement result. Notice that the power of lower-frequency interferences is significant considering the fact that they are out of the main pass-band of the antenna. Total interference power measured in this measurement is approximately

$$I_{100\%} = -33.5 \text{ dBm}, \tag{2.2}$$

where $I_{\text{a}\%}$ denotes the interference power with a% bandwidth usage. If we assume the receiver front-end is band-pass filtered to the frequency range between 780 MHz and 2.05 GHz, which corresponds to 97% usage of antenna system bandwidth, the interference power is reduced to

$$I_{97\%} = -40.9 \text{ dBm}. \tag{2.3}$$

If the frequency range of the potential band-pass filter is between 960 MHz and 1.93 GHz, the interference power is estimated to be

$$I_{86\%} = -60 \text{ dBm}. \tag{2.4}$$

Different types of filters with different pass band can be used to suppress the major interference signals without severely distorting the UWB signal. Figure 2.10 compares the outputs of two different ideal filters with passbands of 780 MHz through 2.05 GHz and 960 MHz through 1.93 GHz, respectively. Waveforms at the filter output were simulated using a measured signal assuming the characteristics of the bandpass filters are ideal. As mentioned above, employment of these filters at the receiver frontend would reduces the interference power by 7.4 dB and 26.5 dB, respectively, however, the received signals are not distorted seriously.

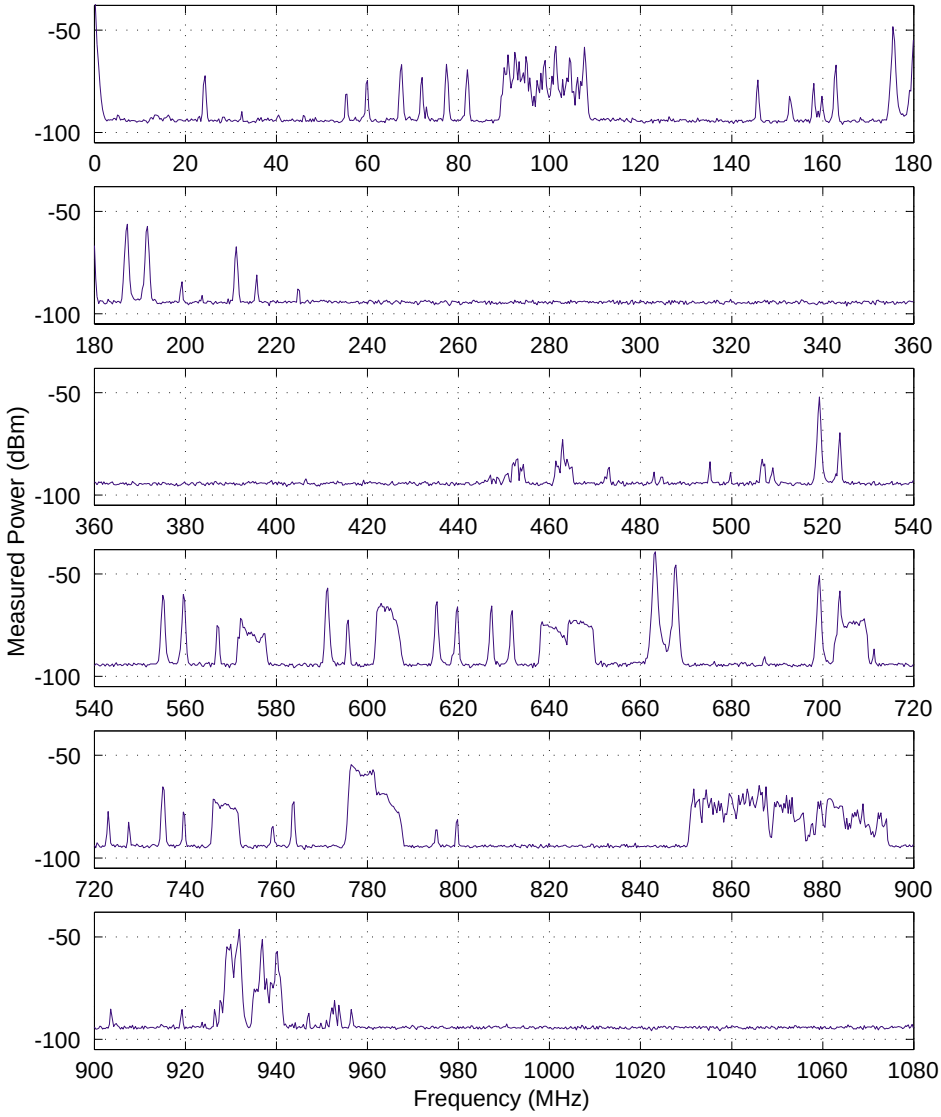

Figure 2.7: Measurement of interference signals using spectrum analyzer. The resolution bandwidth of the spectrum analyzer was 300 kHz and noise floor of the equipment was -94.5 dBm.

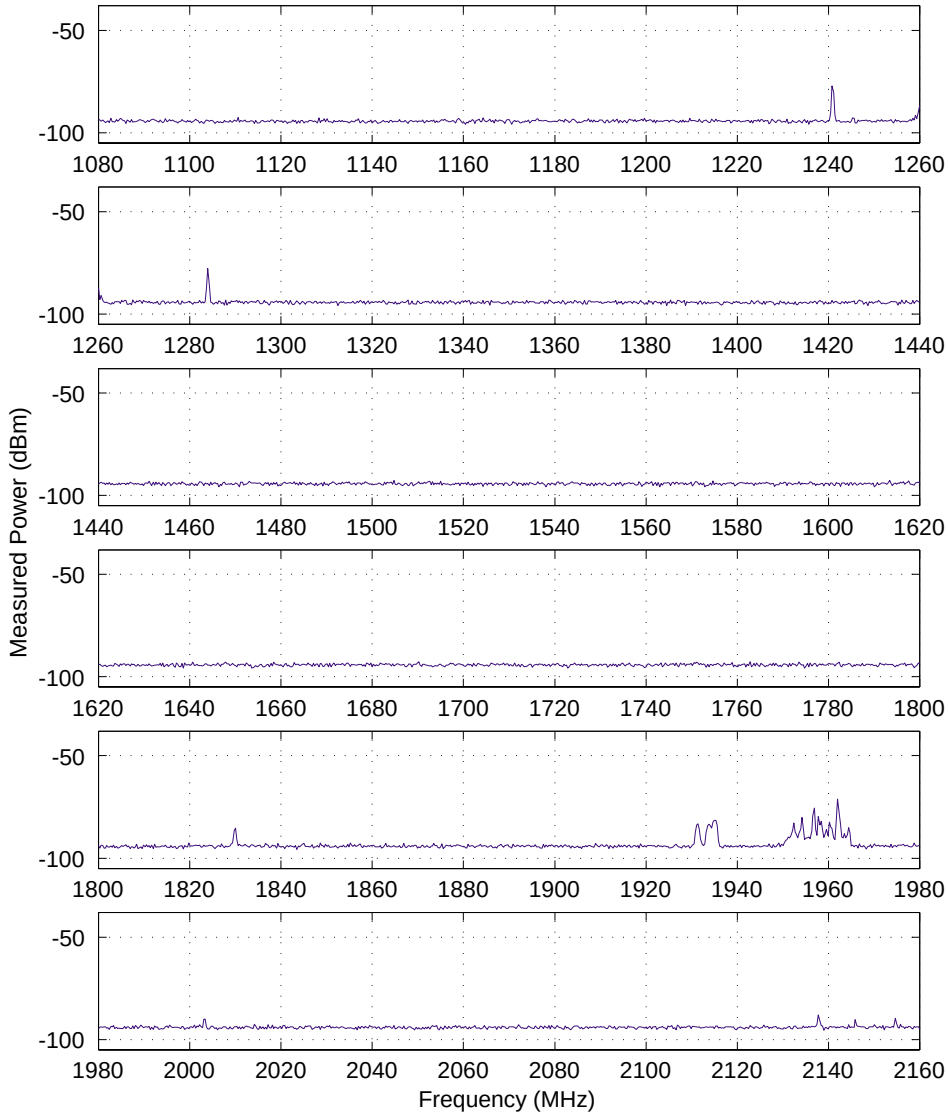

Figure 2.8: Interfering signals in the frequency band from 1.08 Hz to 2.16 GHz. The resolution bandwidth of the spectrum analyzer was 300 kHz and noise floor of the equipment was -94.5 dBm.

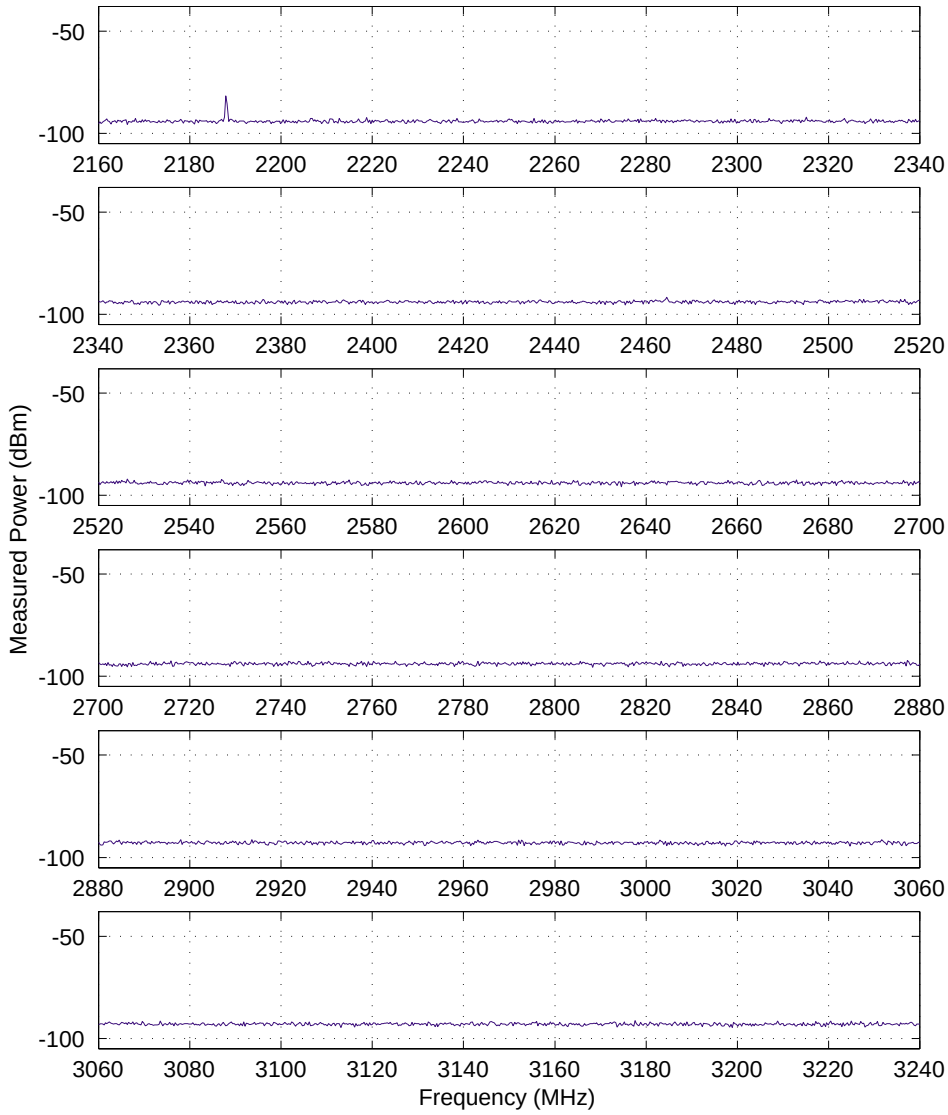

Figure 2.9: Interfering signals in the frequency band from 2.16 Hz to 3.24 GHz. No significant signal but noise floor of the equipment was observed.

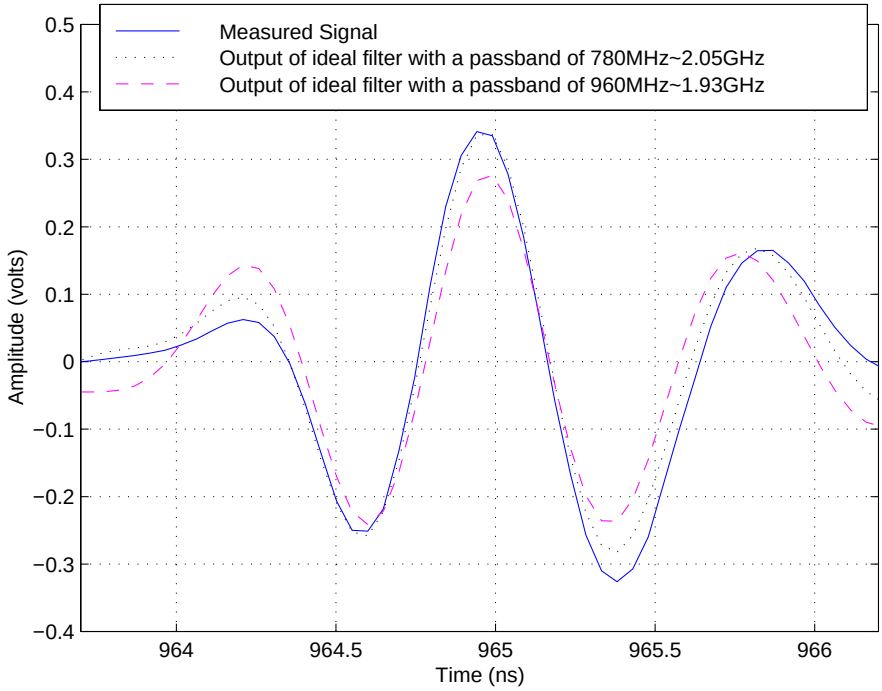

Figure 2.10: Outputs of two ideal bandpass filters whose passbands are 780 MHz - 2.05 GHz and 960 MHz - 1.93 GHz, respectively. The waveform in solid line is the initial portion of a signal measured with a clear LoS.

Chapter 3

ToA Measurement Algorithm for Detection of the Direct Path Signal

3.1 Introduction

Common techniques which have been employed by geo-location systems include time of arrival (ToA), time difference of arrival (TDoA), angle of arrival (AoA), and signal strength measurement. The ranging scheme proposed herein is a time based technique and uses the information of ToA of the direct path signal for range estimation. The direct path is defined as the straight-line path from transmitter to receiver. When the direct path is in fact a viable propagation path, ToA estimation of the direct path signal is useful for ranging. It is not guaranteed that the direct path signal always arrives the earliest even though it does in most cases. For example, suppose the line of sight (LoS) path is blocked by a material with a very high dielectric constant such as a water container, then the there may exist multipath component that arrives earlier than the direct path signal since the direct path

signal suffers a considerable propagation delay. Sometimes the direct path signal is completely blocked by a metallic structure, so that it cannot be observed. In this dissertation, we assume that the direct path signal is the earliest arrival at the receiver. So the estimation technique introduced here is a ToA estiamtion algorithm for the earliest arrival.

3.2 Signal Representation

When a single pulse is transmitted, the received signal can be modeled as a sum of the direct path signal, reflected signals, noise, and interference [38]. Actually, each multipath signal will suffer distortion as well as attenuation depending on the path along which it propagates, however, for the purpose of algorithm design, we assume the signal shape of each multipath component is preserved. Based on this model, the received signal $r_{\mathrm{m}}(t)$ can be represented by

$$r_{\mathrm{m}}(t) = a_{\mathrm{d}} s(t - \tau_{\mathrm{d}}) + \sum_{n=1}^{L} a_n s(t - \tau_n) + n_{\mathrm{m}}(t), \tag{3.1}$$

where $\tau_{\mathrm{d}} < \tau_1 < \tau_2 < \cdots < \tau_L$. The parameters τ_{d} and a_{d} are the arrival time and strength of the direct path signal, respectively, and τ_n and a_n are those of the n^{th} reflected signal component. The waveform $s(t)$ denotes the the canonical single-path signal, used as a correlator template, with a width of T_{p} seconds. The number of multipath signals L is unknown *a priori*. The noise $n_{\mathrm{m}}(t)$ is assumed

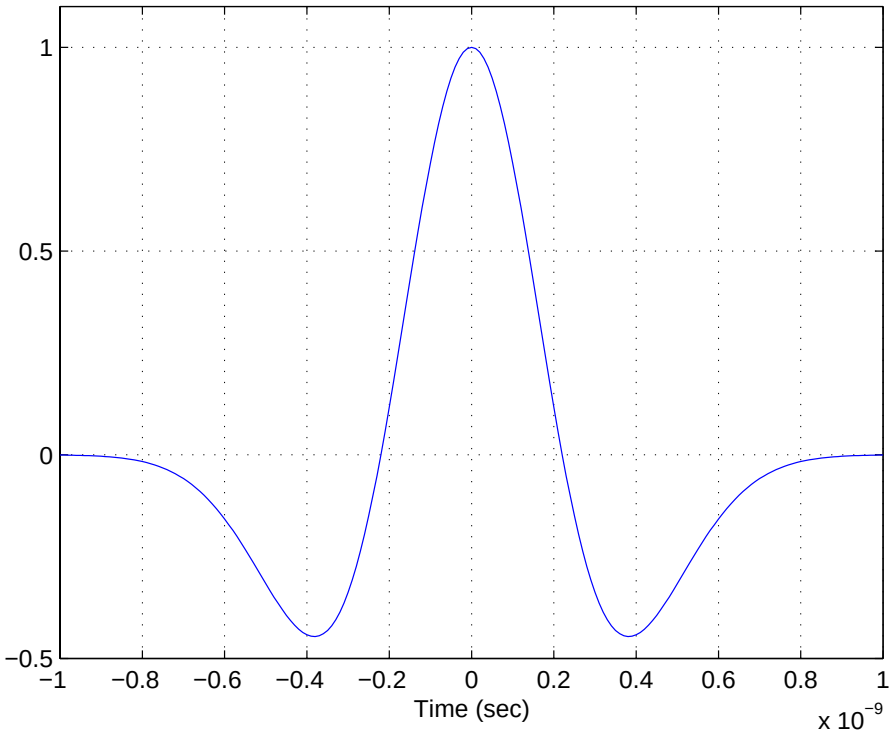

Figure 3.1: Model for the template signal $s(t)$.

to be additive white Gaussian, and interference is assumed to be zero. In this dissertation, the template signal $s(t)$ is modeled as a second derivative of gaussian [37] and represented by

$$s(t) = \Big[1 - 4\pi(t/\tau_m)^2\Big] \exp\Big[-2\pi(t/\tau_m)^2\Big], \tag{3.2}$$

where $\tau_m = 0.781 \times 10^{-9}$.

Figure 3.1 shows the model used for the $s(t)$. Let τ_{peak} and a_{peak} be the arrival time and amplitude of the strongest path and assume these have been determined by

correlation. Then $r_{\rm s}(t)$, a normalized and shifted version of $r_{\rm m}(t)$, can be represented by

$$\begin{aligned} r_{\rm s}(t) &= \frac{1}{|a_{\rm peak}|} r_{\rm m}(t+\tau_{\rm peak}) && (3.3)\\ &= \rho_{\rm d} s(t+\delta) + \sum_{n}^{L} \alpha_n s(t+\beta_n) + n_{\rm s}(t), && (3.4)\\ &= \rho_{\rm d} s(t+\delta) + \sum_{\beta_n \geq 0} \alpha_n s(t+\beta_n) + \sum_{\beta_n < 0} \alpha_n s(t+\beta_n) + n_{\rm s}(t), && (3.5) \end{aligned}$$

where

$$\begin{cases} \delta &= \tau_{\rm peak} - \tau_{\rm d}, \quad \delta \geq 0, \\ \rho_{\rm d} &= a_{\rm d}/|a_{\rm peak}|, \quad 0 < \rho_{\rm d} \leq 1, \\ \beta_n &= \tau_{\rm peak} - \tau_n, \quad \delta > \beta_1 > \beta_2 > \cdots > \beta_L \\ \alpha_n &= a_n/|a_{\rm peak}|, \quad 0 < \alpha_n \leq 1, \ \forall n \leq L. \end{cases} \tag{3.6}$$

The noise $n_{\rm s}(t)$ being a time-shifted version of $n_{\rm m}(t)$, is a white Gaussian noise signal. The third term in (3.5) represents the multipath components which arrive later than the peak path. To simplify the problem, let's restrict our observation to the portion of the signal prior to and including the arrival of the strongest path by truncating $r_{\rm s}(t)$. Let's define $r(t)$, a truncated version of $r_{\rm s}(t)$, as

$$\begin{aligned} r(t) &= r_{\rm s}(t), \ t \leq \frac{T_{\rm p}}{2} && (3.7)\\ &= \rho_{\rm d} s(t+\delta) + \sum_{\beta_k \geq 0} \alpha_k s(t+\beta_k) + n(t), \ t \leq \frac{T_{\rm p}}{2} && (3.8) \end{aligned}$$

$$= \quad \rho_{\mathrm{d}} s(t+\delta) + \sum_{k=1}^{M} \alpha_k s(t+\beta_k) + n(t), \ t \leq \frac{T_{\mathrm{p}}}{2}, \tag{3.9}$$

where $\beta_M = 0$ and $\alpha_M = \pm 1$. The noise $n(t)$ is given by

$$n(t) = \frac{n_{\mathrm{s}}(t)}{|a_{\mathrm{peak}}|}, \tag{3.10}$$

and M denotes the number of signal components that arrived earlier than the peak component. If (and only if) M is equal to 0, then $\delta = 0$, $\rho_{\mathrm{d}} = \pm 1$, and the second term in (3.9) is ignored. The noise $n(t)$ is white Gaussian noise (truncated to the interval $(-\infty, T_{\mathrm{p}}/2)$), whose correlation function is represented by

$$R_{\mathrm{N}}(\tau) = \sigma_{\mathrm{a}}^2 \cdot \delta_{\mathrm{D}}(\tau), \tag{3.11}$$

where σ_{a} is the standard deviation of the noise $n(t)$. Assuming $r(t)$ is sampled, let's represent it as a vector of samples, namely,

$$\underline{r} \quad = \quad \rho_{\mathrm{d}} \underline{s}_{\delta} + \sum_{k=1}^{M} \alpha_k \underline{s}_{\beta_k} + \underline{n}, \tag{3.12}$$

where $\underline{s}_{\beta}$ represents the vector of samples of $s(t+\beta)$ with a same length as $\underline{r}$. The noise vector $\underline{n}$ is a white gaussian vector whose correlation matrix R_{N} is given by

$$R_{\mathrm{N}} = \sigma_{\mathrm{N}}^2 \cdot I, \tag{3.13}$$

where σ_{N} is the standard deviation of the noise and I is an identity matrix. In the next section, ToA estimation of the direct path signal using GML estimation is introduced.

3.3 ToA Algorithm Using GML Estimation

To estimate the ToA of the direct path signal, we have to estimate δ which appears in (3.12) based on the observation vector $\underline{r}$. Let's define $\underline{\alpha}^M$ and $\underline{\beta}^M$ as

$$\underline{\alpha}^M = (\alpha_1, \alpha_2, \cdots, \alpha_M), \tag{3.14}$$

$$\underline{\beta}^M = (\beta_1, \beta_2, \cdots, \beta_M). \tag{3.15}$$

Then ρ_{d}, M, $\underline{\alpha}^M$, and $\underline{\beta}^M$ are nuisance parameters and δ is the parameter to be estimated. Here, we employ maximum likelihood (GML) estimation. All unknown parameters are treated as deterministic and δ is estimated to be

$$\hat{\delta} = \arg\max_{\delta} \Big[\max_{\rho_{\mathrm{d}}, M, \underline{\alpha}, \underline{\beta}} f(\underline{r}|\delta, \rho_{\mathrm{d}}, M, \underline{\alpha}^M, \underline{\beta}^M) \Big]. \tag{3.16}$$

Because $\underline{n}$ is a white Gaussian vector and the unknown parameters are being treated as deterministic, maximum likelihood estimation is equivalent to least square estimation:

$$\hat{\delta} = \arg\min_{\delta} \Big[\min_{\rho_{\mathrm{d}}, M, \underline{\alpha}, \underline{\beta}} \|\underline{r} - \rho_{\mathrm{d}} \underline{s}_{\delta} - \sum_{k=1}^{M} \alpha_k \underline{s}_{\beta_k}\|^2 \Big]. \tag{3.17}$$

Using (3.17) to estimate δ is computation-intensive because $2(M+1)$ unknown parameters are involved. To reduce computational complexity, an iterative nonlinear programming technique is employed, by which the unknown parameters are estimated in a sequential manner [38]. Specifically, the arrival time of each component signal is estimated individually while all other parameters are fixed. Detection of each individual reflected pulse is done in the order of its strength. Even if this dynamic programming approach does not provide an optimal solution for (3.17), it is known to give a suboptimal solution.

Modification of the estimation criterion shown in (3.17) is done as follows. First, the duration of the search region for the time δ of arrival of the direct path signal is limited to prevent the probability of a false detection in the noise only portion of the observed signal from becoming too large. We define θ_δ as a limiting threshold on $\boldsymbol{\delta}$ so that the direct path signal is searched over the portion of $r(t)$ satisfying $t \geq -\theta_\delta$. Secondly, a stopping rule is used to terminate the search, because the value of the norm in (3.17) generally continues to decrease with increasing M. The stopping rule consists of applying a threshold on the relative path strength ρ_{d}. Detailed analysis on error probabilities which are functions of these thresholds are given in chapter 4. Let's define ρ as

$$\rho = |\rho_{\mathrm{d}}|. \tag{3.18}$$

Then the iterative search process stops when no more paths satisfying $\rho \geq \theta_\rho$ are detected in the search region, where θ_ρ is the threshold of ρ. Thirdly, we skip the estimation of some nuisance parameters by ignoring the multipath components that arrive later than already detected paths. By doing this, we can speed up the search process. Following is a brief description of the ToA algorithm:

1. Let $n = 1,\ \omega_1 = 0$, and $\mu_{11} = 1$.

2. Increase n by 1.

3. Find ω_n which satisfies

$$\omega_n = \arg \max_{\omega_{n-1}<\omega<\theta_\delta} (\underline{r} - \sum_{i=1}^{n-1} \mu_{(n-1)i} \underline{s}_{\omega_i})^{\mathrm{t}} \underline{s}_\omega, \tag{3.19}$$

4. Find $(\mu_{n1}, \mu_{n2}, \cdots, \mu_{nn})$ such that

$$(\mu_{n1}, \mu_{n2}, \cdots, \mu_{nn}) = \arg \min_{\mu'_1,\cdots,\mu'_n} \|\underline{r} - \sum_{i=1}^{n} \mu'_i \underline{s}_{\omega_i}\|^2. \tag{3.20}$$

5. If $|\mu_{nn}| \geq \theta_\rho$, go to step 2. Otherwise proceed to the next step.

6. δ is estimated as $\hat{\delta} = \omega_{n-1}$.

Once the location and the strength of the peak path is identified, maximum correlation is searched over the region with a pre-determined length (step 3) and

its path strength is estimated (step 4). If the estimated path strength satisfies the given criterion (step 5), this signal component is subtracted from the received signal. From the remainder of the signal, another maximum correlation is searched from the starting point of the search region up to the location of the path which was already detected (step 3). This process is iterated until there exist no more potential path whose strength is greater than a given threshold level. Figure 3.2 shows an example of the ToA estimation. In this example, the ToA of the direct path signal of signals measured at location 8 and 15 were estimated with various θ_ρ's while θ_δ was fixed at 100 ns. The dashed lines show the ToA of the direct path of each signal which was evaluated with the meausred distance assuming the presence of a clear LoS. The true arrival time is supposed to be greater than this value, since excessive propagation delay is involved in the propagation in the LoS blockage materials. In the ToA estimation of signal 15, large scaled false alarm errors occurred when θ_ρ is less than or equal to 0.1 due to its low SNR. The threshold setting techniques for the ToA algorithm is discussed in detail in chapter 5.

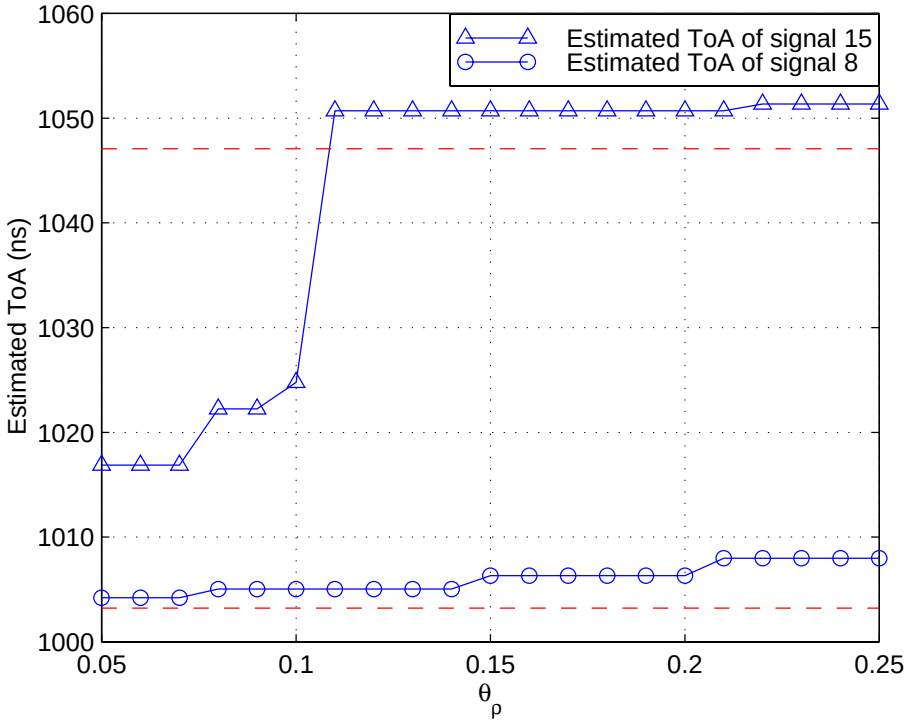

Figure 3.2: Estimated ToA's of signals measured at location 8 and 15. The threshold θ_δ was fixed at 100 ns and θ_ρ was varied. Dashed lines represent of ToA's of each signal evaluated with measured range assuming the presence of a clear LoS. Threshold setting techniques using different criteria are discussed in chapter 5.

Chapter 4

Error Analysis for ToA Algorithm

4.1 Statistical Modeling of Ranging Parameters

The thresholds, θ_δ and θ_ρ, which are used in the ToA algorithm need to be determined so that they satisfy a given performance criteria. This requires a probabilistic analysis for different kinds of error that may occur in the ToA estimation. The parameters $\boldsymbol{\delta}$ and $\boldsymbol{\rho}$ which were defined in 3.2 were modeled statistically for this purpose.

4.1.1 Modeling of Marginal Densities

A set of propagation data taken by Win [39] in an office building was used for this modeling. Figure 4.1 shows the floor plan of the building where measurements were taken. Data was taken in 14 different offices and a hallway. In each office, measurements were taken at 49 different locations which are arranged on 3 feet by 3 feet square grid. A detailed description of the experiment is given in [39]. Out of 720

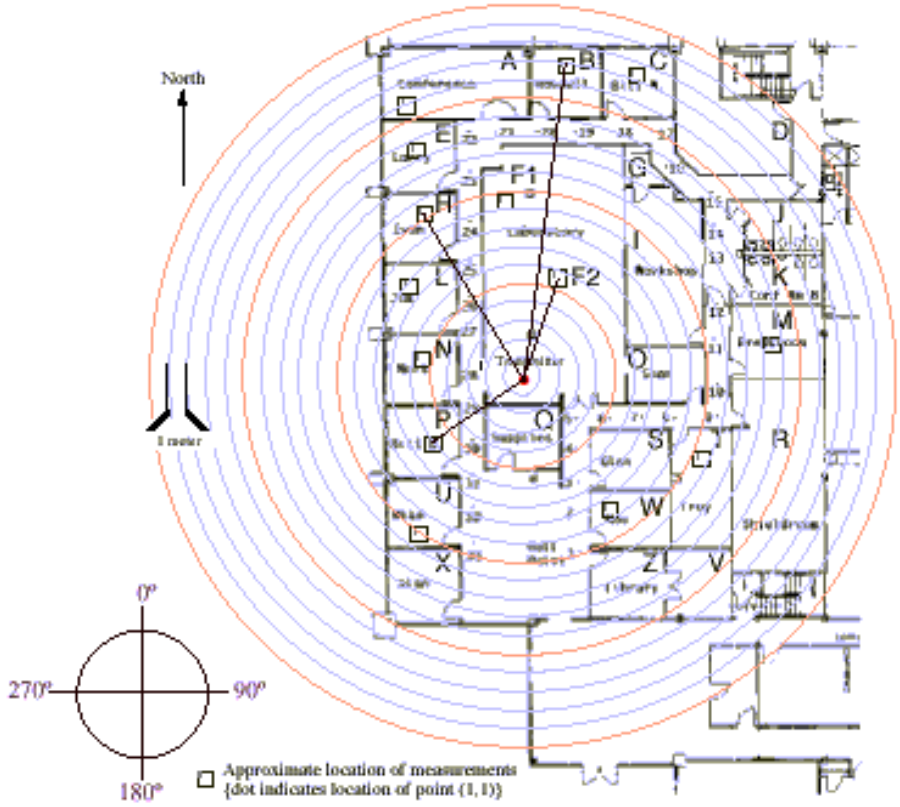

Figure 4.1: Floor plan of the building where the propagation data was taken.

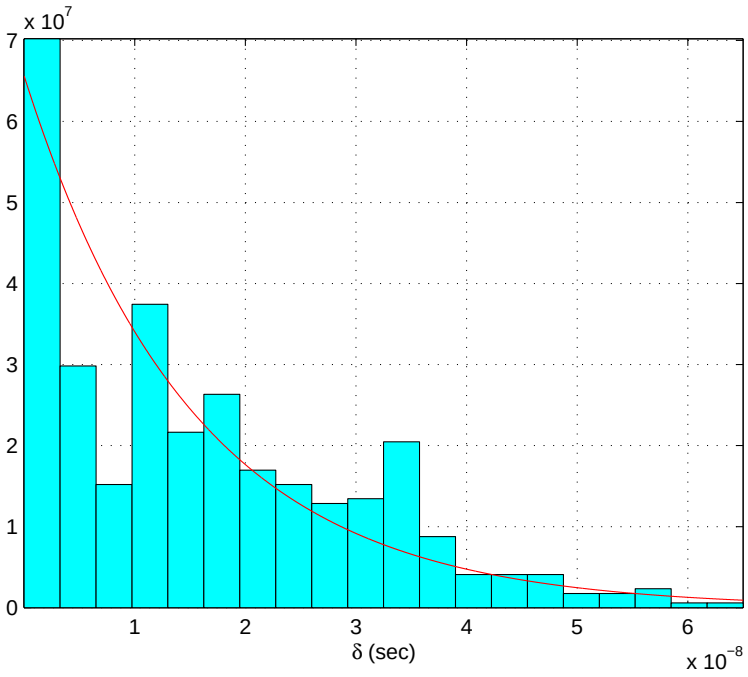

(a)

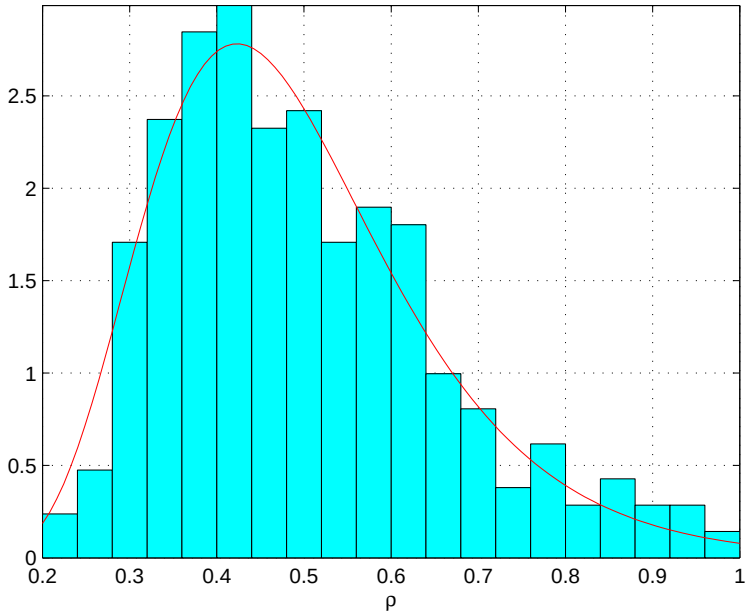

(b)

Figure 4.2: Normalized histograms of (a) $\boldsymbol{\delta}$ and (b) $\boldsymbol{\rho}$ and approximation of marginal densities using curve-fitting.

signals, 622 signals were measured with a blocked LoS and used in modeling. The values of δ's and ρ's for the 622 signals which were measured with a blocked LoS were extracted using the ToA algorithm. The values of θ_δ and θ_ρ used in this process were 70 ns and 0.2, respectively. Some large scale errors relative to the approximately known distance information were corrected by manually adjusting the thresholds. Due to the absence of information on the exact distance of each measurement, it was difficult to collect accurate values of δ. In 95 of 622 observed signals, the direct path signal was the strongest and the others had a stronger multipath component. So if we define P_0 as the probability that $\boldsymbol{\delta}$ is equal to 0 , it can be approximated by

$$P_0 = \Pr(\boldsymbol{\delta} = 0) = \Pr(\boldsymbol{\rho} = 1) = 0.1527. \tag{4.1}$$

Figure 4.2-(a) and (b) are histograms of $\boldsymbol{\delta}$ and $\boldsymbol{\rho}$ which were produced with 527 signals that have a stronger reflected path than the direct path. They were normalized so that their total area equals to one. By curve-fitting on this data, marginal densities of $\boldsymbol{\delta}$ and $\boldsymbol{\rho}$ can be modeled by

$$f_{\boldsymbol{\delta}}(\delta|\boldsymbol{\delta} \neq 0) = \frac{1}{\sigma_\delta} e^{-\delta/\sigma_\delta},\ \delta > 0, \tag{4.2}$$

$$f_{\boldsymbol{\rho}}(\rho|\boldsymbol{\rho} \neq 1) = \frac{1}{\sqrt{2\pi} Q(-\mu_\rho/\sigma_\rho)\sigma_\rho \rho} e^{-(\ln\rho - \mu_\rho)^2/2\sigma_\rho^2}, 0 < \rho < 1, \tag{4.3}$$

where $\sigma_\delta = 1.524 \times 10^{-8}$, $\sigma_\rho = 0.3220$, and $\mu_\rho = -0.7565$. The function $Q(x)$ is defined as

$$Q(x) = \int_{-\infty}^{x} \frac{1}{\sqrt{2\pi}} e^{-y^2/2} dy, \tag{4.4}$$

and $Q(-\mu_\rho/\sigma_\rho)$ appearing in (4.3) is for normalization. Values of σ_δ, σ_ρ, and μ_ρ were determined so that the least square fit is achieved.

4.1.2 Modeling of the Joint Density of (δ, ρ)

To perform error analysis for direct path detection, we need to know the joint density of $\boldsymbol{\rho}$ and $\boldsymbol{\delta}$. Independence between these two parameters was tested using chi-squared test [17, 11]. Chi-squared test uses the contingency data set of categorical variables. Figure 4.3 is the normalized histogram of ρ and δ. Frequency of events of pairs (δ, ρ) were counted corresponding to 11×11 subsections and normalized so that the total volume equals to 1. Let $N = \{n_{ij}\}_{1 \le i \le 11, 1 \le j \le 11}$ be the matrix containing the contents of contingency table of $\boldsymbol{\delta}$ and $\boldsymbol{\rho}$, where n_{ij} represents the frequency of events of pairs (δ, ρ) which belongs to the i^{th} and j^{th} interval of $\boldsymbol{\delta}$ and $\boldsymbol{\rho}$, respectively. Let $n_{i,*}$ and $n_{*,j}$ be i^{th} row sum and j^{th} column sum of matrix N, respectively. Then

$$n_{i,*} = \sum_{j=1}^{11} n_{ij} \tag{4.5}$$

$$n_{*,j} = \sum_{i=1}^{11} n_{ij}. \tag{4.6}$$

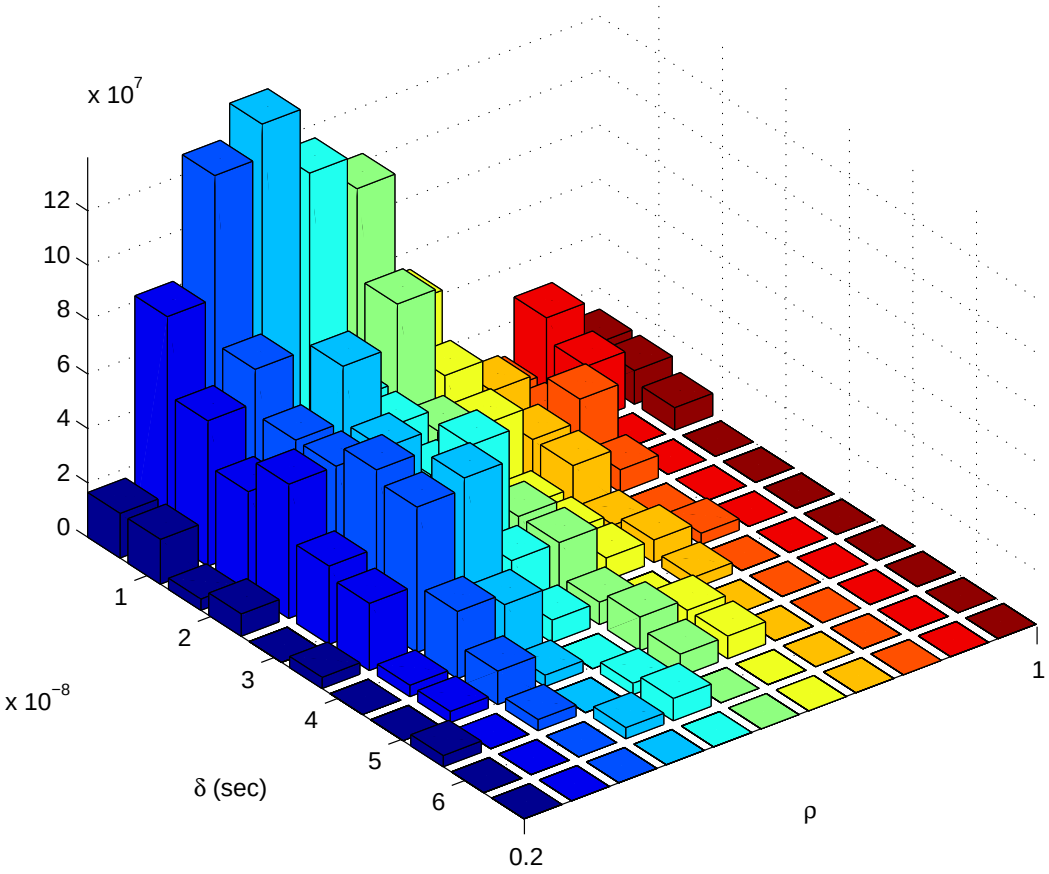

Figure 4.3: Histogram of $\boldsymbol{\rho}$ and $\boldsymbol{\delta}$. Total volume was normalized to 1.

Then, Pearson's statistic $\boldsymbol{\chi}^2$ with degrees of freedom of 10×10 is evaluated by

$$\boldsymbol{\chi}^2 = \sum_{i=1}^{11}\sum_{j=1}^{11} \frac{(n_{ij} - n_{i,*}/n_{\mathrm{tot}})^2}{n_{i,*} \cdot n_{*,j}/n_{\mathrm{tot}}}, \tag{4.7}$$

where n_{tot} is the total number of events,

$$n_{\mathrm{tot}} = \sum_{i=1}^{11}\sum_{j=1}^{11} n_{ij} = \sum_{i=1}^{11} n_{i,*} = \sum_{j=1}^{11} n_{*,j}. \tag{4.8}$$

Let's define H_{ind} as the hypothesis that $\boldsymbol{\delta}$ and $\boldsymbol{\rho}$ are independent. The test procedure consists of comparing Pearson's statistic $\boldsymbol{\chi}^2$ with the critical value c_α corresponding to the significance level α_{s}:

$$\begin{cases} \text{Accept hypothesis } H_{\mathrm{ind}}, & \text{if } \boldsymbol{\chi}^2 < c_\alpha \\ \text{Reject hypothesis } H_{\mathrm{ind}}, & \text{if } \boldsymbol{\chi}^2 \geq c_\alpha, \end{cases} \tag{4.9}$$

where c_α is determined such that

$$\int_0^{c_\alpha} g(x,n)dx = \alpha_{\mathrm{s}}, \tag{4.10}$$

where $g(x,n)$ is the chi-square density with n degrees of freedom, which is

$$g(x,n) = \frac{1}{2^{n/2}\Gamma(n/2)} x^{n/2-1} e^{-x/2}, \ x \geq 0, \tag{4.11}$$

where the gamma function $\Gamma(n)$ is defined as

$$\int_0^\infty y^{n-1}e^{-y}dy,\ y>0. \tag{4.12}$$

So the significance level α_{s} represents the area of the rejection region of the hypothesis test and the larger is α_{s}, the more strict is the hypothesis test. Pearson's statistic $\boldsymbol{\chi}^2$ evaluated using the contingency table is 117.2. Let the significance level α_{s} be 0.1. Then according to the $\boldsymbol{\chi}^2$ distribution, the critical value c_α corresponding to 0.1 significance level and 100 degrees of freedom is 118.5. So hypothesis H_{ind} is accepted with significance level of 10%. Considering the fact that the conventional value of significance level used for independence test is 5%, this result is fairly conservative. Based on the test result, we can model the joint probability density of $\boldsymbol{\delta}$ and $\boldsymbol{\rho}$ by the product of marginal densities:

$$\begin{aligned}
&f_{\boldsymbol{\delta\rho}}(\delta,\rho|\boldsymbol{\delta}\neq 0,\boldsymbol{\rho}\neq 1)\\
&\quad = f_{\boldsymbol{\delta}}(\delta|\boldsymbol{\delta}\neq 0)\cdot f_{\boldsymbol{\rho}}(\rho|\boldsymbol{\rho}\neq 1)\\
&\quad = \frac{1}{\sqrt{2\pi}Q(-\mu_\rho/\sigma_\rho)\sigma_\delta\sigma_\rho\rho}\exp\left\{-\left[\frac{\delta}{\sigma_\delta}+\frac{(\ln\rho-\mu_\rho)^2}{2\sigma_\rho^2}\right]\right\},
\end{aligned} \tag{4.13}$$

where $\delta>0$ and $0<\rho<1$. Figure 4.4 is the plot of this joint probability density function.

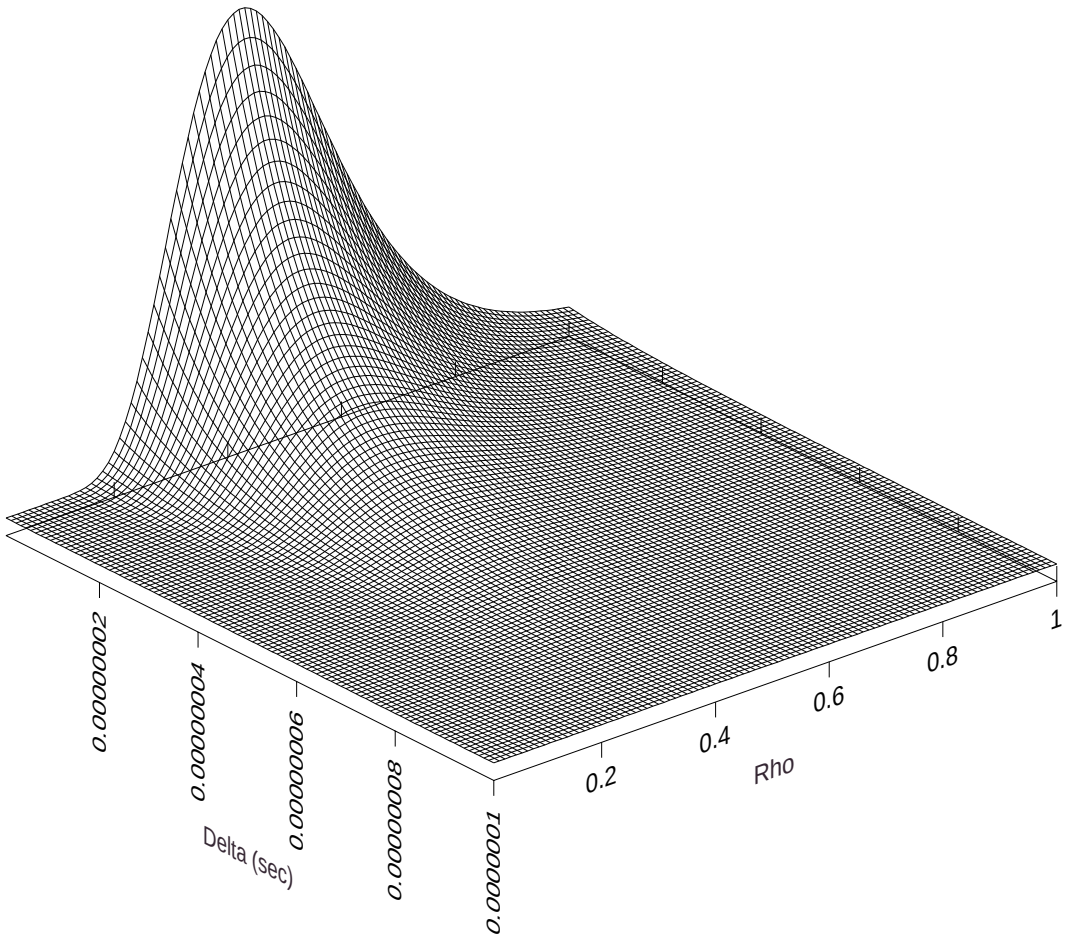

Figure 4.4: Joint probability density function of δ and ρ.

4.2 Error Analysis

Range estimation error can result from two major sources. One is ToA estimation error, and the other is any unknown propagation delay in a LoS blockage structure, which is difficult to estimate without a more thorough knowledge of the blockage. According to test results given in section 5.2, the excessive propagation delay in blockage material is considerable especially when the signal propagates through multiple walls. This can be a limiting factor in UWB ranging through materials. In this section, errors in ToA estimation of the direct path signal are analyzed probabilistically. Based on the error analysis, the thresholds used in ToA algorithm are determined.

We can classify ToA errors into two categories. One is early false alarms which occur when a false detection in the noise-only portion of the signal is regarded as that of direct path signal. Probability of early false alarm increases with increasing θ_δ and decreasing θ_ρ. The other is a missed direct-path error, which occurs when the actual direct path signal is missed and a multipath signal is falsely declared to be the direct path signal. Probability of a missed direct path error increases with decreasing θ_δ and increasing θ_ρ. A ranging error can also occur because of the mismatch between the template waveform and the received pulse waveform.

4.2.1 Probability of an Early False Alarm

An early false alarm probability P_{FA} can be expressed as

$$\begin{aligned} P_{\mathrm{FA}} &= \Pr\left\{ \sup_{\beta\in[-\theta_\delta,-\boldsymbol{\delta}-T_{\mathrm{p}})} \frac{|\underline{n}^t\underline{s}_\beta|}{\|\underline{s}_0\|^2} > \theta_\rho \text{ and } \boldsymbol{\delta} \le \theta_\delta - T_{\mathrm{p}} \right\} && (4.14) \\ &= \int_0^{\theta_\delta} \Pr\left\{ \sup_{\beta\in[-\theta_\delta,-\delta-T_{\mathrm{p}})} \frac{|\underline{n}^t\underline{s}_\beta|}{\|\underline{s}_0\|^2} > \theta_\rho \right\} f_{\boldsymbol{\delta}}(\delta|\boldsymbol{\delta}\neq 0)d\delta \cdot (1-P_0) \\ &\quad +\Pr\left\{ \sup_{\beta\in[-\theta_\delta,-T_{\mathrm{p}})} \frac{|\underline{n}^t\underline{s}_\beta|}{\|\underline{s}_0\|^2} > \theta_\rho \right\} \cdot P_0 && (4.15) \\ &= \int_0^{\theta_\delta} \Pr\left\{ \sup_{\beta\in[-\theta_\delta,-\delta-T_{\mathrm{p}})} \frac{|\underline{w}^t\underline{s}_\beta|}{\|\underline{s}_0\|^2} > \frac{\theta_\rho}{\sigma_{\mathrm{N}}} \right\} f_{\boldsymbol{\delta}}(\delta|\boldsymbol{\delta}\neq 0)d\delta \cdot (1-P_0) \\ &\quad +\Pr\left\{ \sup_{\beta\in[-\theta_\delta,-T_{\mathrm{p}})} \frac{|\underline{w}^t\underline{s}_\beta|}{\|\underline{s}_0\|^2} > \frac{\theta_\rho}{\sigma_{\mathrm{N}}} \right\} \cdot P_0 && (4.16) \end{aligned}$$

where

$$\underline{w} = \frac{1}{\sigma_{\mathrm{N}}}\underline{n}. \tag{4.17}$$

Let's define the peak SNR as the ratio of the peak signal power to the noise power. This can be expressed as

$$\mathrm{SNR}_{\mathrm{p}} = \frac{1}{\sigma_{\mathrm{N}}^2}, \tag{4.18}$$

because the signal was normalized to its peak strength. Substituting (4.18) into (4.16),

$$\begin{aligned} P_{\mathrm{FA}} &= \int_0^{\theta_\delta} \Pr\left\{ \sup_{\beta\in[-\theta_\delta,-\delta-T_{\mathrm{p}})} \frac{|\underline{w}^t\underline{s}_\beta|}{\|\underline{s}_0\|^2} > \theta_\rho\sqrt{\mathrm{SNR}_{\mathrm{p}}} \right\} \cdot f_{\boldsymbol{\delta}}(\delta|\boldsymbol{\delta}\neq 0)d\delta \cdot (1-P_0) \\ &\quad +\Pr\left\{ \sup_{\beta\in[-\theta_\delta,-T_{\mathrm{p}})} \frac{|\underline{w}^t\underline{s}_\beta|}{\|\underline{s}_0\|^2} > \theta_\rho\sqrt{\mathrm{SNR}_{\mathrm{p}}} \right\} \cdot P_0 && (4.19) \end{aligned}$$

Let's define γ and a random process $\boldsymbol{u}(\beta)$ as

$$\gamma = \theta_\rho \cdot \sqrt{\mathrm{SNR_p}}, \tag{4.20}$$

$$\boldsymbol{u}(\beta) = \frac{|\underline{w}^t \underline{s}_\beta|}{\|\underline{s}_0\|^2}. \tag{4.21}$$

Substituting (4.20) and (4.21) into (4.19),

$$P_{\mathrm{FA}} = \int_0^{\theta_\delta} \Pr\left\{ \sup_{\beta \in [-\theta_\delta, -\delta - T_\mathrm{p})} \boldsymbol{u}(\beta) > \gamma \right\} f_{\boldsymbol{\delta}}(\delta | \boldsymbol{\delta} \neq 0) d\delta \cdot (1 - P_0) + \Pr\left\{ \sup_{\beta \in [-\theta_\delta, -T_\mathrm{p})} \boldsymbol{u}(\beta) > \gamma \right\} \cdot P_0. \tag{4.22}$$

$\Pr\{ \sup_{\beta \in [-\theta_\delta, -\delta - T_\mathrm{p})} \boldsymbol{u}(\beta) > \gamma \}$ can be modeled as a high level crossing probability of a random process $\boldsymbol{u}(\beta)$ at a level γ in a given time period $[-\theta_\delta, -\delta - T_\mathrm{p})$. This probability can be approximated by

$$\Pr\left\{ \sup_{\beta \in [-\theta_\delta, -\delta - T_\mathrm{p})} \boldsymbol{u}(\beta) > \gamma \right\} \approx 1 - e^{-(\theta_\delta - \delta - T_\mathrm{p})/E(\boldsymbol{\lambda})}, \tag{4.23}$$

where $\boldsymbol{\lambda}$ represents the time between a down-crossing and the next adjacent up-crossing at a given level γ. Detailed computation of the level crossing probability is given in appendix A. In (4.23), we need the expected value of $\boldsymbol{\lambda}$ to evaluate the level crossing probability. The expected value of $\boldsymbol{\lambda}$ was simulated using a computer generated white Gaussian vector. The white gaussian vector was correlated with the template signal and the value of $\boldsymbol{\lambda}$ for a given γ was observed over 100 occurrences

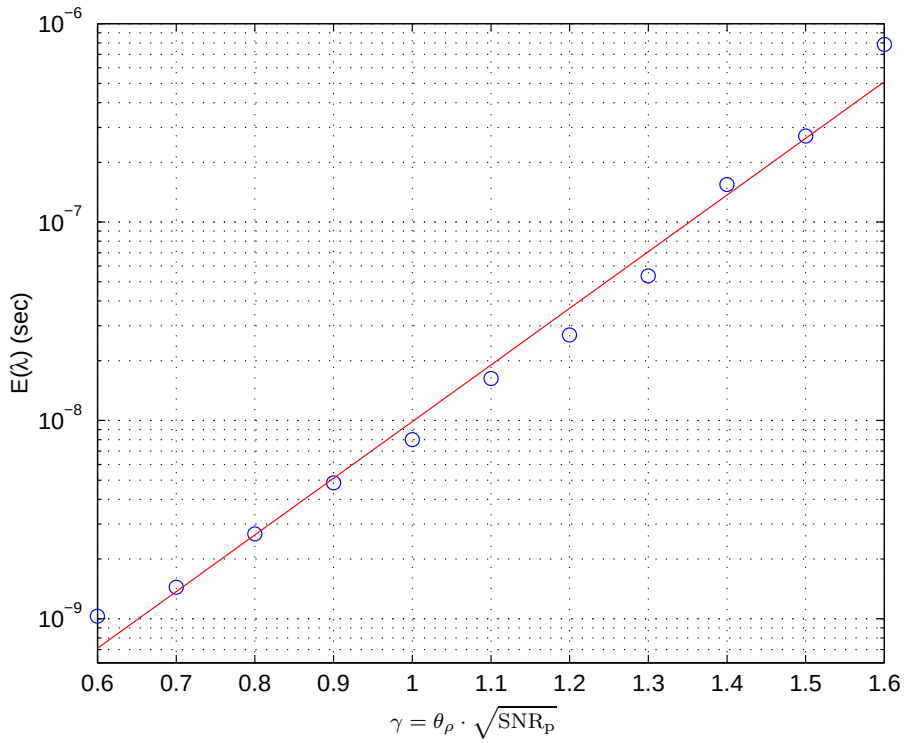

Figure 4.5: Simulation result of $E(\boldsymbol{\lambda})$. $\boldsymbol{u}(\beta)$ was simulated and $\boldsymbol{\lambda}$ for a given γ was observed over 100 occurrences and averaged.

and averaged. Figure 4.5 shows the simulated values of $\boldsymbol{\lambda}$ in log scale. By curve-fitting on the simulation result, $E(\boldsymbol{\lambda})$ can be modeled by

$$E(\boldsymbol{\lambda}) = C \cdot e^{B\gamma}, \tag{4.24}$$

where $B = 6.5757$ and $C = 1.375 \times 10^{-11}$. The constants B and C depend on the structure of the template signal and the signal model defined in (3.2) was used in this simulation. Substituting (4.24) into (4.23),

$$\Pr\left\{\sup_{\beta\in[-\theta_\delta,-\delta-T_\mathrm{p})} \boldsymbol{u}(\beta) > \gamma\right\} = 1 - \exp\left[-\frac{(\theta_\delta - \delta - T_\mathrm{p})}{C} e^{-B\gamma}\right]. \tag{4.25}$$

Substituting (4.2) and (4.25) into (4.22), we get

$$P_{\mathrm{FA}} = 1 - (1 - P_0)\frac{\sigma_\delta e^{-(\theta_\delta - T_{\mathrm{p}})/\sigma_\delta}}{\sigma_\delta - Ce^{B\gamma}} - \frac{P_0\sigma_\delta - Ce^{B\gamma}}{\sigma_\delta - Ce^{B\gamma}} \exp\left[-\frac{(\theta_\delta - T_{\mathrm{p}})}{C} e^{-B\gamma} \right]. \quad (4.26)$$

Substituting (4.20) into (4.26),

$$\begin{aligned} P_{\mathrm{FA}} = 1 - (1 - P_0)&\frac{\sigma_\delta e^{-(\theta_\delta - T_{\mathrm{p}})/\sigma_\delta}}{\sigma_\delta - Ce^{B\theta_\rho\sqrt{\mathrm{SNR_p}}}} \\ &- \frac{P_0\sigma_\delta - Ce^{B\theta_\rho\sqrt{\mathrm{SNR_p}}}}{\sigma_\delta - Ce^{B\theta_\rho\sqrt{\mathrm{SNR_p}}}} \exp\left[-\frac{(\theta_\delta - T_{\mathrm{p}})}{C} e^{-B\theta_\rho\sqrt{\mathrm{SNR_p}}} \right]. \end{aligned} \quad (4.27)$$

4.2.2 Probability of a Missed Direct Path Error

The probability P_{M} of a missed-direct-path error can be evaluated by computing

$$\begin{aligned} P_{\mathrm{M}} &= \Pr(\boldsymbol{\delta} > \theta_\delta \text{ or } \boldsymbol{\rho} < \theta_\rho) \\ &= 1 - \Pr(0 \le \boldsymbol{\delta} \le \theta_\delta \text{ and } \theta_\rho \le \boldsymbol{\rho} \le 1) \\ &= 1 - P_0 - (1 - P_0)\int_{\theta_\rho}^{1}\int_{0}^{\theta_\delta} f_{\boldsymbol{\delta\rho}}(\delta, \rho | \boldsymbol{\delta} \neq 0) d\delta d\rho. \end{aligned} \quad (4.28)$$

Substituting (4.13) into (4.28),

$$P_{\mathrm{M}} = (1 - P_0)\left[1 - (1 - e^{-\theta_\delta/\sigma_\delta})\left(1 - \frac{Q(\frac{\ln\theta_\rho - \mu_\rho}{\sigma_\rho})}{Q(\frac{-\mu_\rho}{\sigma_\rho})} \right) \right]. \quad (4.29)$$

Probabilities of an (a) early false alarm and (b) a missed direct path with a peak SNR of 18 dB are plotted over θ_δ and θ_ρ in figure 4.6.

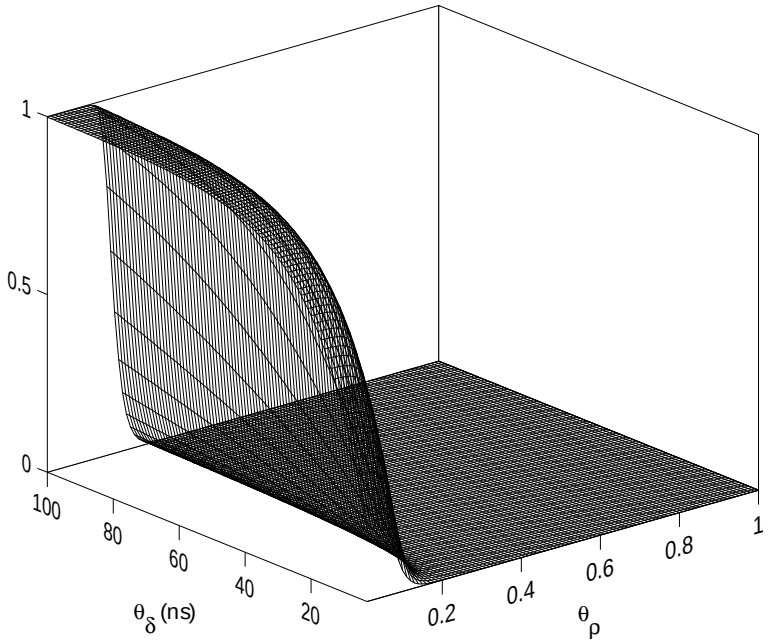

(a)

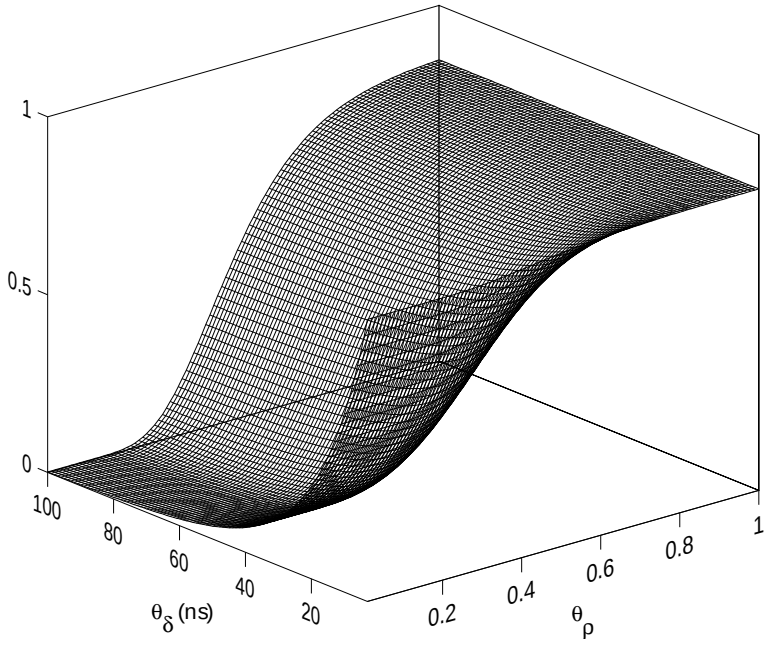

(b)

Figure 4.6: Plot of (a) P_{FA} and (b) P_{M} with a peak SNR of 18 dB.

Chapter 5

Threshold Setting and Test for the ToA Algorithm

5.1 Threshold Setting Criteria

The thresholds, θ_δ and θ_ρ, which are used in the ToA algorithm have to be determined so that they meet the performance criteria. Two kinds of criteria for threshold setting are introduced in this section: (1) early false alarm criterion and (2) the minimum probability of error criterion. The early false alarm criterion determines the thresholds so that the probability of a missed direct path error (P_{M}) is minimized with a given early false alarm setting (α_{F}). The false alarm setting is a conventional method used in radar detection [26, 2] and is also similar to the Neyman-Pearson criterion which is used in hypothesis testing. By the minimum probability of error criterion, which is a special case of Bayes criterion, θ_δ and θ_ρ are determined so that total probability of error ($P_{\mathrm{M}} + P_{\mathrm{FA}}$) is minimized. We can apply these threshold setting criteria in two different ways; First, we can apply the early false alarm criterion (or the minimum probability of error criterion) for the calculation of both

θ_δ and θ_ρ. Second, it is also possible to use these criteria only for setting θ_ρ, while θ_δ is determined so that $\Pr(\boldsymbol{\delta} > \theta_\delta)$ is equal to a given level (α_{M}). The following summarizes four different threshold setting criteria mentioned above:

A. Early false alarm criterion

- Criterion A.1
  - Set θ_δ and θ_ρ so that P_{M} is minimized under the constraint that $P_{\mathrm{FA}} = \alpha_{\mathrm{F}}$.
- Criterion A.2
  - Set θ_δ so that it satisfies $\Pr(\boldsymbol{\delta} > \theta_\delta) = \alpha_{\mathrm{M}}$.
  - Set θ_ρ so that it satisfies $P_{\mathrm{FA}} = \alpha_{\mathrm{FA}}$.

B. Minimum probability of error criterion

- Criterion B.1
  - Set θ_δ and θ_ρ so that $P_{\mathrm{FA}} + P_{\mathrm{M}}$ is minimized.
- Criterion B.2
  - Set θ_δ so that it satisfies $\Pr(\boldsymbol{\delta} > \theta_\delta) = \alpha_{\mathrm{M}}$.
  - Set θ_ρ so that $P_{\mathrm{FA}} + P_{\mathrm{M}}$ is minimized.

Figure 5.1 shows the optimum thresholds based on criterion A.1. Each curve shows the collection of $(\theta_\delta, \theta_\rho)$'s which satisfy the early false alarm setting, $\alpha_{\mathrm{F}} = 0.005$, with a given peak SNR. The circular mark on each curve represents the

thresholds which minimize P_M. According to criterion A.2, θ_δ is determined by solving the following equation:

$$(1 - P_0) \int_{\theta_\delta}^{\infty} f_{\boldsymbol{\delta}}(\delta | \boldsymbol{\delta} \neq 0) d\delta = \alpha_{\mathrm{M}}. \tag{5.1}$$

Substituting (4.2) into (5.1), θ_δ is given by

$$\theta_\delta = \sigma_\delta \ln \frac{1 - P_0}{\alpha_{\mathrm{M}}}, \tag{5.2}$$

and the θ_δ that satisfies the early false alarm setting is evaluated from (4.27). Notice that using criterion A.2, θ_ρ is evaluated independently of PDF of $\boldsymbol{\rho}$, which means the threshold on the signal strength can be set at a fixed level above the noise even before scaling the signal by $\dfrac{1}{|a_{\mathrm{peak}}|}$.

Figure 5.3 shows the optimum thresholds set by criterion B.1. Each circular mark is the $(\theta_\delta, theta_\rho)$ pair which minimizes the total probability of error, $P_{\mathrm{FA}} + P_{\mathrm{FA}}$, for a given peak SNR. Using criterion B.2, θ_δ is set in a manner similar to criterion A.2., which is given by (5.2). Threshold θ_ρ is set so that $P_{\mathrm{FA}} + P_{\mathrm{FA}}$ is minimized for the given θ_δ. Figure 5.4 is a plot of P_{M} vs. P_{FA} with $\alpha_{\mathrm{M}} = 0.001$ and the circular mark on each curve represents the thresholds that satisfy the minimum probability of error criterion.

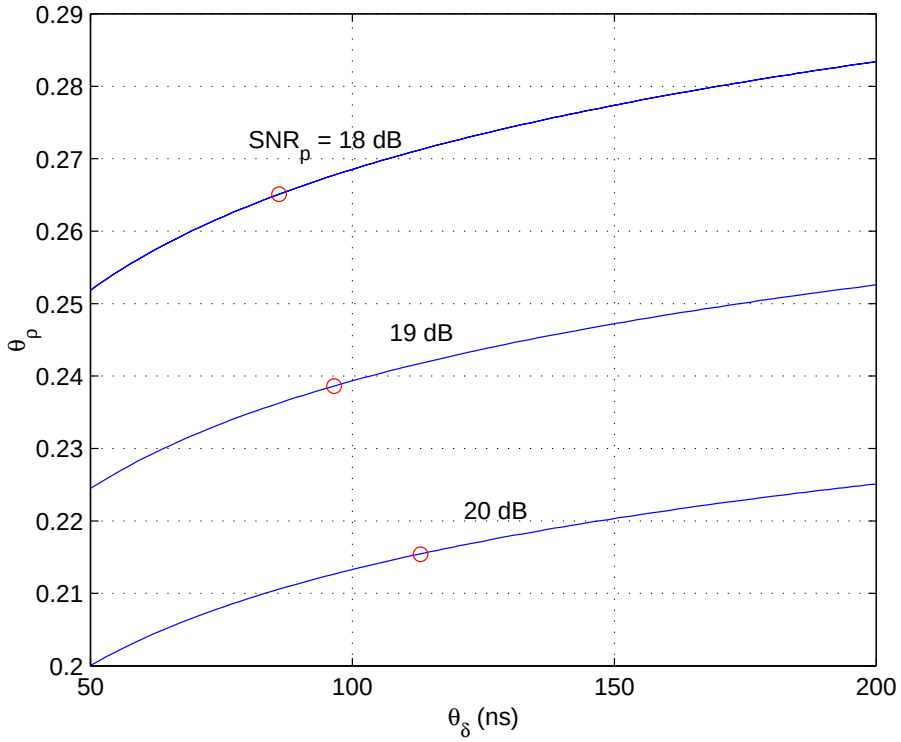

Figure 5.1: Threshold setting using criterion A.1 with $\alpha_{\mathrm{FA}} = 0.005$. Each curve is the collection of θ_δ and θ_ρ which satisfy $P_{\mathrm{FA}} = \alpha_{\mathrm{FA}}$. The circular mark on each curve represents the thresholds that minimize P_{M}.

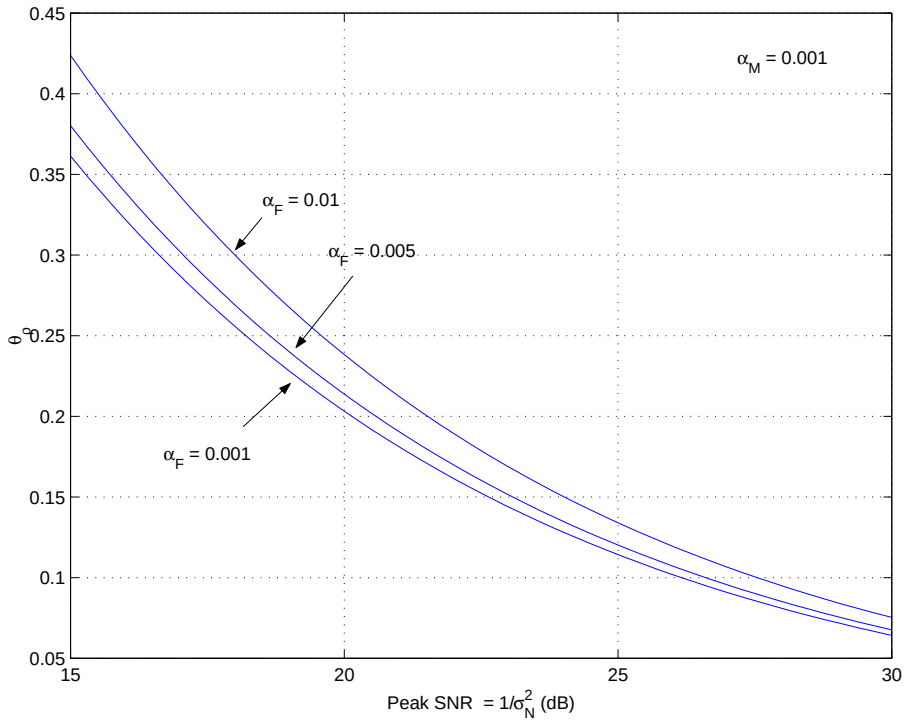

Figure 5.2: Threshold setting using criterion A.2. The value of θ_δ corresponding to $\alpha_{\mathrm{M}} = 0.001$ is 102.8 ns and each curve represents θ_ρ's which satisfy the given early false alarm setting (α_{F}). Notice that with this criterion, θ_ρ is set independently of the PDF of $\boldsymbol{\rho}$.

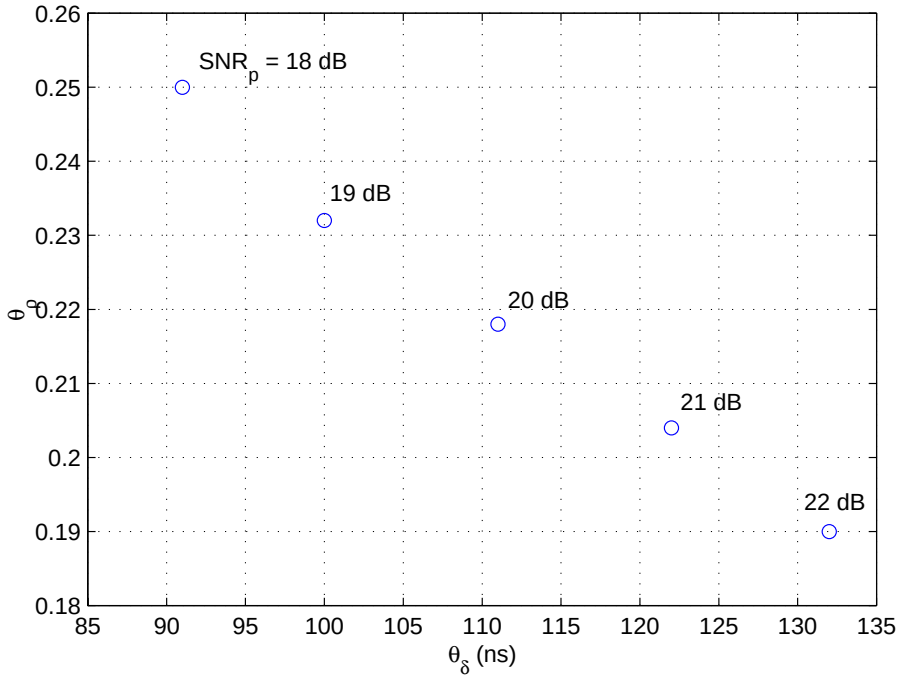

Figure 5.3: Threshold setting using criterion B.1. Each circular mark represents the optimum θ_δ and θ_ρ that minimize $P_{\mathrm{FA}} + P_{\mathrm{M}}$ with a given peak SNR.

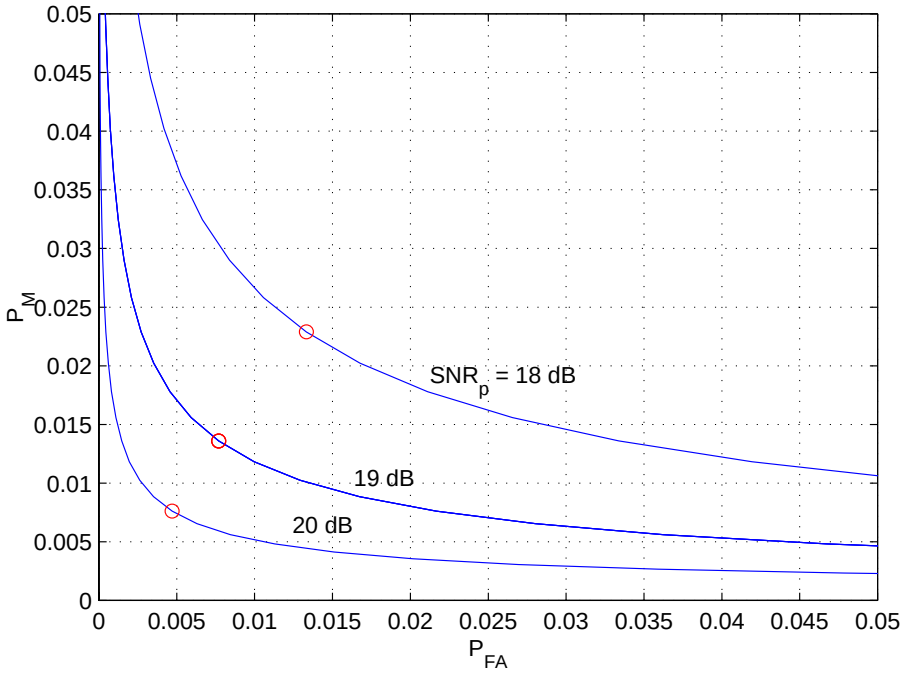

Figure 5.4: Threshold setting with criterion B.2. The value of θ_δ corresponding to $\alpha_{\mathrm{M}} = 0.001$ is 102.8 ns and each curve is a plot of P_{M} vs. P_{FA} with a given peak SNR. Circular mark on each curve represents the optimum θ_δ and θ_ρ that minimize $P_{\mathrm{FA}} + P_{\mathrm{M}}$.

5.2 Test on Measured Data

ToA algorithm was tested on the propagation data. In each test, the thresholds, θ_δ and θ_ρ were set with criterion B.2 described in the previous section. The value of θ_δ was set at 102.8 ns which corresponds to $\alpha_{\mathrm{M}} = 0.001$, and θ_ρ was set by the peak SNR of each signal. Figure 5.5 through figure 5.12 show of test results on the signals measured at locations 2 through 17 described in section 2.1. In each example, the upper plot is the measured waveform and the lower one shows the reconstructed signal with the paths detected in the ToA algorithm. The vertical line appearing in each plot indicates the expected arrival time of the direct-path signal in the presence of a clear LoS path, based on physical range measurements. We can observe discrepancies up to a few nanoseconds of delay in each example between location of this line and the signal frontend. This probably is caused by excessive propagation delay in the LoS blockage and a systematic error in the distance measurement. This unknown delay makes it difficult to measure the length of the direct propagation path. In figure 5.12, notice the large error which is due to the metallic LoS blockage (elevators). In this case, signal components detected are reflected or diffracted.

Figure 5.13 shows the range estimation errors incurred in this test at the locations marked in Figure 2.3. Notice that larger errors occurred at long ranges, probably because the structure of LoS blockage was more complex at these locations.

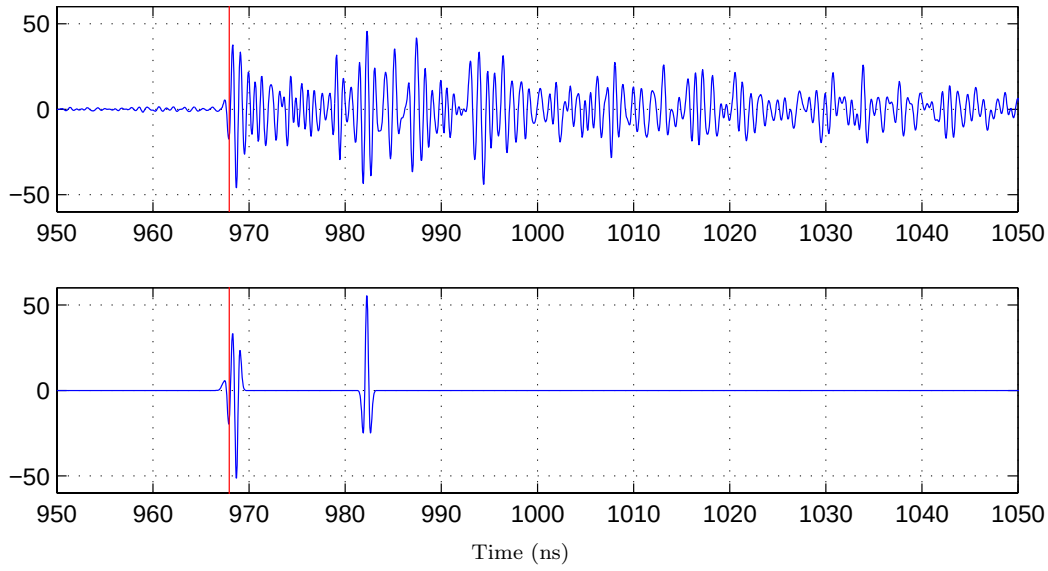

(a)

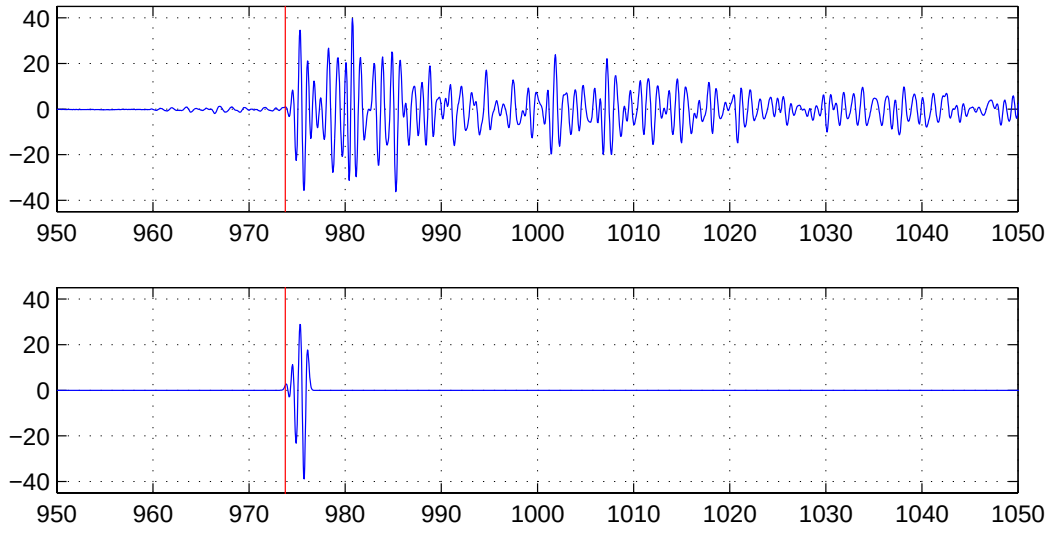

(b)

Figure 5.5: ToA algorithm tested on measured signal at location 2 and 3 with thresholds set by criterion B.2. The vertical scale is in millivolts. Vertical line in each plot show the ToA of the direct path signal based on true measured range, assuming the presence of a clear LoS. The threshold θ_δ was set at 102.8 ns with $\alpha_{\mathrm{M}} = 0.001$ and the values of θ_ρ were (a) 0.060 and (b) 0.056. Notice that the ToA of the signal was defined as the center of the pulse. (See figure 3.1)

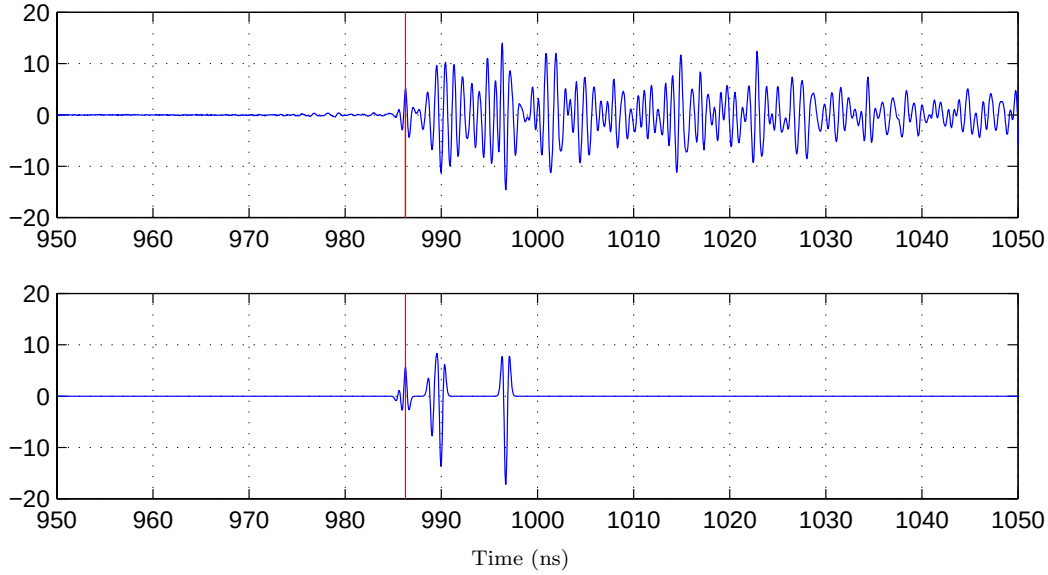

(a)

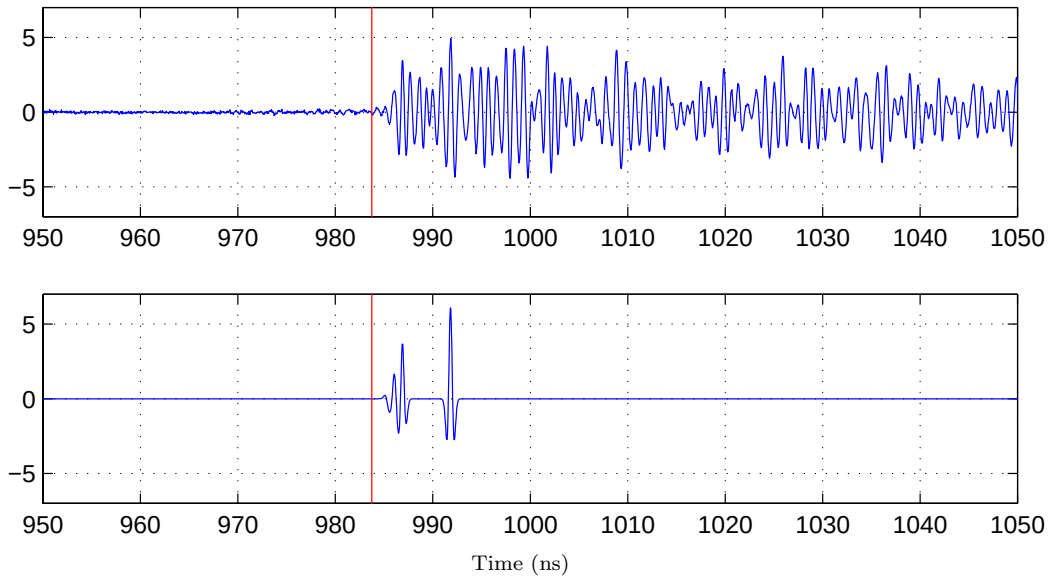

(b)

Figure 5.6: ToA algorithm tested on measured signal at location 4 and 5 with thresholds set by criterion B.2. Vertical line in each plot show the ToA of the direct path signal based on true measured range, assuming the presence of a clear LoS. The threshold θ_δ was set at 102.8 ns with $\alpha_{\mathrm{M}} = 0.001$ and the values of θ_ρ were (a) 0.038 and (b) 0.060. Notice that the ToA of the signal was defined as the center of the pulse. (See figure 3.1)

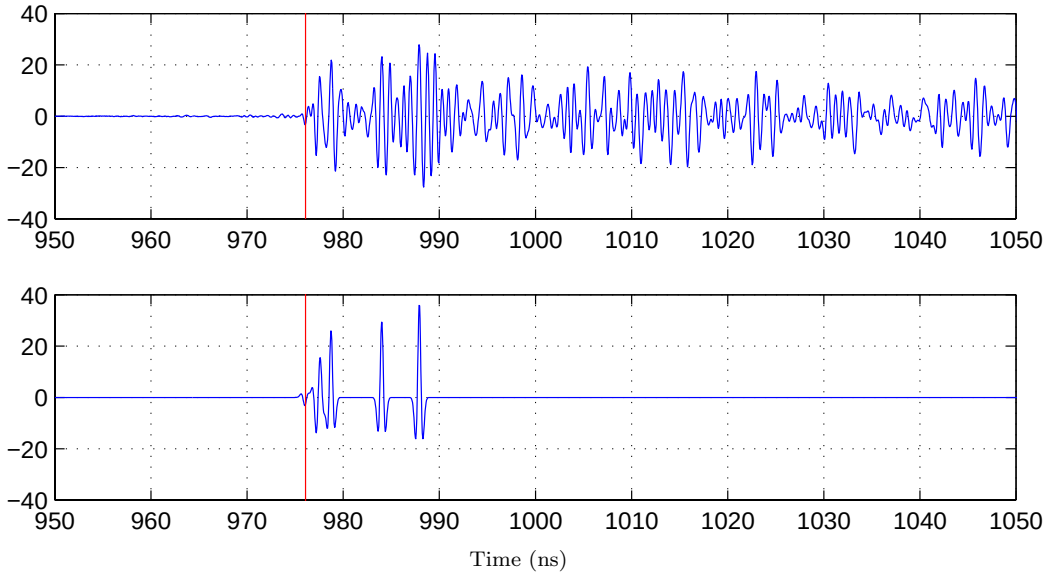

(a)

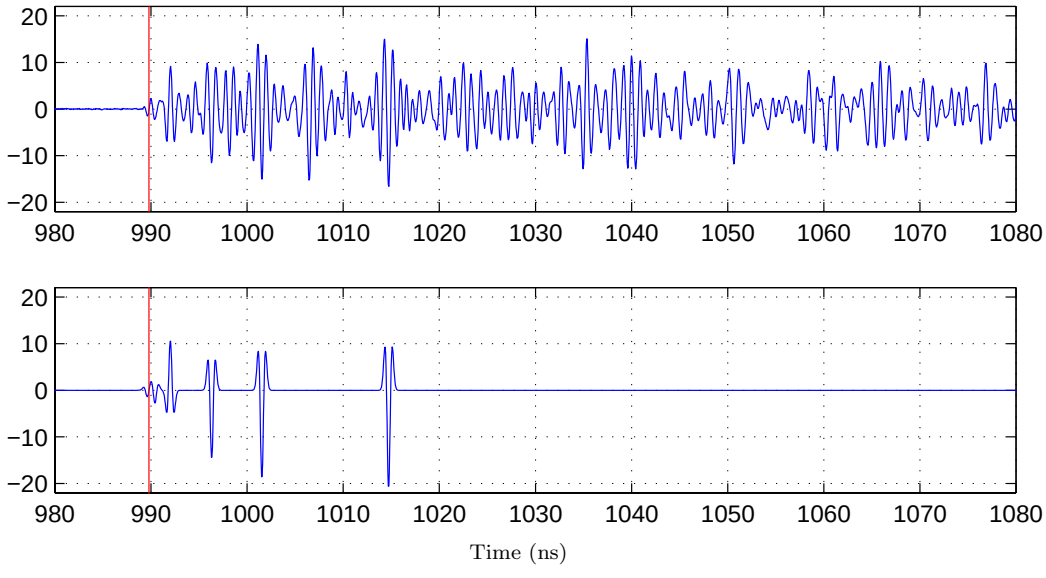

(b)

Figure 5.7: ToA algorithm tested on measured signal at location 6 and 7 with thresholds set by criterion B.2. Vertical line in each plot show the ToA of the direct path signal based on true measured range, assuming the presence of a clear LoS. The threshold θ_δ was set at 102.8 ns with $\alpha_{\mathrm{M}} = 0.001$ and the values of θ_ρ were (a) 0.034 and (b) 0.020. Notice that the ToA of the signal was defined as the center of the pulse. (See figure 3.1)

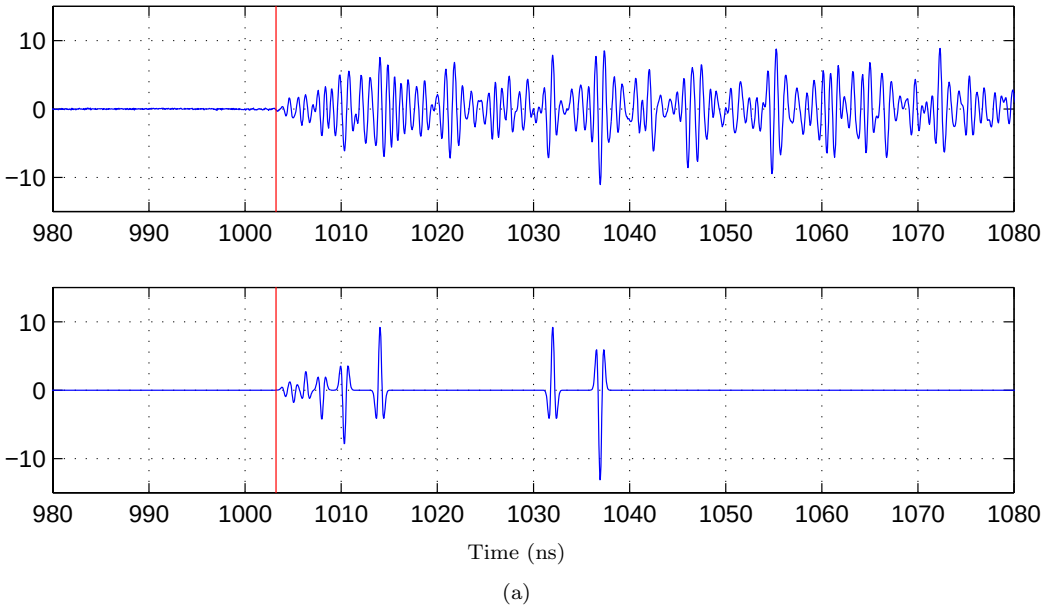

(a)

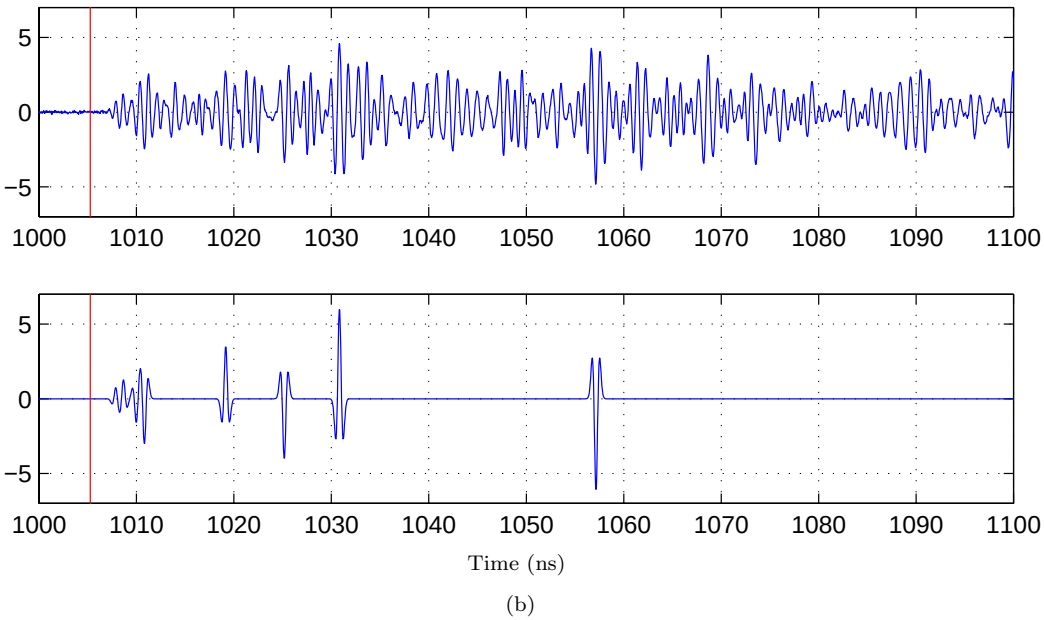

(b)

Figure 5.8: ToA algorithm tested on measured signal at location 8 and 9 with thresholds set by criterion B.2. Vertical line in each plot show the ToA of the direct path signal based on true measured range, assuming the presence of a clear LoS. The threshold θ_δ was set at 102.8 ns with $\alpha_{\mathrm{M}} = 0.001$ and the values of θ_ρ were (a) 0.030 and (b) 0.050. Notice that the ToA of the signal was defined as the center of the pulse. (See figure 3.1)

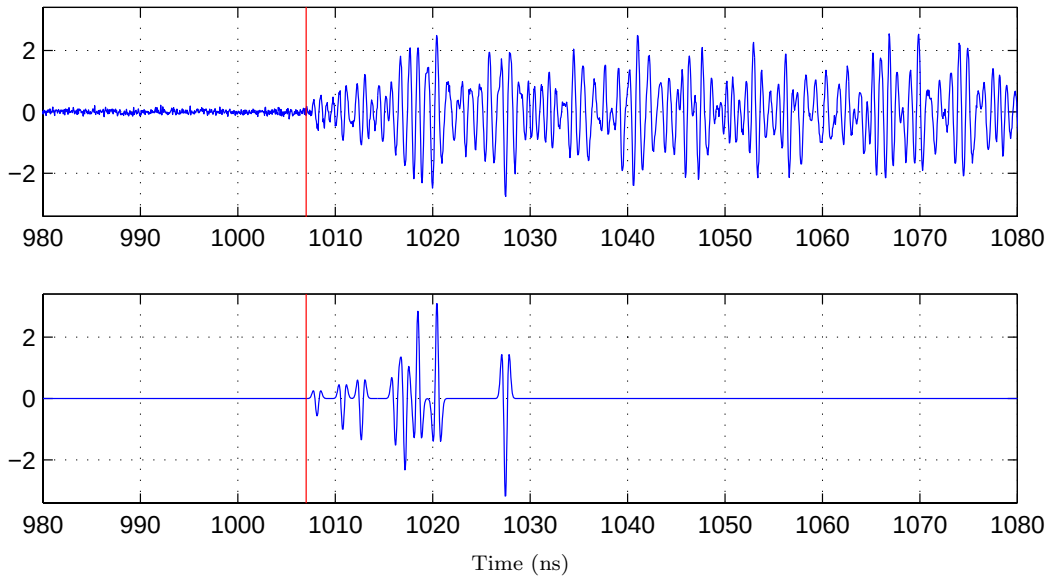

(a)

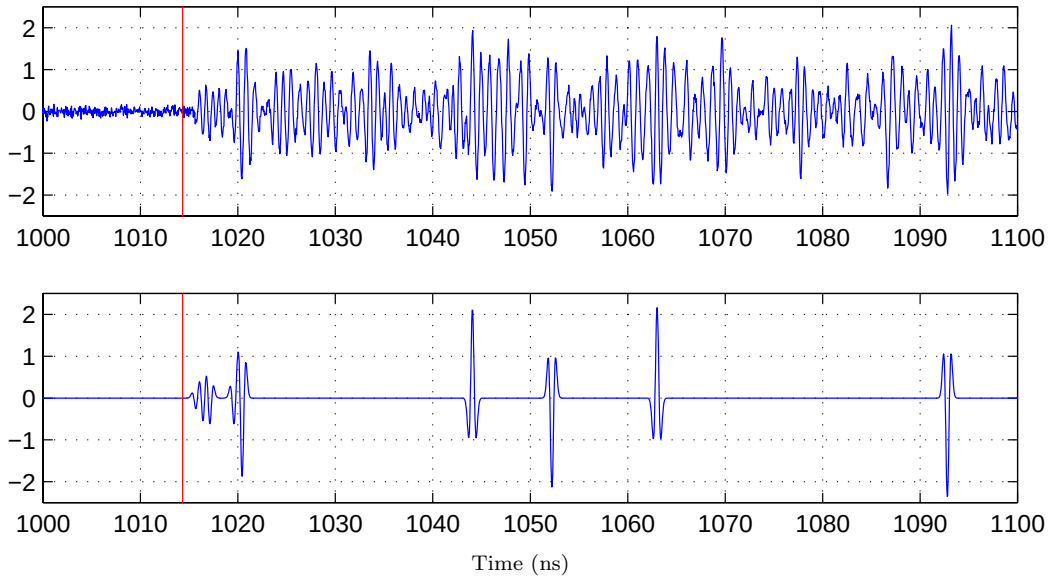

(b)

Figure 5.9: ToA algorithm tested on measured signal at location 10 and 11 with thresholds set by criterion B.2. Vertical line in each plot show the ToA of the direct path signal based on true measured range, assuming the presence of a clear LoS. The threshold θ_δ was set at 102.8 ns with $\alpha_{\mathrm{M}} = 0.001$ and the values of θ_ρ were (a) 0.082 and (b) 0.102. Notice that the ToA of the signal was defined as the center of the pulse. (See figure 3.1)

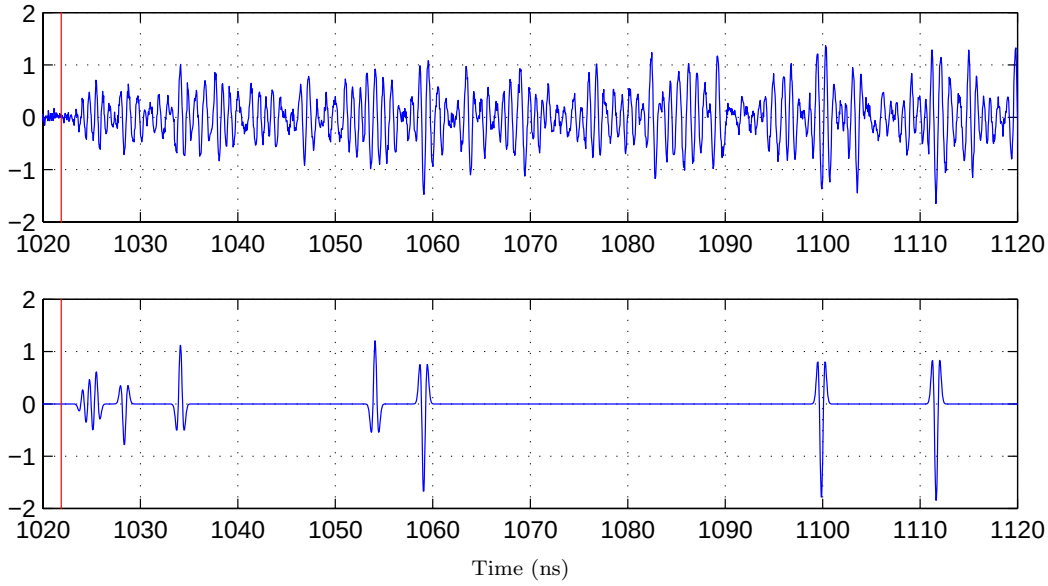

(a)

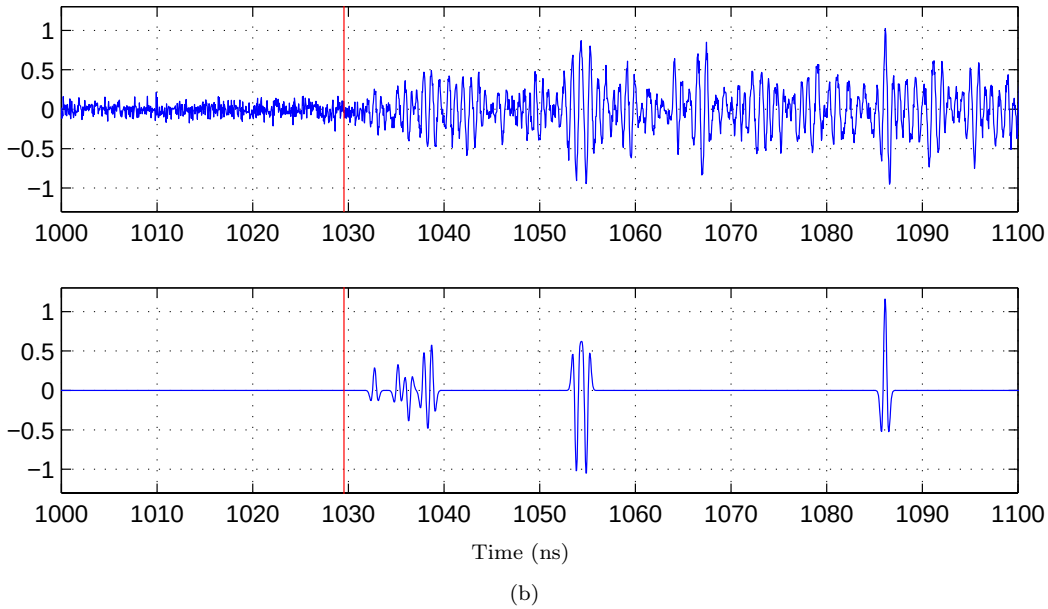

(b)

Figure 5.10: ToA algorithm tested on measured signal at location 12 and 13 with thresholds set by criterion B.2. Vertical line in each plot show the ToA of the direct path signal based on true measured range, assuming the presence of a clear LoS. The threshold θ_δ was set at 102.8 ns with $\alpha_{\mathrm{M}} = 0.001$ and the values of θ_ρ were (a) 0.112 and (b) 0.154. Notice that the ToA of the signal was defined as the center of the pulse. (See figure 3.1)

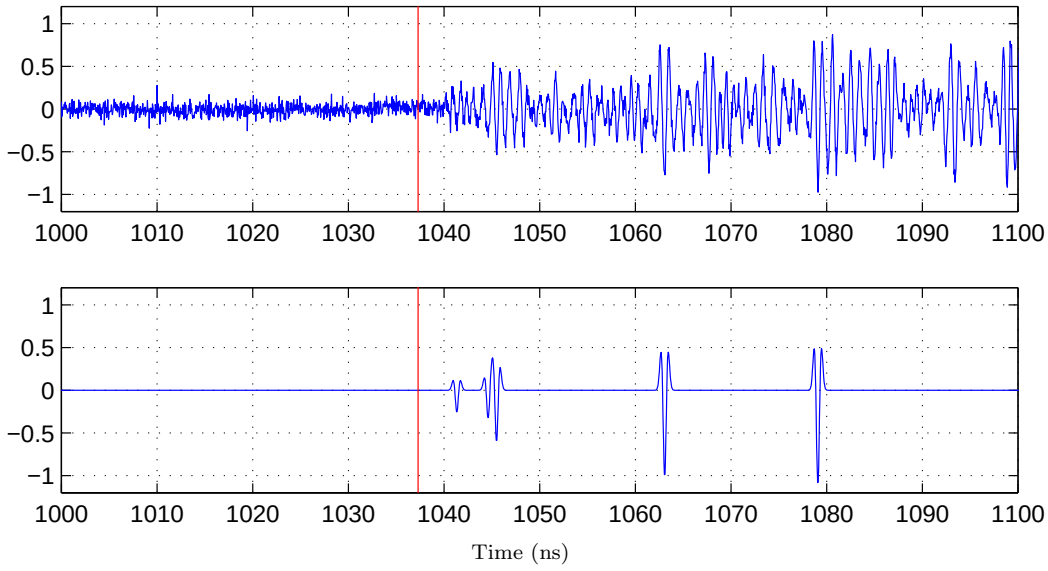

(a)

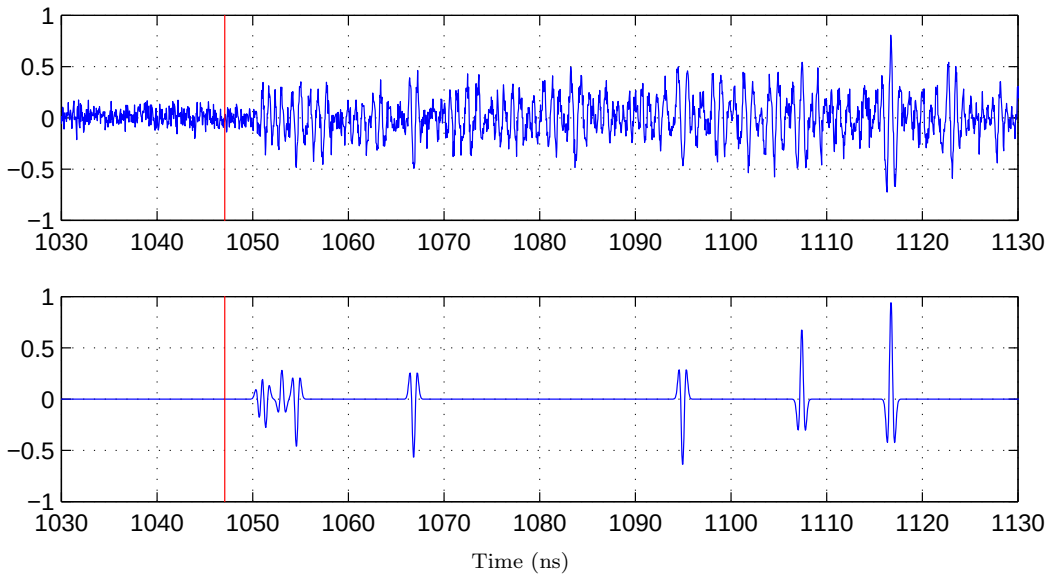

(b)

Figure 5.11: ToA algorithm tested on measured signal at location 14 and 15 with thresholds set by criterion B.2. Vertical line in each plot show the ToA of the direct path signal based on true measured range, assuming the presence of a clear LoS. The threshold θ_δ was set at 102.8 ns with $\alpha_{\mathrm{M}} = 0.001$ and the values of θ_ρ were (a) 0.152 and (b) 0.184. Notice that the ToA of the signal was defined as the center of the pulse. (See figure 3.1)

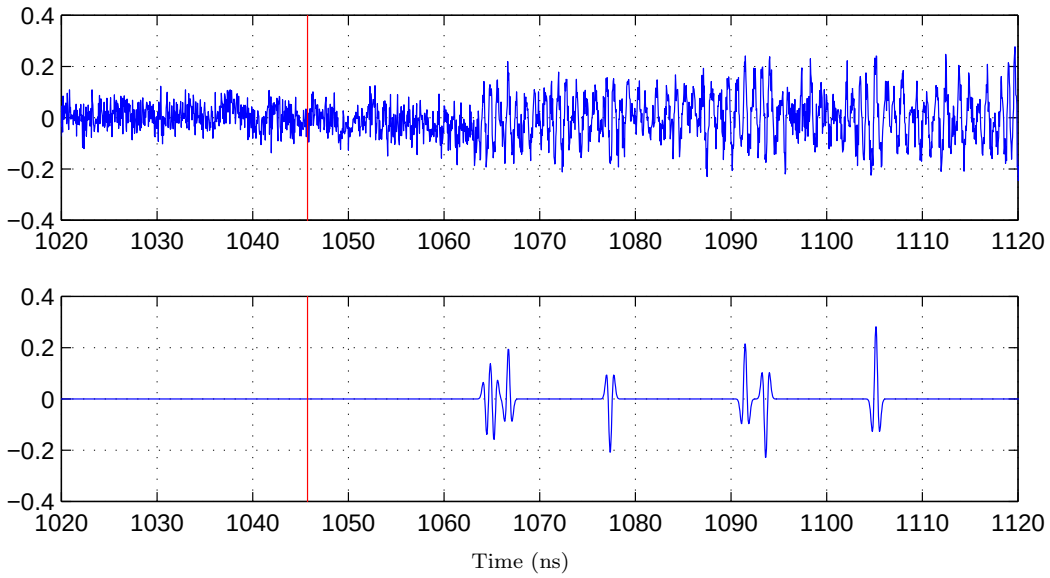

(a)

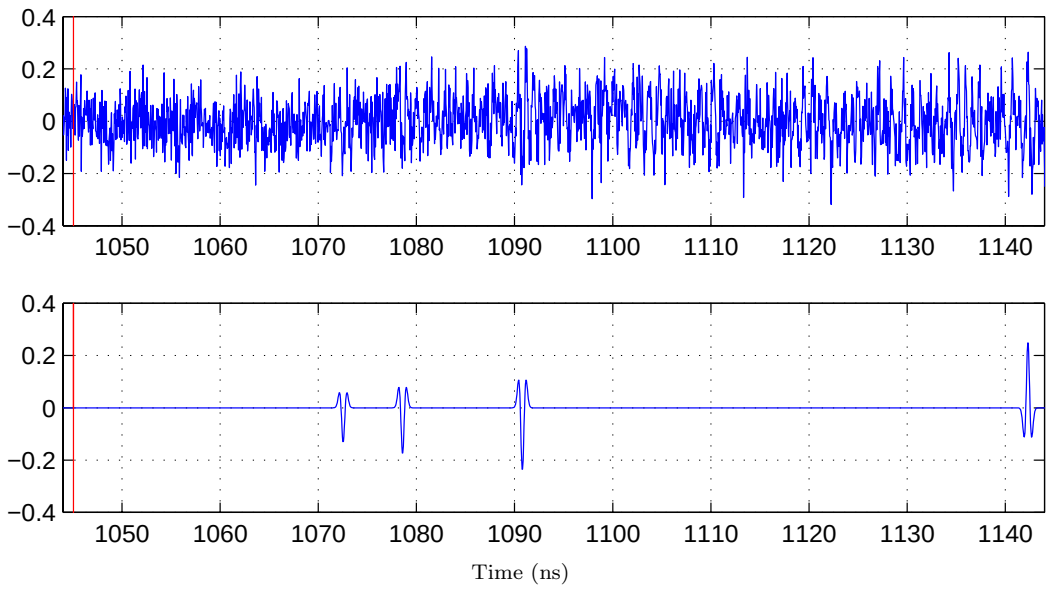

(b)

Figure 5.12: ToA algorithm tested on measured signal at location 16 and 17 with thresholds set by criterion B.2. Vertical line in each plot show the ToA of the direct path signal based on true measured range, assuming the presence of a clear LoS. The threshold θ_δ was set at 102.8 ns with $\alpha_{\mathrm{M}} = 0.001$ and the values of θ_ρ were (a) 0.288 and (b) 0.458. Notice that the ToA of the signal was defined as the center of the pulse. (See figure 3.1)

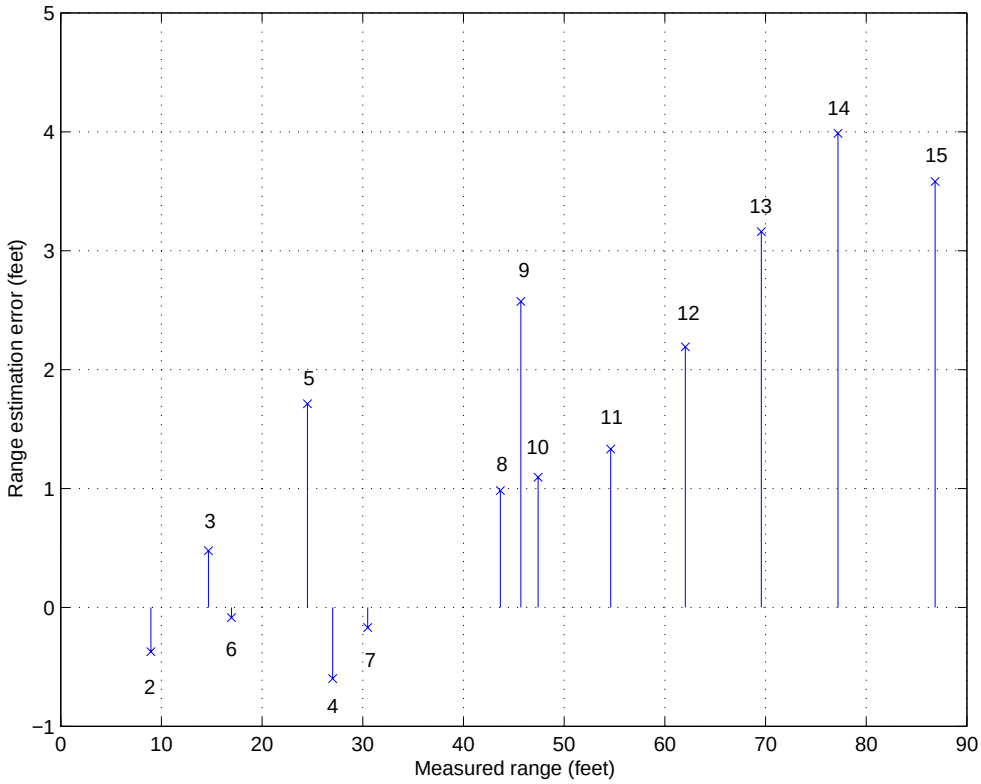

Figure 5.13: Range estimation errors (estimated range - measured range) incurred in the test using threshold setting criterion B.2. The numbers are the index of measurement positions.

Chapter 6

Design of an UWB Ranging System

6.1 Introduction

In previous chapters, a ToA measurement algorithm using generalized maximum likelihood was introduced and tested on a set of propagation data. Utilizing the fine range resolution of the signal and statistical information on the arrival time and strength, the direct path signal can be detected with reasonable accuracy. The data used for the test of the ranging algorithm is a set of sampled waveforms whose sampling frequency is 20.5 GHz, which is conservatively high considering the bandwidth of the UWB signal even though it is not band-limited. The sampling frequency of the waveform affects the accuracy of ToA estimation. So to achieve accuracy in ToA estimation, the ranging system should have a rapid measurement capability.

Withington et al. [40] introduced an UWB scanning receiver system which, using two correlators, has the capability of simultaneous communication and channel pulse response measurement. What is interesting with this UWB scanning receiver system

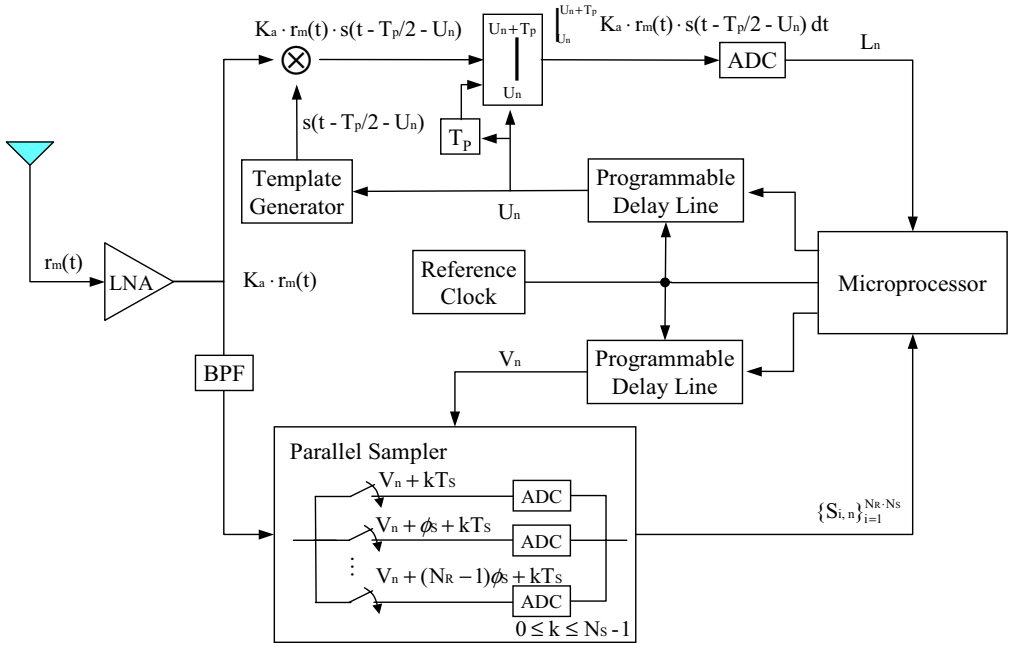

Figure 6.1: Receiver schematic of UWB ranging system.

is that it does not require a common clock between the transceiver for the measurement of the signal but derives timing for the channel response measurements from the synchronous communication clock. In this chapter, the UWB ranging system using a correlator and a parallel sampler to enable a higher speed measurement of signals is introduced. This system utilizes the ToA algorithm introduced in chapter 3 and employs two-way ranging scheme for the range estimation between transceiver without a common timing reference.

6.2 System Description

Figure 6.1 shows the receiver block diagram of the UWB ranging system. This system is composed of a correlator, a parallel receiver, and a microprocessor. The correlator locks on the received signal and the parallel receiver collect samples from the signal. The microprocessor controls the times of the correlator and sampler and perform the signal processing with collected samples.

At the receiver frontend, a wideband low noise amplifier (LNA) with a gain of K_{a} is used to amplify the received signal. When the signal is received, it is correlated with the template signal $s(t)$ of width of T_{p} sec. The correlator synchronizes with the received signal, specifically with one path. The quantity U_n is the time-tracking point in the n^{th} time frame. The digitized correlator output L_n in the n^{th} time frame is used for tracking and evaluation of noise power. Once the correlator is locked, the parallel sampler starts sampling the incoming signal under the time control of a trigger signal. The trigger time V_n in the n^{th} time frame is controlled relative to the tracking time U_n. The signal is filtered by a band-pass filter and then sampled by the parallel sampler which is composed of a bank of N_{R} individual samplers and N_{R} analog-to-digital converters (ADC). Each individual sampler performs uniform sampling at a sampling rate of $1/T_{\mathrm{s}}$ Hz and takes N_{s} samples per time frame. The

samples taken at one location are averaged given number of times later to increase SNR. In n^{th} time frame, the i^{th} individual sampler takes samples at

$$t = V_n + (N_{\text{R}} - 1)\phi + kT_{\text{s}}, \text{ where } 0 \leq k \leq N_{\text{s}} - 1. \tag{6.1}$$

The offset in the sampling times of any two adjacent individual samplers is ϕ_{s}, which satisfies

$$\phi_{\text{s}} \cdot N_{\text{R}} = T_{\text{s}}. \tag{6.2}$$

A Total of $N_{\text{s}} \cdot N_{\text{R}}$ samples are taken in each time frame by this parallel sampler and the overall sampling rate is $1/\phi_{\text{s}}$ Hz. The overall sampling frequency is proportional to the number of individual samplers employed, however, it is limited by an implementation issue. To acquire an acceptable SNR, each sample is integrated over several time frames. Once the samples are averaged over a given number of times, samples at different locations are taken by changing the relative trigger time of the sampler to the time-tracking point, which results in the increase of the sampling frequency of the measured signal. The samples of the signal taken with an acceptable SNR are used to estimate the arrival time of the direct path signal. Assuming that the overall sampling rate of the measured signal is high enough compared to signal bandwidth, we can directly apply the ToA algorithm described in chapter 3.

Let's take a system which employs 10 individual samplers with a sampling rate of 100 MHz each as an example. If the transmitter and receiver are time-multiplexed

with a period of 0.2 msec, then each radio would take samples for 0.1 ms per time-multiplex period. Assume that the pulse repetition rate is 10 Mpps, which corresponds to the frame time of 0.1μsec, and each individual samplers take 8 samples per time frame. Then total number of samples taken by each radio per time-multiplex period, N_{T}, is given by

$$N_{\mathrm{T}} = 10 \times 10^6 \times 0.1 \times 10^{-3} \times 8 \times 10 = 8000. \tag{6.3}$$

If samples are averaged over 32 times and time displacement between any two adjacent samples is 0.05 ns, then signal can be measured with 20 GHz of overall sampling frequency and 125 ns of time span, which provides data with a high enough sampling rate to apply ToA algorithm.

6.3 Evaluation of Noise Power

To determine the thresholds used in the ToA algorithm, the SNR of the peak path must be evaluated, so the noise power of the received signal has to be estimated. A traditional method to estimate the noise power is to send training signals or send no signal at all, which necessitates a separate time interval for the noise estimation. However, in the UWB ranging system, we can take advantage of the fact that the tracking correlator is locked on a specific path with a constant amplitude, assuming

that the channel is stationary during the evaluation. We utilize the correlator output for the noise power estimation.

Let $\boldsymbol{L}_n$ be the random variable representing the digitized correlator output at n^{th} time frame. Then $\boldsymbol{L}_n$ is evaluated by

$$\boldsymbol{L}_n = \int_{U_n}^{U_n+T_\text{p}} s(t-U_n-T_\text{p}/2)r(t)dt. \tag{6.4}$$

Let's assume that there is no other path which overlaps with the locked path, then $\boldsymbol{L}_n$ can be approximated by

$$\boldsymbol{L_n} \approx \int_{U_n}^{U_n+T_\text{p}} s(t-U_n-T_\text{p}/2)[A_\text{Lock}s(t-U_n-T_\text{p}/2)+n(t)]dt, \tag{6.5}$$

where A_Lock is the amplitude of the locked path. The noise $n(t)$ is assumed to be white gaussian with correlation function is given by

$$R_\text{N}(\tau) = \sigma_\text{b}^2\delta_\text{D}(\tau). \tag{6.6}$$

The expected value of $\boldsymbol{L_n}$ can be evaluated by

$$\begin{aligned} E\{\boldsymbol{L}_n\} &= E\left\{\int_{U_n}^{U_n+T_\text{p}} s(t-U_n-T_\text{p}/2)[A_\text{Lock}s(t-U_n-T_\text{p}/2)+n(t)]dt\right\} \\ &= A_\text{Lock}\int_{U_n}^{U_n+T_\text{p}} s^2(t-U_n-T_\text{p}/2)dt + \int_{U_n}^{U_n+T_\text{p}} E\{s(t-U_n-T_\text{p}/2)n(t)\}dt \\ &= E_\text{s}\cdot A_\text{Lock}. \end{aligned} \tag{6.7}$$

The variance of $\boldsymbol{L_n}$ is

$$\begin{aligned}
Var\{\boldsymbol{L_n}\} &= E\{(\boldsymbol{L_n} - E_{\mathrm{s}}A_{\mathrm{Lock}})^2\} \\
&= E\Bigg\{\Big[\int_{U_n}^{U_n+T_{\mathrm{p}}} A_{\mathrm{Lock}}s^2(t-U_n-T_{\mathrm{p}}/2)dt \\
&\quad + \int_{U_n}^{U_n+T_{\mathrm{p}}} s(t-U_n-T_{\mathrm{p}}/2)n(t)dt - E_{\mathrm{s}}A_{\mathrm{Lock}}\Big]^2\Bigg\} \\
&= E\Bigg\{\Big[\int_{U_n}^{U_n+T_{\mathrm{p}}} s(t-U_n-T_{\mathrm{p}}/2)n(t)dt\Big]^2\Bigg\} \\
&= E\Bigg\{\int_{U_n}^{U_n+T_{\mathrm{p}}}\int_{U_n}^{U_n+T_{\mathrm{p}}} s(t-U_n-T_{\mathrm{p}}/2)s(t'-U_n-T_{\mathrm{p}}/2)n(t)n(t')dtdt'\Bigg\} \\
&= \int_{U_n}^{U_n+T_{\mathrm{p}}}\int_{U_n}^{U_n+T_{\mathrm{p}}} s(t-U_n-T_{\mathrm{p}}/2)s(t'-U_n-T_{\mathrm{p}}/2)\sigma_{\mathrm{b}}^2\delta_{\mathrm{D}}(t-t')dtdt' \\
&= \int_{U_n}^{U_n+T_{\mathrm{p}}} \sigma_{\mathrm{b}}^2 s^2(t-U_n-T_{\mathrm{p}}/2)dt \\
&= E_{\mathrm{s}}\cdot\sigma_{\mathrm{b}}^2, \qquad (6.8)
\end{aligned}$$

If we assume the channel is stationary during the measurement and the noise is white gaussian, the sequence $\{\boldsymbol{L_n}\}$ is independent, identically distributed, and A_{lock} and σ_{b}^2 can be evaluated using the weak law of large number:

$$\begin{aligned}
A_{\mathrm{lock}} &= \frac{E\{\boldsymbol{L_n}\}}{E_{\mathrm{s}}} \\
&= \frac{1}{E_{\mathrm{s}}}\lim_{p\to\infty}\frac{1}{p}\sum_{n=1}^{p}\boldsymbol{L_n}, \qquad (6.9) \\
\sigma_{\mathrm{b}}^2 &= \frac{1}{E_{\mathrm{s}}}Var\{\boldsymbol{L_n}\} \\
&= \frac{1}{E_{\mathrm{s}}}\lim_{p\to\infty}\frac{1}{p}\sum_{n=1}^{p}(\boldsymbol{L_n} - A_{\mathrm{Lock}})^2. \qquad (6.10)
\end{aligned}$$

Let N_{T} be the number of pulses transmitted during T_{M} sec and assume it is very large, then A_{lock} and σ_{b}^2 can be approximated to be

$$\hat{A}_{\mathrm{lock}} = \frac{1}{E_{\mathrm{s}} N_{\mathrm{T}}} \sum_{n=1}^{N_{\mathrm{T}}} \boldsymbol{L_n}, \tag{6.11}$$

$$\hat{\sigma}_{\mathrm{b}}^2 = \frac{1}{E_{\mathrm{s}} N_{\mathrm{T}}} \sum_{n=1}^{N_{\mathrm{T}}} (L_n - A_{\mathrm{Lock}} E_{\mathrm{s}})^2. \tag{6.12}$$

The noise variance would be further reduced since each sample is integrated. Let's assume samples are integrated over N_{A} times to get a reasonable SNR, then the noise variance is reduced by $\frac{1}{N_{\mathrm{A}}}$ times,

$$\hat{\sigma}_{\mathrm{b}}^2 = \frac{1}{E_{\mathrm{s}} N_{\mathrm{T}} N_{\mathrm{A}}} \sum_{n=1}^{N_{\mathrm{T}}} (L_n - A_{\mathrm{Lock}} E_{\mathrm{s}})^2. \tag{6.13}$$

6.4 Two-Way Ranging Scheme

A UWB ranging system estimates the range using a completely wireless two-way link without a common timing reference. The range estimate is based on the measured signal round-trip time between the transceiver. This ranging scheme uses a two-way remote synchronization technique [19] employed in satellite systems.

Figure 6.2 is the timing diagram of this approach. A pair of UWB radios are time multiplexed with a period of T_{M}. Each radio switches between a transmission mode and a reception mode every $T_{\mathrm{M}}/2$ sec and the clocks are assumed to be locked. Radio 1 transmits signal 1 which is a train of pulses without modulation. It is received by

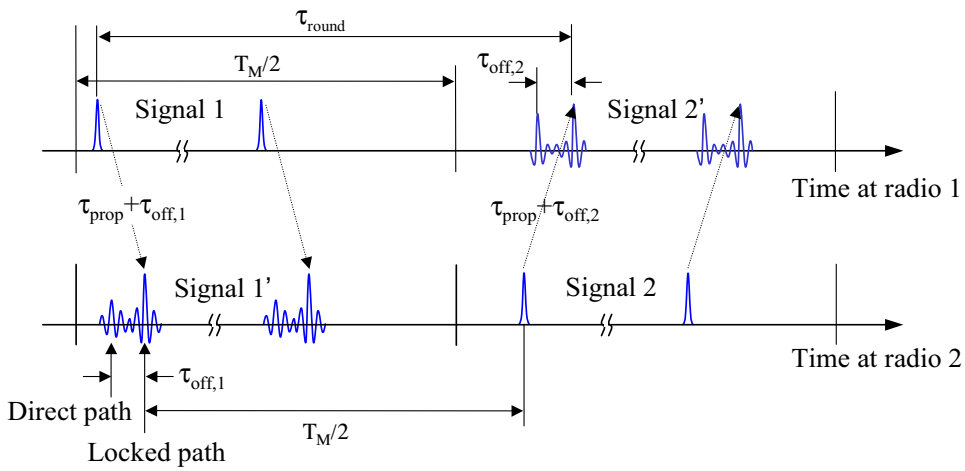

Figure 6.2: Evaluation of the signal round-trip time using 2-way ranging technique.

radio 2 and signal 1′ denotes the captured signal. The time-multiplex period T_{M} is assumed to be large enough relative to the temporal profile of the received signal so that it does not affect the next transmission. The delay between transmission and reception of this signal is $\tau_{\mathrm{prop}} + \tau_{\mathrm{off},1}$, where τ_{prop} is the propagation time and $\tau_{\mathrm{off},1}$ represents the time offset between the locked path and the direct path. With a known delay of $T_{\mathrm{M}}/2$ from the front end of signal 1′, radio 2 transmits signal 2 and it is captured by radio 1. Signal 2′ denotes the captured signal by radio 1. Similarly, a delay of $\tau_{\mathrm{prop}} + \tau_{\mathrm{off},2}$ exists in this direction. The structures of signal 2 and signal 2′ are similar to those of signal 1 and signal 1′, respectively. Radio 1 can measure the signal round-trip time, τ_{round}, which is

$$\tau_{\mathrm{round}} \approx 2\tau_{\mathrm{prop}} + \frac{T_{\mathrm{M}}}{2} + \tau_{\mathrm{off},1} + \tau_{\mathrm{off},2}. \tag{6.14}$$

Then the signal propagation time can be approximated by

$$\tau_{\text{prop}} \approx \frac{\tau_{\text{round}} - T_{\text{M}}/2 - \tau_{\text{off},1} - \tau_{\text{off},2}}{2}. \tag{6.15}$$

Radio 2 informs radio 1 of $\tau_{\text{off},1}$ afterwards with a few bits of information so that radio 1 can evaluate the signal propagation time. Radio 2 also sends the information on SNR of measured signal to radio 1. If SNR's of the measured signals at both sides are not large enough to achieve desired performance, the two radios increase the signal measurement time by repeating the same measurement in the next time-multiplex period. This post-processing is necessary because with an unacceptable SNR, desired accuracy in ToA estimation cannot be achieved.

Chapter 7

Application of ToA algorithm for UWB Scanning Receiver

In this chapter, the application of the ToA algorithm for an existing technology, UWB scanning receiver system which was developed by Time Domain Corporation, is discussed. The UWB scanning receiver has a communication and signal measurement capability and employs two correlators, one of which is used for tracking and the other is for sampling. A detailed description of this system is given in [40]. Since the sampling correlator takes one sample per time frame, the measurement speed of this system is not high enough to achieve high sampling frequency. Since the ToA algorithm proposed in chapter 3 assumes the presence of measurement data with a high enough sampling rate, the algorithm is modified to be applied to under-sampled data.

7.1 Modification of the Algorithm

The ToA algorithm of chapter 3 requires the knowledge of location and strength of the peak path of received signal. To get this information in a UWB scanning receiver, a separate search for the peak signal has to be performed once the tracking correlator is locked, since the locked path is not necessarily the peak. This consumes a considerable amount of time because of the low sampling rate. Further, it is difficult to perform the GML estimation with under-sampled data.

The modified algorithm is as follows. First, the search region for the direct path signal with a given length of θ_δ is set in the forward direction from the location of the locked path. Considering that the synchronization strategy is based on threshold detection, by which the tracking correlator is locked on the first level crossing point at the threshold, we can assume that the tracking correlator is locked on a path which arrives earlier than the peak path. As a consequence, the probability of an early false alarm would increase since the length of the noise only portion of the signal over which the search is conducted increases, while the risk of missing the direct path signal beyond the range of search would decrease. Secondly, the threshold of the amplitude is determined only by the noise floor without considering the relative path strength due to the absence of the knowledge of the peak strength. Thirdly, the first level crossing point is regarded as the ToA of direct path signal since computation of GML estimation cannot be done with the under-sampled data.

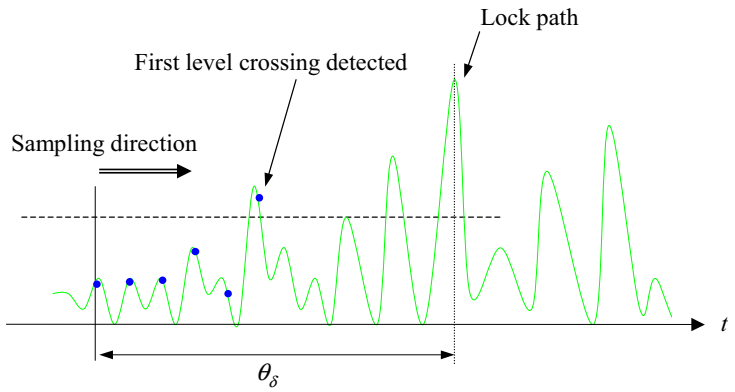

Figure 7.1: Search for the earliest arrival of the signal using uniform sampling. Search is performed in a positive direction along the time axis.

Figure 7.1 illustrates the search process. Search by sampling is done in the positive direction along the time axis and terminated once the first level crossing is detected. To perform search for the earliest arrival with a low sampling rate, effective sampling design is very important. In the next section, issues related to the sampling scheme is discussed.

7.2 Sampling Issues

As discussed in the previous section, in the modified ToA algorithm, the earliest arrival is detected by searching the first level crossing time by sampling the correlator output. To achieve an accurate detection in a limited measurement, which is determined by sampling rate, length of search region, and the number of integration, effective sampling design is critical. To determine the sampling strategy, it is necessary to know the minimum sampling frequency required. For example, the larger

is the distance between adjacent two samples, the higher is the risk of missing the level crossing point between them.

While it is very difficult to evaluate the probability of missing level crossing between samples, we can think of some ways to measure this risk. One of them is to quantify the interpolation error caused by under-sampling, assuming the signal is deterministic. Since the signal from which the samples are taken is not band-limited, it is impossible to sample at the Nyquist rate and as a consequence, the signal spectra would overlap [22]. The amount of energy of high frequency components lost due to aliasing will provide one way of measuring the sampling quality. Another is to evaluate the error variance in minimum mean square error (MMSE) estimation, assuming the correlator output signal is a wide sense stationary (w.s.s.) process. Figure 7.2 shows an example of MMSE estimation using two samples. In this figure, $\hat{w}(t')$ denotes the MMSE estimate of $w(t')$ evaluated with observation vector of samples, namely $\underline{m}$, which is

$$\underline{m} = \begin{bmatrix} w(t_1) \\ \\ w(t_2) \end{bmatrix}. \tag{7.1}$$

The solid line represents the reconstructed signal using MMSE estimation and the dotted line represents the standard variation of the estimation error. The closer the dotted line is to the threshold level at which the crossing is searched, the larger is

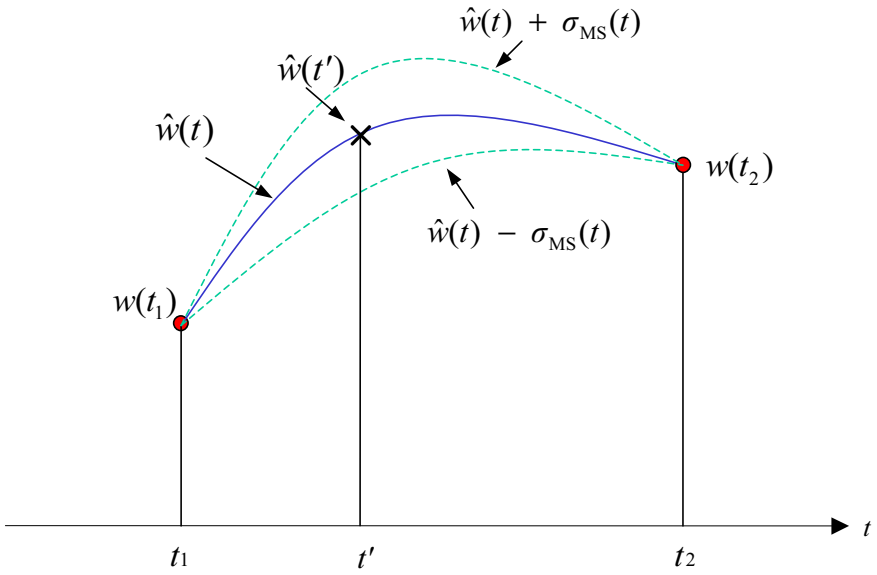

Figure 7.2: Reconstruction of signal using MMSE estimation based on two samples. Solid curve indicates the reconstructed signal and the dotted line shows the error deviation.

the probability of missing the occurrence of crossing. MMSE estimate of $w(t')$ and the error variance $\sigma^2_{\rm MS}(t')$ are given by

$$\hat{w}(t') = R_{\hat{\rm w}{\rm m}} R_{\rm m}^{-1} \underline{m}, \tag{7.2}$$

$$\sigma^2_{\rm MS}(t') = {\rm Tr}(R_{\hat{\rm w}} - R_{\hat{\rm w}{\rm m}} R_{\rm m}^{-1} R_{{\rm m}\hat{\rm w}}), \tag{7.3}$$

where $R_{\hat{\rm w}}$ and $R_{\rm m}$ are correlation matrix $\hat{w}(t')$ and $\underline{m}$, respectively, $R_{\hat{\rm w}{\rm m}}$ is the cross-correlation matrix of $\hat{w}(t')$ and $\underline{m}$, and ${\rm Tr}(\cdot)$ is the trace function. Correlation matrices appearing in (7.2) are evaluated by computing

$$R_{\hat{\rm w}} = R_{\rm w}(0), \tag{7.4}$$

Figure 7.3: Transmission and reception of signal in UWB scanning receiver system link. The channel function $h_{\rm b}(t)$ can be approximated using the measured antenna system function.

$$R_{\rm m} = \begin{bmatrix} R_{\rm w}(0) & R_{\rm w}(t_1 - t_2) \\ R_{\rm w}(t_2 - t_1) & R_{\rm w}(0) \end{bmatrix}, \tag{7.5}$$

$$R_{\hat{w}m} = [R_{\rm w}(t' - t_1)\ R_{\rm w}(t' - t_2)], \tag{7.6}$$

where $R_{\rm w}(\tau)$ denotes the auto-correlation function of $w(t)$. As shown in (7.2) through (7.6), to calculate $\hat{w}(t')$ and $\sigma^2_{\rm MS}(t')$, auto-correlation function of the correlator output signal needs to be evaluated.

Figure 7.3 is the block diagram of a matched filter system which is equivalent to a scanning receiver system link. A transmitted UWB pulse $p(t)$ goes though the channel including antennas whose impulse response is $h_{\rm b}(t)$, and the resulting output is correlated is the template signal $u(t)$. Assuming the correlator output $w(t)$ is a wide sense stationary random process, the energy spectral density $S_{\rm w}(f)$ of $w(t)$ can be approximated by

$$S_{\rm w}(f) = |U(f)|^2 |H_{\rm b}(f)|^2 S_{\rm p}(f), \tag{7.7}$$

where $S_{\mathrm{p}}(f)$ is the energy spectral density of $p(t)$. The channel function $H_{\mathrm{b}}(f)$ can be modeled using the measured antenna system function $H_{\mathrm{a}}(f)$ shown in figure 2.6, which is

$$H_{\mathrm{b}}(f) = c_{\mathrm{a}} \cdot H_{\mathrm{a}}(f), \tag{7.8}$$

where the unknown constant c_{a} is the attenuation factor. Let's define $S'_{\mathrm{w}}(f)$ and $R'_{\mathrm{w}}(\tau)$ as

$$\begin{aligned} S'_{\mathrm{w}}(f) &= |U(f)|^2 |H_{\mathrm{a}}(f)|^2 S_{\mathrm{p}}(f), & (7.9) \\ R'_{\mathrm{w}}(\tau) &= F^{-1}\{S'_{\mathrm{w}}(f)\}. & (7.10) \end{aligned}$$

Then, $S_{\mathrm{w}}(f)$ and $R_{\mathrm{w}}(\tau)$ satisfies

$$\begin{aligned} S_{\mathrm{w}}(f) &= c_{\mathrm{a}}^2 \cdot S'_{\mathrm{w}}(f), & (7.11) \\ R_{\mathrm{w}}(\tau) &= c_{\mathrm{a}}^2 \cdot R'_{\mathrm{w}}(\tau). & (7.12) \end{aligned}$$

In figure 7.4 and figure 7.5, plots of $S_{\mathrm{p}}(f)$, $|U(f)|^2$, $S'_{\mathrm{w}}(f)$, and $R'_{\mathrm{w}}(\tau)$ are shown. The template $u(t)$ was assumed to be $s(t)$ whose mathematical model is given in (3.2). The unknown constant c_{a} can be evaluated using (7.12), which is

$$c_{\mathrm{a}} = \sqrt{\frac{R_{\mathrm{w}}(0)}{R'_{\mathrm{w}}(0)}}$$

$$= \sqrt{\frac{E_{\mathrm{w}}}{R'_{\mathrm{w}}(0)}}, \tag{7.13}$$

where E_{w} is the total energy of $w(t)$. So calculation of c_{a} requires knowledge of the total energy of $w(t)$, which is difficult to estimate without knowledge of the channel.

Figure 7.6 and figure 7.7 are examples of the standard deviation of error, $\sigma_{\mathrm{MS}}(t)$, assuming c_{a} is equal to 1. Figure 7.6 compares $\sigma_{\mathrm{MS}}(t)$ with different sampling rates, assuming the number of samples used for the estimation is 2. Notice that the peak of each curve is located at the midpoint between the two samples. Figure 7.7 shows another comparison of $\sigma_{\mathrm{MS}}(t)$ with a different number of observations used for the estimation, while the sampling rate is fixed at 2 GHz, assuming the closest samples are used for estimation. The error deviation decreases as the number of observations used increases.

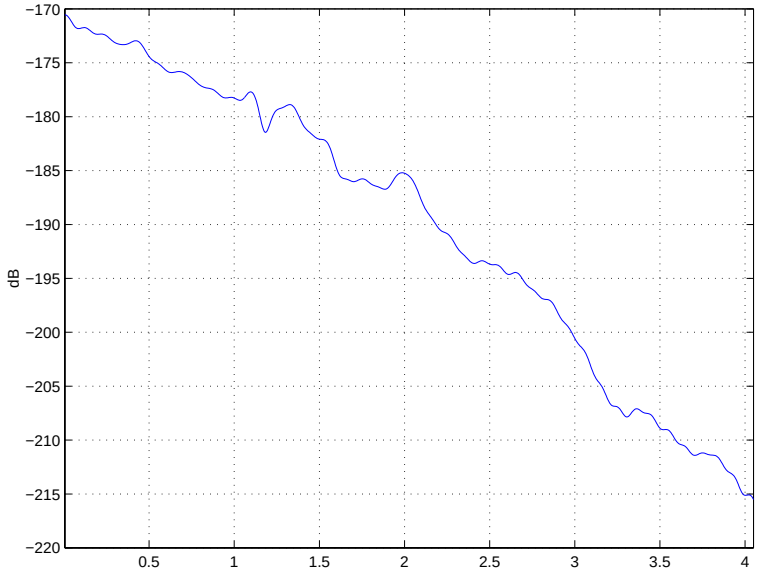

(a) $S_{\mathrm{p}}(f)$

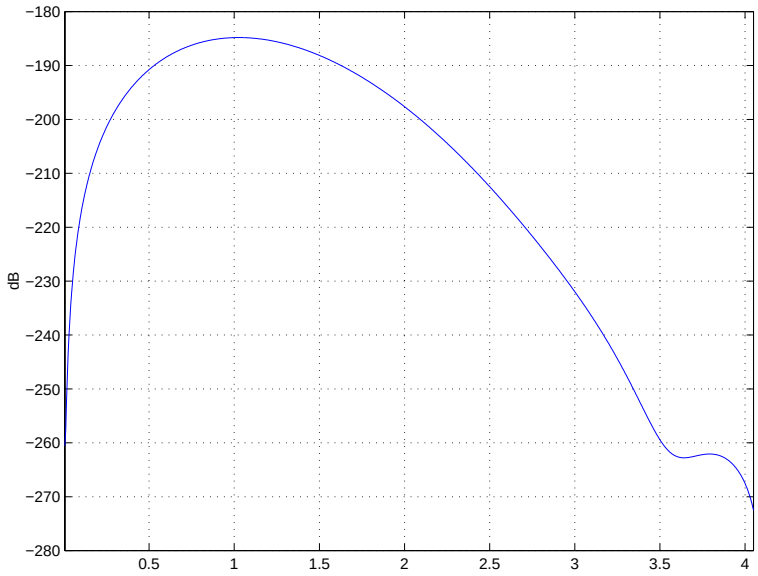

(b) $|U(f)|^2$

Figure 7.4: Spectral density of $p(t)$ and $u(t)$. The template signal $u(t)$ was modeled using $s(t)$ shown in figure 3.1

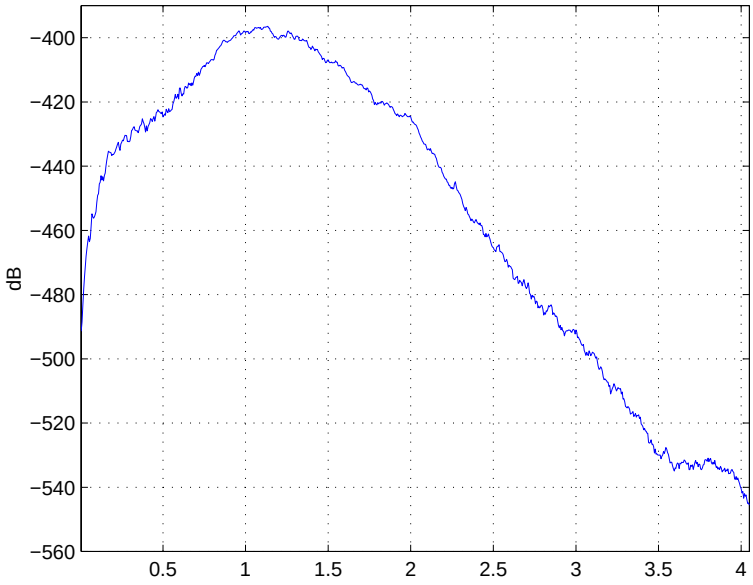

(a) $S'_{\mathrm{w}}(f)$

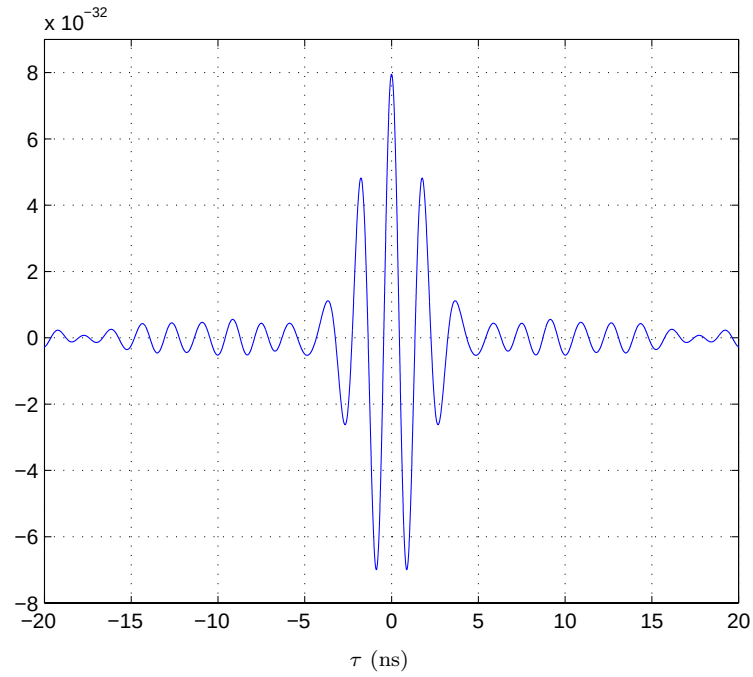

(b) $R'_{\mathrm{w}}(\tau)$

Figure 7.5: Plots of (a) $S'_{\mathrm{w}}(f)$ and (b) $R'_{\mathrm{w}}(\tau)$. $S'_{\mathrm{w}}(f)$ is evaluated by (7.7).

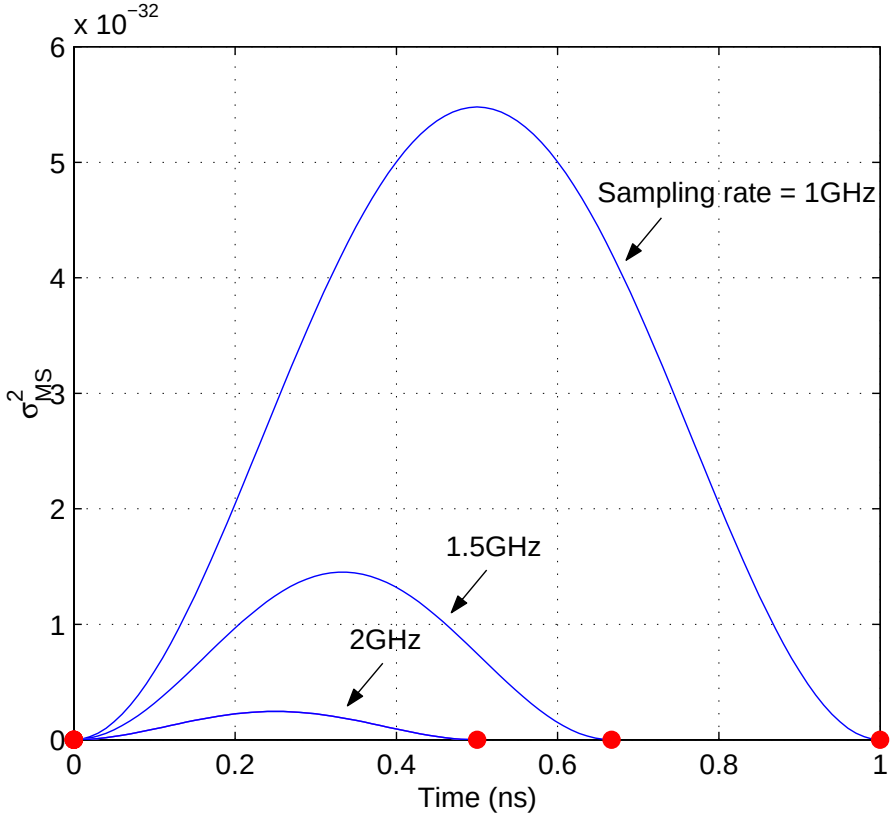

Figure 7.6: Evaluation of error variance in MMSE estimation based on 2 samples. Error variance decreases with sampling rate.

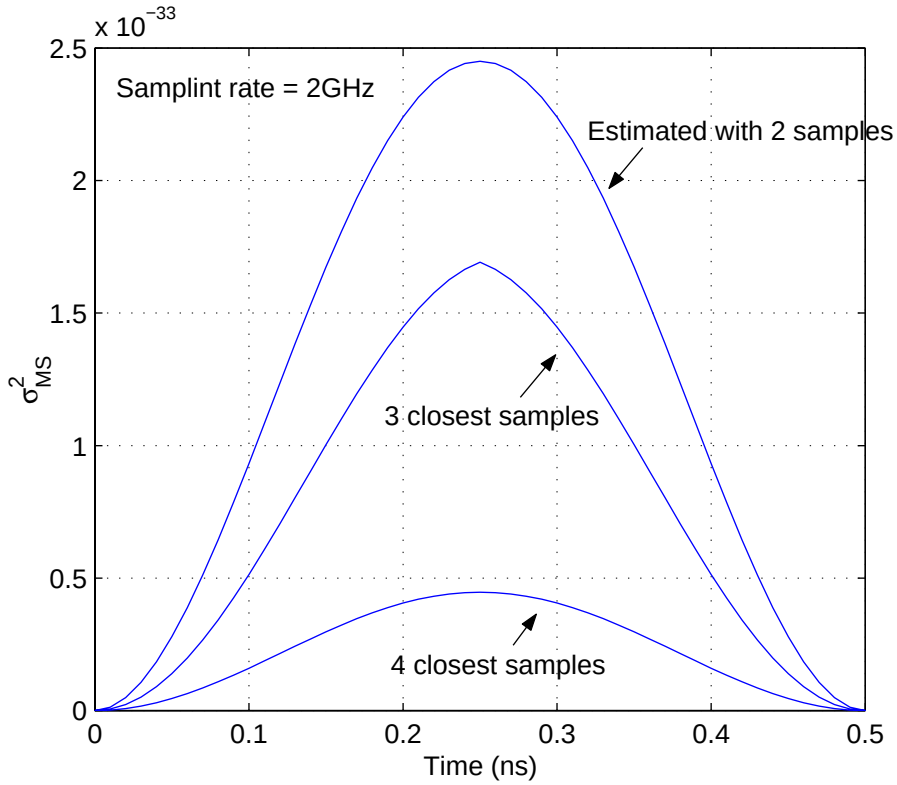

Figure 7.7: Evaluation of error variance in MMSE estimation based on different number of samples. Sampling rate was fixed at 2GHz and it was assumed that estimation was done with given number of closest samples.

Chapter 8

Conclusion

The target of this dissertation was to design a UWB ranging system with a decent multipath immunity for the application in dense multipath environments. A ToA based ranging scheme was adopted and a ranging algorithm for the detection of the direct path signal was developed. A set of propagation data was used for probabilistic analysis related to the ToA algorithm and another set of measurements were made to test the algorithm. The UWB ranging system was designed utilizing the ToA algorithm based on two-way ranging scheme. Thus, this work was composed of two main parts, development of processing algorithm for ToA estimation of the direct path signal and design of the system using this algorithm.

The ToA algorithm introduced in chapter 3 is based on a deterministic assumption, as most multipath resolution techniques developed for narrow band are. So it was developed independently of UWB channel model, even if some statistical information of a few critical parameters were used for threshold setting, and this is why the algorithm does not achieve the optimality. Nevertheless, the search algorithm

based on GML provided a sup-optimal solution and the tests on the measured data showed a reasonable performance in terms of its accuracy. Furthermore, even if there has been similar deterministic approaches for ToA estimation, direct path signal detection using critical parameters of the signal and threshold setting based on a decent statistical model which was acquired from measurement data is one of the novel aspects of this work. A study of ToA measurement using different estimation technology based on a stochastic scenario would be of interest. This work would incorporate modeling of the UWB channel.

The design of the UWB ranging system which consists of two main parts, tracking and sampling, is based on the structure of the UWB scanning receiver system [40] developed at Time Domain. An employment of a parallel receiver instead of a sampling correlator is for the purpose of improving the measurement speed and this is what makes this system distinguishing. The two-way ranging scheme introduced in chapter 6 assumes that the clocks are locked. So the clock synchronization is an important issue for the utilization of this technique and a further study is required.

Reference List

[1] M. Ali, "The system applications of novel methods of location and tracking of cellular mobiles," in *IEE Colloquium on Novel Methods of Location and Tracking of Cellular Mobiles and Their System Applications*, 1999, pp. 6/1–6/4.

[2] David K. Barton, *Radar System Analysis*, Artech, Dedham, 1976.

[3] James L. Caffery and Gordon L. Stuber, "Radio location in urban cdma microcells," *Proceedings of the Personal, Indoor and Mobile Radio Communications (PIMRC '95)*, vol. 2, pp. 858–862, 1995.

[4] Mats Cedervall, "Mobile positioning for third generation WCDMA systems," in *Proc. IEEE 1998 International Conference on Universal Personal Communications (ICUPC '98)*, 1998, vol. 2, pp. 1373–1377.

[5] J. M. Cramer, R. A. Scholtz, and M. Z. Win, "Evaluation of an ultra-wideband propagation channel," *IEEE Transactions on Antennas and Propagation*, 2002, to be published.

[6] J. M. Cramer, M.Z. Win, and R. A. Scholtz, "Evaluation of multipath characteristics of the impulse radio channel," in *Proc. PIMRC '98*, 1998, vol. 2, pp. 864–868.

[7] J. M. Cramer, R. A. Scholtz, and M.Z. Win, "Spatio-temporal diversity in ultra-wideband radio," in *Proc. WCNC '99*, 1999, vol. 2, pp. 888–892.

[8] J. Durbin, "The first passage density of a continuous process to a general boundary," *Jour. Appl. Prob.*, vol. 22, no. 1, pp. 99–122, 1985.

[9] Rebeca Estrada, David Munoz-Rodriguez, Carlos Molina, and Kalyan Basu, "Cellular position location techniques a parameter detection approach," in *Proc. VTC '99*, Jul 1999, vol. 2, pp. 1166–1171.

[10] Meir Feder and Ehud Weinstein, "Parameter estimation of superimposed signals using the EM algorithm," *IEEE Transactions on Acoustics, Speech, and Signal Processing*, vol. 36, no. 4, pp. 477–489, Apr 1988.

[11] Priscilla E. Greenwood and Mikhail S. Nikulin, *A Guide to Chi-Squared Testing*, A Wiley-Interscience Publication, New York, 1975.

[12] Malek G. M. Hussain, "Principles of high-resolution radar based on nonsinusoidal waves - part II : Generalized ambiguity function," *IEEE Transactions on Electrmagnetic Compatibility*, vol. 31, no. 4, pp. 369–375, Nov 1989.

[13] Yangseok Jeong, Heungryeol You, and Chungyong Lee, "Calibration of nlos error for positioning systems," *Proc. VTC '01*, vol. 4, pp. 2605–2608, 2001.

[14] Hiroyuki Kameda, "On the probability distribution of the number of crossings of a certain response level in random vibration," *Mem. Fac. Engrg., Kyoto Univ*, vol. 34, pp. 68–83, 1972.

[15] Joon-Yong Lee and R. A. Scholtz, "Time of arrival estimation of the direct path signal in UWB communications," in *Proc. URSI*, Jan 2001.

[16] Joon-Yong Lee and Robert A. Scholtz, "Ranging in dense multipath environments using an uwb radio link," *IEEE Journal on Selected Areas in Communications*, 2002, Submitted.

[17] E. L. Lehmann, *Nonparametrics: Statistical Methods Based on Ranks*, McGraw-Hill Book Company, San Francisco, 1975.

[18] Jian Li and Renbiao Wu, "An efficient algorithm for time delay estimation," *IEEE Transactions on Signal Processing*, vol. 46, no. 8, pp. 2231–2235, 1998.

[19] W.C. Lindsey and M.K. Simon, *Phase and doppler measurements in two-way phase-coherent tracking systmes*, Dover Pubs, 1991.

[20] Tom Logsdon, *Understanding the NAVSTAR: GPS, GIS, and IVHS*, Van Norstrand Reinhold, New York, 2nd edition, 1995.

[21] T. G. Manickam, R. J. Vaccaro, and D. W. Tufts, "A least-squares algorithm for multipath time-delay estimation," *IEEE Transactions on Signal Processing*, vol. 42, no. 11, pp. 3229–3233, Nov. 1994.

[22] Robert J. Marks II, *Introduction to Shannon Sampling And Interpolation Theory*, Springer-Verlag New York Inc., New York, 1991.

[23] G. G. Messier and J. S. Nielsen, "An analysis of TOA-based location for IS-95 mobiles," in *Proc. VTC '99*, 1999, vol. 2, pp. 1067 –1071.

[24] T. L. Mikhaleva and V. I. Piterbarg, "On the distribution of the maximum of a gaussian field with constant variance on a smooth manifold," *Theory Prob. Appl.*, vol. 41, no. 2, pp. 1650–1654, 1996.

[25] Kaveh Pahlavan, Prashant Krishnamurthy, and Jacques Beneat, "Wideband radio propagation modeling for indoor geolocation applications," *IEEE Communications Magazine*, vol. 36, no. 4, pp. 60–65, April 1998.

[26] Jr Peyton Z. Peebles, *Radar Principles*, Wiley Interscience Publication, New York, 1998.

[27] L.P. Remmerswaal and D. Van Willigen, "Some aspects of interferenc on Loran-C," *IEE Proceedings*, vol. 136, no. 3, pp. 109–117, June 1989.

[28] James R. Rice, "First-occurrence time of high-level crossings in a continuous random process," *Jour. Acoust. Soc. Amr.*, vol. 39, no. 2, pp. 323–335, 1966.

[29] Harri Saarnisaari, "TLS-ESPRIT in a time dealy estimation," in *Proc. VTC '97*, 1997, vol. 3, pp. 1619–1623.

[30] H. G. Schantz and L. Fullerton, "The diamond dipole: A gaussian impulse antenna," in *Proceedings of the 2001 IEEE AP-S International Symposium*, Boston, July 2001.

[31] R. A. Scholtz et al., "UWB radio deployment challenges," in *Proc. Personal, Indoor and Mobile Radio Communications (PIMRC 2000)*, 2000, vol. 1, pp. 620–625.

[32] M. I. Silventoinen and T. Rantalainen, "Mobile station emergency locaing in gsm," *IEEE International Conference on Personal Wireless Communications*, pp. 232–238, February 1996.

[33] Merrill I. Skolnik, *Radar Handbook*, McGraw-Hill Book Company, New York, 1970.

[34] M. Oguz Sunay and Ibrahim Tekin, "Mobile location tracking in DS CDMA networks using forward link time difference of arrival and its application to zone-based billing," in *Proc. GLOBECOM '99*, 1999, vol. 1a, pp. 143–147.

[35] Eric Villier, Luis Lopes, and Brendan Ludden, "Performance of a handset-assisted positioning method for GSM," in *Proc. VTC '99*, 1999, vol. 3, pp. 1967 –1972.

[36] Owen Wilkes and Nils Petter Gleditsch, *Loran-C and Omega*, Norwegian University Press, 1987.

[37] M. Z. Win and R. A. Scholtz, "Ultra-wide bandwidth time-hopping spread-spectrum impulse radio for wireless multiple-access communications," *IEEE Transactions on Communications*, vol. 48, no. 4, pp. 679–689, Apr 2000.

[38] M. Z. Win and R. A. Scholtz, "Energy capture vs. correlator resources in ultra-wide bandwidth indoor wireless communications channels," in *Proc. Milcom '97*, Nov 1997.

[39] M.Z. Win and R. A. Scholtz, "Ultra-wide bandwidth signal propagation for indoor wireless communications," in *Proc. ICC '97*, Jun 1997.

[40] P. Withington, R. Reinhardt, and R. Stanley, "Preliminary results of an ultra-wideband (impulse) scanning receiver," in *Proc. MILCOM '99*, 1999, vol. 2, pp. 1186–1190.

[41] Sung-Shik Woo, Heung-Ryeol You, and Jong-Seog Koh, "The nlos technique for position location using is-95 cdma networks," in *Proc. VTC '00*, 2000, vol. 6, pp. 2556 – 2560.

[42] Marilynn P. Wylie and Jack Holtzman, "The non-line of sight problem in mobile location estimation," *IEEE International Conference on Universal Personal Communications*, vol. 2, pp. 827–831, 1996.

[43] Ilan Ziskind and Mati Wax, "Maximum likelihood localization of multiple sources by alternating projection," *IEEE Transactions on Acoustics, Speech, and Signal Processing*, vol. 36, no. 10, pp. 1553–1560, 1988.

Appendix A

Evaluation of High Level Crossing Probability of a Continuous Random Process

In (4.22), $\Pr\{\sup_{\beta\in[-\theta_\delta,-\delta-T_\mathrm{p})} \boldsymbol{u}(\beta) > \gamma\}$ can be evaluated by computing the level crossing probability of the random process $\boldsymbol{u}(\beta)$ at a given level γ. This problem has been studied [28, 14, 8, 24] with different assumptions about the random process. We look for the probability that the random process $\boldsymbol{u}(\beta)$ crosses the level γ within the time period $\beta \in [-\theta_\delta, -\delta - T_\mathrm{p})$, assumming that $\boldsymbol{u}(-\theta_\delta) < \gamma$. The random process $\boldsymbol{u}(\beta)$ is colored gaussian process whose autocorrelation function satisfies

$$R_{\boldsymbol{u}}(\tau) = 0, \text{ if } |\tau| > T_\mathrm{p}. \tag{A.1}$$

Since $\boldsymbol{u}(\beta)$ is a stationary process, it also satisfies

$$Pr\{\sup_{\beta\in[-\theta_\delta,-\delta-T_\mathrm{p})} \boldsymbol{u}(\beta) > \gamma\} = Pr\{\sup_{\beta\in[0,\theta_\delta-\delta-T_\mathrm{p})} \boldsymbol{u}(\beta) > \gamma\}, \tag{A.2}$$

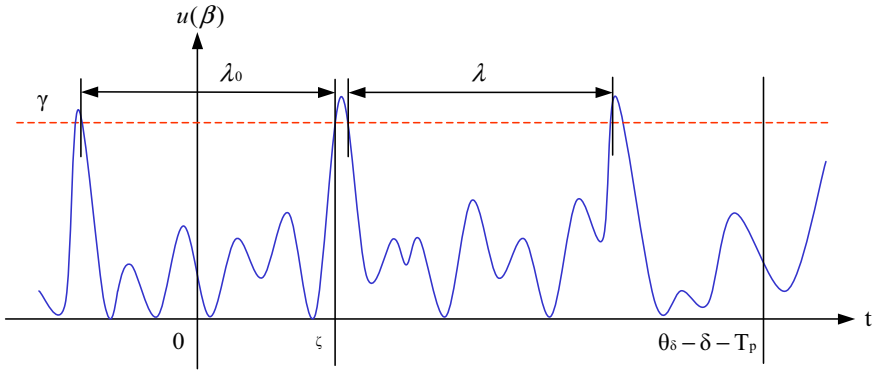

Figure A.1: Evaluation of level crossing probability. λ denotes the time between successive down-crossing and up-crossing and ζ is the first occurrence time.

where $\boldsymbol{u}(0) < \gamma$.

Let's define $\zeta(> 0)$ as the time of the first occurrence of crossing at $\boldsymbol{u}(\beta) = \gamma$ and $\boldsymbol{\lambda}$ as the time between successive down-crossing and up-crossing. (See figure A.1.) The quantitiy $\boldsymbol{\lambda}_0$ denotes the time interval between a down-crossing and the next adjacent up-crossing which contains the origin. Assuming the time of a down-crossing is uniformly distributed along the time axis, probability that the origin belongs to an interval between successive down-crossing and up-crossing with a length of λ_0 is proportional to λ_0. So PDF of $\boldsymbol{\lambda}_0$ satisfies

$$f_{\boldsymbol{\lambda}_0}(\lambda_0) \propto \lambda_0 \cdot f_{\boldsymbol{\lambda}}(\lambda_0). \tag{A.3}$$

Normalizing (A.3),

$$f_{\boldsymbol{\lambda}_0}(\lambda_0) \;=\; \frac{\lambda_0 \cdot f_{\boldsymbol{\lambda}}(\lambda_0)}{\int_0^\infty \lambda \cdot f_{\boldsymbol{\lambda}}(\lambda) d\lambda}$$

$$= \frac{\lambda_0 \cdot f_{\boldsymbol{\lambda}}(\lambda_0)}{E(\boldsymbol{\lambda})}, \tag{A.4}$$

where $E(\boldsymbol{\lambda})$ is the expected value of $\boldsymbol{\lambda}$. Considering the uniformity of location of the origin in the interval $\boldsymbol{\lambda_0}$,

$$f_{\boldsymbol{\zeta}}(\zeta \mid \boldsymbol{\lambda_0} = \lambda_0) = \begin{cases} 1/\lambda_0, & \text{if } \zeta < \lambda_0 \\ 0, & \text{otherwise} \end{cases} \tag{A.5}$$

Using (A.4) and (A.5), $f_{\boldsymbol{\zeta}}(\zeta)$ is given by

$$\begin{aligned} f_{\boldsymbol{\zeta}}(\zeta) &= \int_0^\infty f_{\boldsymbol{\zeta}}(\zeta|\boldsymbol{\lambda_0} = \lambda_0) \cdot f_{\boldsymbol{\lambda_0}}(\lambda_0) d\lambda_0 \\ &= \int_\zeta^\infty \frac{1}{\lambda_0} \frac{\lambda_0}{E(\boldsymbol{\lambda})} f_{\boldsymbol{\lambda}}(\lambda_0) d\lambda_0 \\ &= \frac{1}{E(\boldsymbol{\lambda})}[1 - \int_0^\zeta f_{\boldsymbol{\lambda}}(\lambda_0) d\lambda_0]. \end{aligned} \tag{A.6}$$

Let's assume that

$$\boldsymbol{\zeta} > T_{\mathrm{p}}, \tag{A.7}$$

then the first occurrence time is not affected by the past history of $\boldsymbol{u}(\beta)$, which means its distribution has memoryless character. So $f_{\boldsymbol{\zeta}}(\zeta)$ satisfies

$$f_{\boldsymbol{\zeta}}(\zeta) = f_{\boldsymbol{\lambda}}(\zeta). \tag{A.8}$$

Substituting (A.8) into (A.6),

$$f_{\boldsymbol{\zeta}}(\zeta) = \frac{1}{E(\boldsymbol{\lambda})}[1 - \int_0^{\zeta} f_{\boldsymbol{\zeta}}(\lambda_0)d\lambda_0]. \tag{A.9}$$

Solving the integral equation (A.9),

$$f_{\boldsymbol{\zeta}}(\zeta) = \frac{1}{E(\boldsymbol{\lambda})}e^{-\zeta/E(\boldsymbol{\lambda})}. \tag{A.10}$$

So the level crossing probability that we desire is equivalent to

$$\begin{aligned} Pr\{\sup_{\beta\in[0,\theta_\delta-\delta-T_{\rm p})} \boldsymbol{u}(\beta) > \gamma | \boldsymbol{u}(0) < \gamma\} &= Pr(0 \le \zeta \le \theta_\delta - \delta - T_{\rm p} | \boldsymbol{u}(0) < \gamma) \\ &= \int_0^{\theta_\delta-\delta-T_{\rm p}} f_{\boldsymbol{\zeta}}(\zeta)d\zeta \\ &= 1 - e^{-(\theta_\delta-\delta-T_{\rm p})/E(\boldsymbol{\lambda})}. \end{aligned} \tag{A.11}$$

Appendix B

UWB Ambiguity Function

B.1 Derivation UWB Ambiguity Function

In a narrow-band system, the ambiguity function has two parameters [33] representing time mismatch at the matched filter and frequency mismatch caused by the doppler frequency offset related to radial velocity uncertainties. In defining the UWB ambiguity function, doppler frequency offset is not considered due to the absence of a carrier. Instead, we consider a scaling factor caused by the offset in the radial velocities. Let's assume a signal $s_{\mathrm{t}}(t)$ is transmitted by the transmitter, which is

$$s_{\mathrm{t}}(t) = A_{\mathrm{t}} s(t), \tag{B.1}$$

where A_{t} is the amplitude of the signal. The transmitted signal is then time delayed by τ_{r} and time scaled by α due to the radial velocity. The received signal $s_{\mathrm{r}}(t)$ can be represented by

$$s_{\mathrm{r}}(t) = A_{\mathrm{r}} s\Big(\alpha(t-\tau_{\mathrm{r}})\Big), \tag{B.2}$$

where A_{r} is the amplitude of received signal. At the receiver, the received signal is matched filtered to signal $s\mathrm{m}(t)$, which is

$$s_{\mathrm{m}}(t) = A_{\mathrm{m}} s(t-\tau_{\mathrm{m}}), \tag{B.3}$$

and the matched filter output $z(t)$ is given by

$$\begin{aligned} z(t) &= A_{\mathrm{r}}A_{\mathrm{m}} \int_{-\infty}^{\infty} s(t-\tau_{\mathrm{m}}) s\Big(\alpha(t-\tau_{\mathrm{r}})\Big) dt \\ &= A_{\mathrm{r}}A_{\mathrm{m}} \int_{-\infty}^{\infty} s(t) s\Big(\alpha(t-(\tau_{\mathrm{r}}-\tau_{\mathrm{m}}))\Big) dt \\ &= A_{\mathrm{r}}A_{\mathrm{m}} \int_{-\infty}^{\infty} s(t) s\Big(\alpha(t-\tau)\Big) dt \\ &= \frac{A_{\mathrm{r}}A_{\mathrm{m}}}{\sqrt{\alpha}} \underbrace{\int_{-\infty}^{\infty} \sqrt{\alpha} s(t) s\Big(\alpha(t-\tau)\Big) dt}_{\mathrm{Ambiguityfunction}}, \end{aligned} \tag{B.4}$$

where

$$\tau = \tau_{\mathrm{r}} - \tau_{\mathrm{m}}. \tag{B.5}$$

UWB ambiguity function, namely $\chi_{\mathrm{u}}(\tau, \alpha)$, can be defined as

$$\chi_{\mathrm{u}}(\tau, \alpha) = \int_{-\infty}^{\infty} \sqrt{\alpha} s(t) s(\alpha(t - \tau)) dt, \tag{B.6}$$

where $\sqrt{\alpha}$ is for normalization so that the signal energy is kept constant. As for the conventional narrow-band ambiguity function, the UWB ambiguity function satisfies

$$\chi_{\mathrm{u}}(\tau, \alpha) \leq \chi_{\mathrm{u}}(0, 1) = E_{\mathrm{s}}, \tag{B.7}$$

where E_{s} denotes the energy of $s(t)$. If α is equal to 1, $\chi_{\mathrm{u}}(\tau, \alpha)$ can be interpreted as the auto-correlation function of $s(t)$.

The function $\chi_{\mathrm{u}}(\tau, \alpha)$ can be expanded near $(0, 1)$ using Taylor series expansion, which is

$$\begin{aligned} \chi_{\mathrm{u}}(\tau, \alpha) = \chi_{\mathrm{u}}(0, 1)[1 + A_\tau \tau + A_\alpha(\alpha - 1) + \frac{1}{2} B_\tau \tau^2 + \frac{1}{2} B_\alpha (\alpha - 1)^2 \\ + \frac{1}{2} B_{\tau\alpha} \tau (\alpha - 1)], \end{aligned} \tag{B.8}$$

where A_τ, A_α, B_τ, B_α, and $B_{\tau\alpha}$ are defined as

$$\begin{cases} A_\tau &= \dfrac{1}{\chi_{\rm u}(0,1)}\dfrac{\partial}{\partial\tau}\chi_{\rm u}(\tau,\alpha)\Big|_{\tau=0,\alpha=1}, \\ A_\alpha &= \dfrac{1}{\chi_{\rm u}(0,1)}\dfrac{\partial}{\partial\alpha}\chi_{\rm u}(\tau,\alpha)\Big|_{\tau=0,\alpha=1}, \\ B_\tau &= \dfrac{1}{\chi_{\rm u}(0,1)}\dfrac{\partial^2}{\partial\tau^2}\chi_{\rm u}(\tau,\alpha)\Big|_{\tau=0,\alpha=1}, \\ B_\alpha &= \dfrac{1}{\chi_{\rm u}(0,1)}\dfrac{\partial^2}{\partial\alpha^2}\chi_{\rm u}(\tau,\alpha)\Big|_{\tau=0,\alpha=1}, \\ B_{\tau\alpha} &= \dfrac{1}{\chi_{\rm u}(0,1)}\dfrac{\partial^2}{\partial\tau\partial\alpha}\chi_{\rm u}(\tau,\alpha)\Big|_{\tau=0,\alpha=1}. \end{cases} \tag{B.9}$$

The coefficients A_τ and A_α can be evaluated by

$$\begin{aligned} A_\tau &= \frac{1}{\chi_{\rm u}(0,1)}\frac{\partial}{\partial\tau}\int_{-\infty}^{\infty}\sqrt{\alpha}s(t)s(\alpha(t-\tau))dt\Big|_{\tau=0,\alpha=1} \\ &= -\frac{1}{\chi_{\rm u}(0,1)}\int_{-\infty}^{\infty}\alpha\sqrt{\alpha}s(t)s'(\alpha(t-\tau))dt\Big|_{\tau=0,\alpha=1} \\ &= -\frac{1}{\chi_{\rm u}(0,1)}\int_{-\infty}^{\infty}s(t)s'(t)dt \\ &= -\frac{1}{\chi_{\rm u}(0,1)}\left[\frac{1}{2}s^2(t)\right]_{-\infty}^{\infty} \\ &= 0, \end{aligned} \tag{B.10}$$

$$\begin{aligned} A_\alpha &= \frac{1}{\chi_{\rm u}(0,1)}\frac{\partial}{\partial\alpha}\int_{-\infty}^{\infty}\sqrt{\alpha}s(t)s(\alpha(t-\tau))dt\Big|_{\tau=0,\alpha=1} \\ &= \frac{1}{\chi_{\rm u}(0,1)}\int_{-\infty}^{\infty}s(t)\left[\frac{1}{2\sqrt{\alpha}}s(\alpha(t-\tau))+\sqrt{\alpha}(t-\tau)s'(\alpha(t-\tau))\right]dt\Big|_{\tau=0,\alpha=1} \\ &= \frac{1}{\chi_{\rm u}(0,1)}\int_{-\infty}^{\infty}\frac{1}{2}s^2(t)dt+\frac{1}{\chi_{\rm u}(0,1)}\int_{-\infty}^{\infty}ts(t)s'(t)dt \\ &= \frac{1}{\chi_{\rm u}(0,1)}\left[\frac{1}{2}ts^2(t)\right]_{-\infty}^{\infty} \end{aligned}$$

$$= \quad 0. \tag{B.11}$$

According to (B.10) and (B.11), the coefficients of the first order terms are 0 if the pulse is time limited. The coefficients of the second order terms B_τ, B_α, and $B_{\tau\alpha}$ can be evaluated by computing the second order partial derivatives of $\chi_{\mathrm{u}}(\tau,\alpha)$, which are

$$\begin{aligned}
B_\tau &= \frac{1}{\chi_{\mathrm{u}}(0,1)}\frac{\partial^2}{\partial\tau^2}\int_{-\infty}^{\infty}\sqrt{\alpha}s(t)s(\alpha(t-\tau))dt\Big|_{\tau=0,\alpha=1} \\
&= \frac{1}{\chi_{\mathrm{u}}(0,1)}\int_{-\infty}^{\infty}\alpha^2\sqrt{\alpha}s(t)s(t)''(\alpha(t-\tau))dt\Big|_{\tau=0,\alpha=1} \\
&= \frac{1}{\chi_{\mathrm{u}}(0,1)}\int_{-\infty}^{\infty}s(t)s(t)''dt \\
&= -\frac{1}{\chi_{\mathrm{u}}(0,1)}\int_{-\infty}^{\infty}(2\pi f)^2|S(f)|^2df,
\end{aligned} \tag{B.12}$$

$$\begin{aligned}
B_\alpha &= \frac{1}{\chi_{\mathrm{u}}(0,1)}\frac{\partial^2}{\partial\alpha^2}\int_{-\infty}^{\infty}\sqrt{\alpha}s(t)s(\alpha(t-\tau))dt\Big|_{\tau=0,\alpha=1} \\
&= \frac{1}{\chi_{\mathrm{u}}(0,1)}\int_{-\infty}^{\infty}s(t)\Big[-\frac{1}{4\alpha\sqrt{\alpha}}s(\alpha(t-\tau))+\frac{1}{\sqrt{\alpha}}(t-\tau)s'(\alpha(t-\tau)) \\
&\quad +(t-\tau)^2\sqrt{\alpha}s''(\alpha(t-\tau))\Big]dt\Big|_{\tau=0,\alpha=1} \\
&= \frac{1}{\chi_{\mathrm{u}}(0,1)}\Big[-\frac{1}{4}\int_{-\infty}^{\infty}s^2(t)dt+\int_{-\infty}^{\infty}ts'(t)s(t)dt+\int_{-\infty}^{\infty}t^2s''(t)s(t)dt\Big] \\
&= \frac{1}{\chi_{\mathrm{u}}(0,1)}\Big[-\frac{1}{4}\int_{-\infty}^{\infty}s^2(t)dt+\Big[\frac{1}{2}ts^2(t)\Big]_{-\infty}^{\infty}-\frac{1}{2}\int_{-\infty}^{\infty}s^2(t)dt \\
&\quad +\int_{-\infty}^{\infty}t^2s''(t)s(t)dt\Big] \\
&= \frac{1}{\chi_{\mathrm{u}}(0,1)}\Big[-\frac{3E_{\mathrm{s}}}{4}+\int_{-\infty}^{\infty}t^2s(t)s''(t)dt\Big],
\end{aligned} \tag{B.13}$$

$$
\begin{aligned}
B_{\tau\alpha} &= \frac{1}{\chi_{\mathrm{u}}(0,1)}\frac{\partial^2}{\partial\tau\partial\alpha}\int_{-\infty}^{\infty}\sqrt{\alpha}s(t)s(\alpha(t-\tau))dt\Big|_{\tau=0,\alpha=1} \\
&= \frac{1}{\chi_{\mathrm{u}}(0,1)}\int_{-\infty}^{\infty}s(t)\Big[-\frac{3}{2}\sqrt{\alpha}s'(\alpha(t-\tau))-\alpha\sqrt{\alpha}(t-\tau)s''(\alpha(t-\tau))\Big]dt\Big|_{\tau=0,\alpha=1} \\
&= \frac{1}{\chi_{\mathrm{u}}(0,1)}\Big[-\frac{3}{2}\int_{-\infty}^{\infty}s(t)s'(t)dt-\int_{-\infty}^{\infty}ts(t)s'(t)dt\Big] \\
&= -\frac{1}{\chi_{\mathrm{u}}(0,1)}\int_{-\infty}^{\infty}ts(t)s''(t)dt. \qquad \text{(B.14)}
\end{aligned}
$$

If we define the effective bandwidth B_{eff} as

$$
B_{\mathrm{eff}} = \Big[\int_{-\infty}^{\infty}(2\pi f)^2|S(f)|^2df\Big]^{\frac{1}{2}}, \qquad \text{(B.15)}
$$

then B_τ can be interpreted as a function of bandwidth, which is

$$
B_\tau = -\frac{1}{\chi_{\mathrm{u}}(0,1)}B_{\mathrm{eff}}^2. \qquad \text{(B.16)}
$$

B.2 Computer Plots of UWB Ambiguity functions

In this section, UWB ambiguity functions with different formats are evaluated using computer simulations. The UWB pulse $s(t)$ was assumed to be the one which was modeled in (3.2). (See figure 3.1.) Figure B.1 shows the ambiguity function of a single UWB pulse. Considering the scale of potential mismatch in the radial velocities, the velocity resolution is not very good, while the time resolution is very

fine and the shape of resulting ambiguity function of a single UWB pulse can be classified as the knife-edge type.

Suppose the UWB ranging system transmits and receives a train of pulses. Because of the absence of a common clock, there may exist mismatch in the clock periods of the transmitter and receiver. The order of the clock period mismatch can be possibly as large as 0.1%, which is considerable compared to the the mismatch caused by typical radial velocity uncertainties. So we can ignore the velocity mismatch and instead, consider the clock misalignment or drift as the second factor of the UWB ambiguity function. The UWB ambiguity function of a train of N_{p} periodic pulses are given by

$$\chi_{\mathrm{u}}(\tau,\alpha)=\int_{-\infty}^{\infty}\sum_{i=1}^{N_{\mathrm{p}}-1}\sum_{j=1}^{N_{\mathrm{p}}-1}s(t-iT_{\mathrm{f}})s(t-j\alpha T_{\mathrm{f}})dt, \tag{B.17}$$

where T_{f} is the clock period and α is the scaling factor due to the clock period differences, which is equal to

$$\alpha=\frac{T_{\mathrm{f}}}{T_{\mathrm{f}}+T_{\mathrm{d}}}, \tag{B.18}$$

where T_{d} denotes the clock period mismatch. Detailed evaluation of the ambiguity function of the periodic gaussian pulses is given in [12] and figure B.2 is a simulated ambiguity function. The number of pulses was assumed to be 64 and pulse repetition rate is 10 Mpps. We can still measure the range with a fine resolution but with an

ambiguity and the clock frequency resolution is also fine considering its scale. Figure B.3 is the ambiguity function of a train of time hopped pulses, which is represented by

$$s_{\text{hop}}(t) = \sum_{j=0}^{N_{\text{p}}-1} s\left(t - jT_{\text{f}} - c_j(u)T_{\text{c}} + \frac{(N_{\text{p}}-1)T_{\text{f}}}{2}\right) \tag{B.19}$$

where N_{p} is the total number of pulses and T_{f} and T_{c} denote frame time and chip time, respectively. The time hopping sequence $\{c_j(u)\}$ satisfies

$$0 \leq c_j(u) \leq N_h - 1. \tag{B.20}$$

It was assumed that $N_{\text{p}} = 64$, $N_{\text{h}} = 16$, $T_{\text{f}} = 100$ ns, and $T_{\text{c}} = 2$ ns. Figure B.4 shows ambiguity function another time-hopped pulses with $N_{\text{h}} = 32$, which is more smoothly spread than the plot shown in figure B.3, since the fraction of the frame time over which time-hopping is allowed is larger.

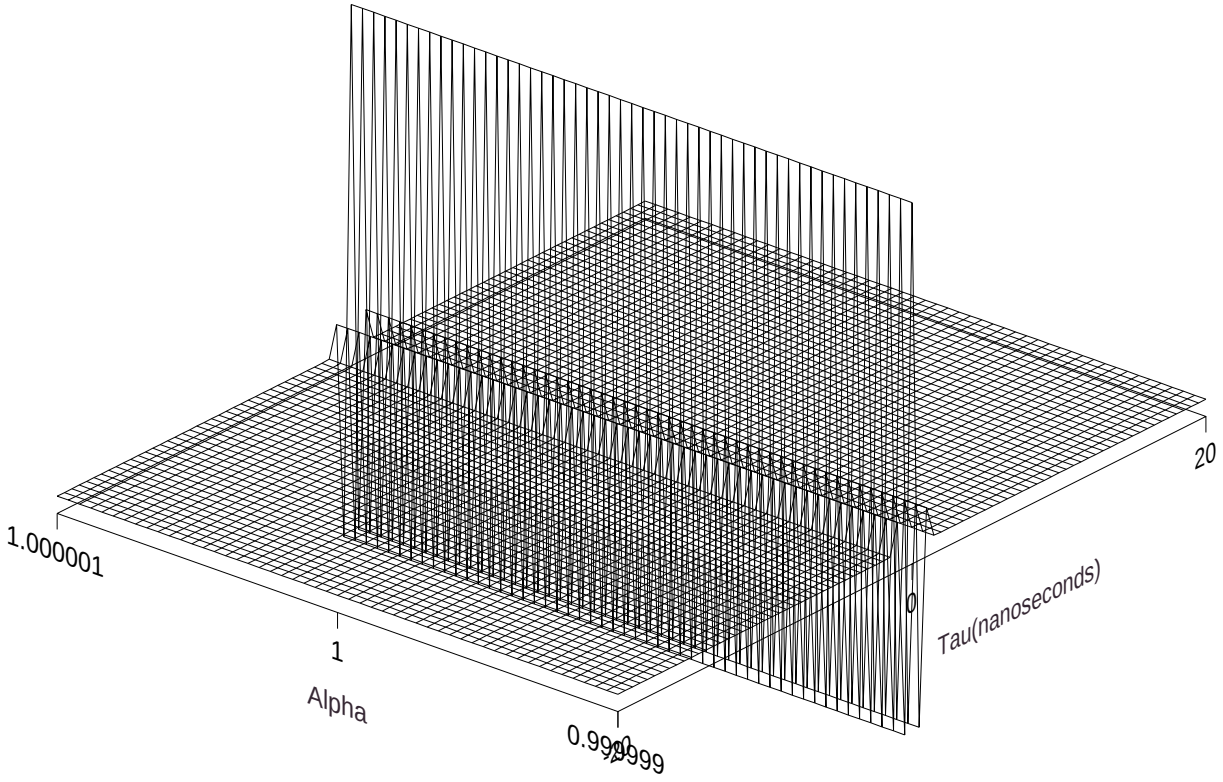

Figure B.1: UWB ambiguity function of a single pulse.

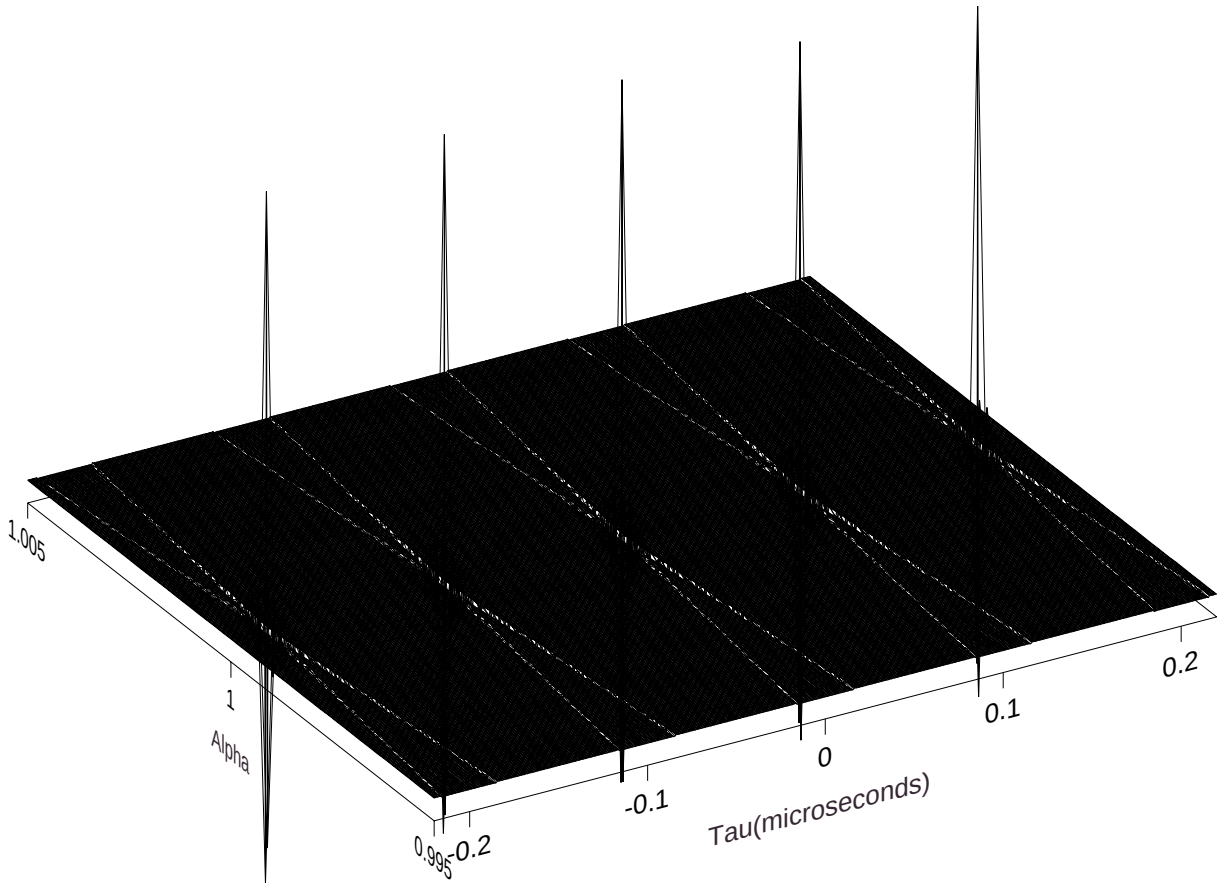

Figure B.2: UWB ambiguity function of a periodic train of 64 pulses. The pulse repetition rate is 10 Mpps.

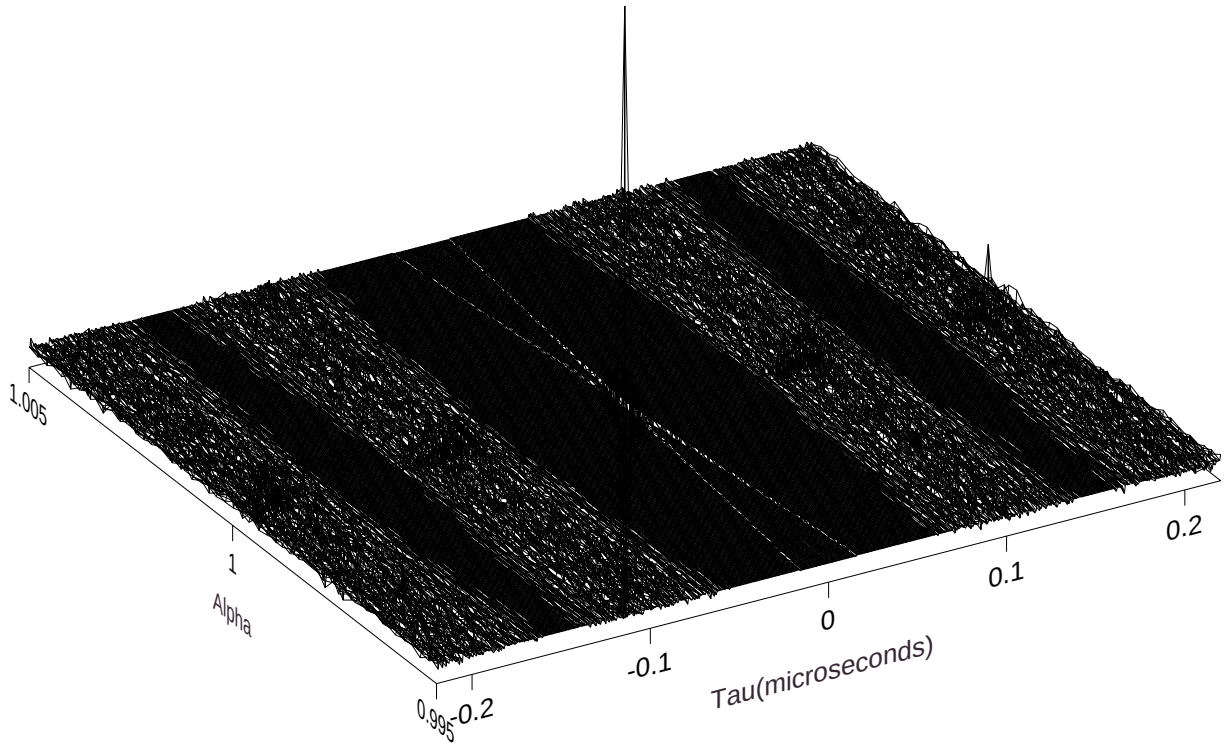

Figure B.3: UWB ambiguity function of 64 time hopped pulses with $N_{\mathrm{h}} = 16$, $T_{\mathrm{f}} = 100$ ns, and $T_{\mathrm{c}} = 2$ ns.

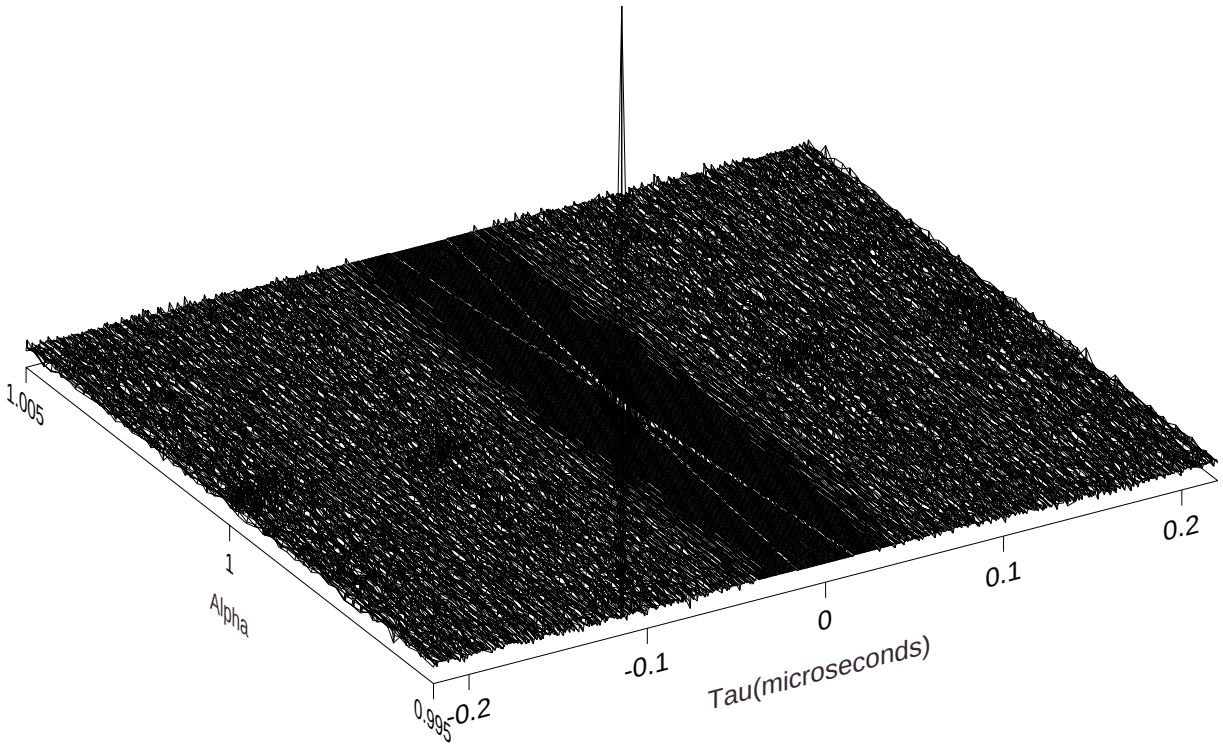

Figure B.4: UWB ambiguity function of 64 time hopped pulses with $N_{\mathrm{h}} = 32$, $T_{\mathrm{f}} = 100$ ns, and $T_{\mathrm{c}} = 2$ ns.

Appendix C

Maximum A Posteriori Estimation for ToA Measurement: Two-Path Model

C.1 Introduction

In chapter 3, time of arrival of the direct path signal was estimated using generalized maximum likelihood (GML) estimation. In this Appendix, ToA estimation using maximum a posteriori (MAP) estimation is presented. Complete evaluation using MAP estimation requires a reasonable model of UWB channel, which is not currently available. Estimation using a simple two-path model is presented to initiate the discussion.

In (3.12), the observation vector $\underline{r}$ was represented by the sum of the direct path signal, multipath signals up to the arrival of the peak path, and white gaussian noise. If M is equal to 0, then $\delta = 0$, $\rho = 1$, and $\underline{r}$ is equivalent to

$$\underline{r} = \underline{s}_0 + \underline{n}. \tag{C.1}$$

When M is greater than 0, then $\underline{r}$ can be represented by

$$\begin{aligned} \underline{r} &= \rho \underline{s}_{\delta} + \sum_{k=1}^{M} \alpha_k \underline{s}_{\beta_k} + \underline{n} \\ &= \rho \underline{s}_{\delta} + \sum_{k=1}^{M'} \alpha_k \underline{s}_{\beta_k} + \underline{s}_0 + \underline{n}, \end{aligned} \tag{C.2}$$

where $M' = M - 1$ and $M' \geq 0$. The second term in (C.2 represents the reflected signals which arrive between the direct path and the peak path and is ignored when M' is equal to 0. Define the inter-arrival time β'_k as

$$\begin{cases} \beta'_k &= \beta_{k-1} - \beta_k, \ i \geq 1 \\ \beta'_1 &= \delta - \beta_1. \end{cases} \tag{C.3}$$

Then (C.2) is equivalent to

$$\underline{r} = \rho \underline{s}_{\delta} + \sum_{k=1}^{M'} \alpha_k \underline{s}_{[\delta - \sum_{i=1}^{k} \beta'_i]} + \underline{s}_0 + \underline{n}. \tag{C.4}$$

Let's define hypothesis H_0 and H_1 as

$$\begin{cases} H_0 : \delta = 0 \text{ and } \rho = 1, \\ H_1 : \delta \neq 0 \text{ and } \rho \neq 1. \end{cases} \tag{C.5}$$

Then given an observation $\underline{r}$, we can establish a hypothesis test,

$$\begin{cases} \text{Accept } H_0, \text{ if } f(\underline{r}|H_0)p_0 > f(\underline{r}|H_1)(1-p_0) \\ \text{Accept } H_1, \text{ otherwise,} \end{cases} \tag{C.6}$$

where p_0 is as defined in (4.1). The probability density function $f(\underline{r}|H_0)$ is a gaussian density and $f(\underline{r}|H_1)$ can be evaluated by

$$\begin{aligned} f(\underline{r}|H_1) &= \sum_{m=1}^{\infty} \int \cdots \int f(\underline{r}|\delta, \rho, \underline{\alpha}, \underline{\beta}', M' = m) f(\delta, \rho, \underline{\alpha}, \underline{\beta}', m|\rho, \delta) \\ &\quad \cdot f(\rho) f(\delta)\ d\underline{\alpha} d\underline{\beta}' d\rho d\delta. \end{aligned} \tag{C.7}$$

If the hypothesis H_0 is accepted, then the estimate of δ is equal to 0, while if H_1 is accepted $\hat{\delta}$ is evaluated by computing

$$\begin{aligned} \hat{\delta} &= \arg\max_{\delta} f(\underline{r}|\delta) f(\delta|\delta \neq 0) \\ &= \sum_{m=1}^{\infty} \int \cdots \int f(\underline{r}|\rho, \delta, \underline{\alpha}, \underline{\beta}', M' = m) f(\rho, \delta, \underline{\alpha}, \underline{\beta}', M'|\rho, \delta) f(\rho) \\ &\quad \cdot f(\delta)\ d\underline{\alpha} d\underline{\beta}' d\rho \cdot \Pr(M' = m|\boldsymbol{\delta} = \delta). \end{aligned} \tag{C.8}$$

Estimation using maximum likelihood requires the probability density function $f(\rho, \delta, \underline{\alpha}, \underline{\beta}', M'|\rho, \delta)$, which is the channel model for the paths which arrive between the direct path and the peak path. Even if this PDF was available, analytical evaluation of multiple the integrals appearing in (C.8) would be very challenging. Here we present a ML estimation approach to ToA estimation using a simple two

path model, which assumes there is no signal component between the direct path signal and the peak.

C.2 ToA Estimation Using a Two-Path Model

Let's assume M' is equal to 0 in (C.2), then the received signal can be represented by

$$\underline{r} = \rho \underline{s}_\delta + \underline{s}_0 + \underline{n}, \tag{C.9}$$

where $\underline{r}$ is modeled as a sum of the direct path signal, peak path signal, and the noise. Then MAP estimate of δ is given by

$$\begin{aligned} \hat{\delta} &= \arg\max_{\delta} f(\delta|\underline{r}) \\ &= \arg\max_{\delta} f(\underline{r}|\delta) f(\delta|\delta \neq 0) \\ &= \arg\max_{\delta} \int_{-1}^{1} f(\underline{r}|\delta,\rho) f(\rho|\rho \neq 1) d\rho \cdot f(\delta|\delta \neq 0). \end{aligned} \tag{C.10}$$

The probability density function (PDF) of ρ was modeled as a lognormal density in (4.3), however, we alternatively use Rayleigh model for computational simplicity,

even if the fitness is not as good as lognormal. Using Rayleigh model, PDF of ρ can be modeled by

$$f(\rho|\rho \neq 1) = \frac{1}{\sigma_\rho^2(1 - e^{-1/2\sigma_\rho^2})} e^{-\rho^2/2\sigma_\rho^2},\ 0 < \rho < 1, \tag{C.11}$$

where σ_ρ is 0.3715. Substituting (4.2) and (C.11) into (C.10),

$$\hat{\delta} \ = \ \arg\max_{\delta} e^{-\delta/\sigma_\delta} \int_{-1}^{1} \exp\Big[-\frac{1}{2\sigma_{\rm N}^2} \|\underline{r} - \rho\underline{s}_\delta - \underline{s}_0\|^2 \Big] \cdot |\rho| e^{-\rho^2/2\sigma_\rho^2}\ d\rho. \tag{C.12}$$

Assuming the direct path signal and the peak signal does not overlap,

$$\hat{\delta} = \arg\max_{\delta} e^{-\delta/\sigma_\delta} \int_{-1}^{1} |\rho| \exp\Big[-\frac{1}{2\sigma_{\rm N}^2}\Big(\rho^2\|\underline{s}_0\|^2 - 2\rho\underline{r}^t\underline{s}_\delta\Big) - \frac{1}{2\sigma_\rho^2}\rho^2 \Big]\ d\rho. \tag{C.13}$$

Let's define g and $h(\delta, \underline{r})$ as

$$g \ = \ \frac{1}{2}\left[\frac{\|\underline{s}_0^2\|}{\sigma_{\rm N}^2} + \frac{1}{\sigma_\rho^2} \right], \tag{C.14}$$

$$h(\delta, \underline{r}) \ = \ \frac{\underline{r}^t \underline{s}_\delta}{2\sigma_{\rm N}^2}, \tag{C.15}$$

then

$$\hat{\delta} \ = \ \arg\max_{\delta} \int_{-1}^{1} |\rho| \exp\left[-g\Big(\rho - \frac{h(\delta, \underline{r})}{g}\Big)^2 \right] d\rho\ \exp\left[\frac{h^2(\delta, \underline{r})}{g} - \frac{\delta}{\sigma_\delta} \right]$$

$$= \arg\max_{\delta} \Big[\Big[1 - \exp\Big[2h(\delta, \underline{r}) - g\Big]\Big] \exp\Big[-\delta/\sigma_{\delta}\Big]. \tag{C.16}$$

According to (C.16), $\hat{\delta}$ is given by a simple expression, however it cannot be evaluated before the correlator output is available since it involves the maximization of the quantity which is a function of both the correlator output ($h(\delta, \underline{r})$) and δ. In real channel responses, there may exist multipath components which arrive between the direct path and the peak path, which can cause errors if δ is evaluated based on (C.16). So modeling of these potential signal components to eliminate the nuisance parameters appearing in (C.8) which is mathematically very challenging.